The antimycotic drug fluconazole induces reabsorption of water by promoting the redistribution of water channel aquaporin-2

DISSERTATION

Inaugural-Dissertation
to obtain the academic degree
Doctor rerum naturalium (Dr. rer. nat.)

submitted to the Department of Biology, Chemistry and Pharmacy
of Freie Universität Berlin

by

TANJA VUKIĆEVIĆ

from Niš, Serbia

Berlin 2017

This work was conducted from August 2014 until May 2017 at the Max-Delbrück Center for Molecular Medicine in Berlin under the supervision of Priv.-Doz. Dr. Enno Klußmann.

1. Reviewer: Priv.-Doz. Dr. Enno Klußmann
2. Reviewer: Univ.- Prof. Dr. Matthias F. Melzig

Dissertation submitted on: 18. 5. 2017

Date of Disputation: 10. 7. 2017

I hereby declare that the following work was performed by me alone, only with the use of literature and materials listed. I further declare that to the best of my knowledge this work is novel and does not conflict with any earlier published work.

Berlin, May 2017

Tanja Vukićević

Acknowledgments

First and foremost I would like to thank Priv.-Doz. Dr. Enno Klußmann for giving me an opportunity to be a member of his lab. I would also like to thank him for helping me design a project, which was tailored to my interest of working. I especially appreciate all the time and patience that he has given me while clarifying my concerns and suggesting improvements towards my experimental goals.

I owe a gratitude to Univ.- Prof. Dr. Matthias F. Melzig for taking me as a second supervisor.

I am grateful from the bottom of my heart to the previous and present members of AG Klußmann especially Alessandro Dema, Maike Schulz, Dr. Katharina Schrade, Dr. Ekaterina Perets, Mohamed Elkewedi and Dr. Dörte Faust for their kindness, day to day guidance through my experimental procedures and constant reassurance.

A special thank you to Jenny Eichhorst and Dr. Burkhard Wiesner for all the help with confocal microscopy.

I am thankful to Andrea Geelhaar and Beate Eisermann for the huge support and excellent technical assistance.

I would like to thank my collaborators Dr. med. Christian Hinze from AG Schmidt-Ott, Prof. Dr. Kai M. Schmidt-Ott, Univ.- Prof. Dr. Wolf Hagen Schunck and Maximilian Blum from AG Schunck.

I also thank to Priv.-Doz. Dr. Enno Klußmann, Dr. Jelena Ivanovska, Katarina Stevanović, Dr. Sarah Ashley, Maike Schulz and Alessandro Dema for fast and accurate corrections of my thesis.

I would like to thank Maike Schulz for translation of the summary into German.

Many thanks go to Dipl.-Ing. Adela Sesto for professional expertise in drawing the figures used in this thesis.

Lastly, I would like to thank my family, friends and loved ones for their continuous love, support, for giving me strength to work abroad, and most importantly for encouraging me constantly to make this dream come true.

1 Table of Contents

ABBREVATIONS

AC	adenylyl cyclase
ADH	antidiuretic hormone
AKAPs	a-kinase anchoring proteins
ANF	atrial natriuretic factor
ATP	adenosine triphosphate
ADPKD	autosmal policystic kidney disease
ANOVA	analysis of variance
AQP	aquaporin
bp	base pare
BSA	bovine serum albumin
BMP-2	bone morphogenetic protein-2
bw	body weight
cAMP	cyclic adenosine-3',5'-monophosphate
cGMP	cyclic guanosine-3',5'-monophosphate
CD8	primary kidney cell line
CDK	cyclin-dependent kinase
Cdc42	the small GTPase
COX-2 inhibitor	directly targets cyclooxygenase-2
COPD	chronic obstructive pulmonary disease
CYP	cytochrome P450
DAPI	4', 6-diamidine-2'-phenylindole dihydrochloride
DBcAMP	N^6,O2'-Dibutyryladenosin-3',5'-monophosphat
dDAVP	desmopressin
diHOME	linoleic acid metabolite
DMEM	Dulbecco's modified eagle medium
DI	Diabetes insipidus
DMSO	dimethylsulfoxide
EET	epoxyeicosatrineoic acids
EDTA	ethylenediaminetetraacetic acid
eNOS	endothelial nitric oxide synthase
EP	prostaglandin receptor
ERK	extracellular signal–regulated kinases
ET-1	endothelin
F-actin	filamentous actin
Flu	fluconazole
FCS	fetal calf serum
FELASA	Federation of european laboratory animal science associacions
FMP	Leibniz-Institut für Molekulare Pharmakologie
FSK	forskolin
G-actin	globular actin
GEFs	guanine nucleotide exchange factors
GDI	guanosine nucleotide dissociation inhibitor
GDP	guanosine diphosphat
GTP	guanosine triphosphate
h	hour(s)
HELLP	syndrome including hemolysis, elevated liver enzymes and low platelets
HCTZ	hydrochlorthiazide
HMG-CoA	3-hydroxy-m-methylglutharyl-coenzyme A
HSP90	heat-shock protein 90
HSP70	heat-shock protein 70
HET-0016	*N*-hydroxy-*N*9-(4-butyl-2methylphenyl)formamidine
20-HETE	20- hydroxyeicosatetraenoic acid
H27	rabbit-derived anti-AQP2 antibody
H27-Cy3	rabbit-derived anti-AQP2 antibody plus Cy3-conjugated secondary antibody
IF	immunofluorescence
IMCD	inner medulla collecting duct

i.p.	intraperitoneal
JNK	c-Jun N-terminal kinase
kg	kilogram
L	litre
LaGeSo	Landesamt für Gesundheit und Soziales
LIMK	LIM kinase
LLC-AQP2	renal epithelial cell line
LSM	laser scanning microscope
MCD4	mouse collecting duct cells
MDC	Max-Delbrück-Zentrum für Molekulare Medizin
mEq	milliequivalent
mg	milligram
min	minute
MLC	myosin light chain
MLCK	myosin light chain kinase
mpkCCD	murine immortalized cortical collecting duct cells
mPGES-1	PGE_2 synthase-1
NO	nitric oxide
NSAIDs	nonsteroidal anti-inflammatory drug
ONO-AE-329	EP_4 receptor antagonist
PAGE	polyacrylamide gel electrophoresis
p	value used for statistic assessment
p38-MAPK	p38-mitogen-activated protein kinase
pSer256	AQP2, phosphorylated at serine 256
pSer261	AQP2, phosphorylated at serine 261
pSer264	AQP2, phosphorylated at serine 264
pSer269	AQP2, phosphorylated at serine 269
PAI-1	plasminogen activator inhibitor-1
PBS	phosphate-buffered saline
PD	pulldown
PDE	phosphodiesterase
PFA	paraformaldehyde
PGE_2	prostaglandin E_2
PGI_2	prostacyclin
PKA	protein kinase A
PKC	protein kinase C
PKG	protein kinase G
POD	peroxidase
PP	protein phosphatase
pNP	para-Nitrophenol
pNPP	para-Nitrophenylphosphate
PVDF	polyvinylidene fluoride
Rab3a	GTP-binding protein
Rab5	the small GTPase
Rab11	the small GTPase
RBD	Rho binding domain
R subunit	regulatory subunit of PKA
RhoA	Ras homolog family member A
Rac1	Ras-related C3 botulinum toxin substrate 1
ROCK	Rho-associated protein kinase
SDS	sodium dodecyl sulfat
SEM	standard error of mean
sEH	solubile epoxyde hydrolaze
SIPA111	signal-induced proliferation-associated 1 like 1
SIADH	syndrome of inappropriate antidiuretic hormone secretion
SDS-PAGE	SDS-polyacrylamide gel electrophoresis
SLB	standard lysis buffer
SNARE	soluble N-ethylmaleimide-sensitive-factor-attachment receptor
SNP	sodium nitroprusside
sEH	solubile epoxyde hydrolase
TAE	tris-acetate-EDTA
TBS	tris-buffered saline
TBS-T	TBS + tween
TEA	triethylamine
t-PA	tissue-type plasminogen activator
Tris	tris(hydroxymethyl)-aminomethane
Tol	tolvaptan

TxA2	tromboxane A_2
unt	untreated
V	volt
VAMP8	vesicle-associated membrane protein 8
V2R	vasopressin receptor type 2
WB	Western blotting
°C	degree celsius
µ	micro

LIST OF TABLES

LIST OF FIGURES

2 INTRODUCTION

Parts of the thesis introduction have been published in a review: Vukićević T, Schulz M, Faust D, Klussmann E. The Trafficking of the Water Channel Aquaporin-2 in Renal Principal Cells-a Potential Target for Pharmacological Intervention in Cardiovascular Diseases. Front Pharmacol. 2016 Feb 11;7:23. doi: 10.3389/fphar.2016.00023. eCollection 2016.
.

2.1 Kidney function in water reabsorption

Maintaining water homeostasis is achieved by controlling both blood volume and blood osmolality and this is crucial for the most of the physiological processes. The body fluid homeostasis is mostly controlled through the water intake and urine excretion. In kidneys, around 180 L of plasma are filtered by glomeruli each day. Most functions of the kidney are accomplished by filtration, reabsorption and secretion in the nephron, which is the main functional unit of the kidney (Figure 1). Before urine is produced and stored in the bladder, filtrate passes through the proximal convoluted tubules, the descending and ascending limb of Henle, where around 90 % of water gets reabsorbed. The reabsorption of the remaining 10 % occurs in the distal convoluted tubule and, finally, in the collecting duct where reabsorption of water is hormonally regulated. About 1 % of the 180 L of primary urine is excreted as the final urine (Noda et al., 2004).

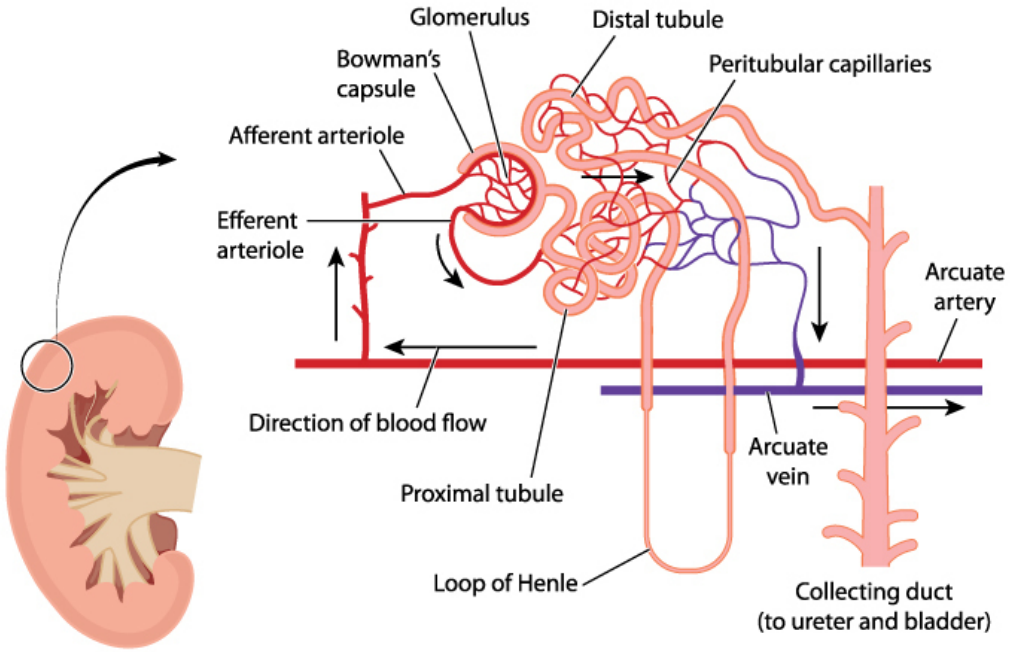

Figure 1. The nephron. The nephron is the functional unit of the kidney. Each kidney consists of approximately one million nephrons. Nephrons consist of capsules and a set of tubular structures surrounded by a capillary network leading to venules. Venules form veins leaving the kidney into the inferior vena cava *en route* to the heart (Adapted from: A nephron of the Kidney Cortex, Blamb *via* Shutterstock.com).

2.2 Vasopressin-regulated water reabsorption

Aquaporins (AQP) are membrane proteins that are responsible for the water transport across the membranes. Eight of the thirteen human AQP isoforms are located in the human kidneys. Several of them contribute to maintain the body's water homeostasis (Preston and Agre, 1991; Su et al., 2017). Each AQP possesses six membrane-spanning alpha-helices and central water pore (Murata et al., 2000). Four AQP monomers form tetramers, which represent the functional unit in the membrane. If at least three of the four monomers are phosphorylated, AQP2 redistributes to the plasma membrane (Kamsteeg et al., 2000). Although water is able to pass the lipid barrier of biological membranes by passive diffusion, the insertion of AQPs into the plasma membrane facilitates high-rate water movement.

Renal water excretion is mostly regulated by the antidiuretic hormone (arginine vasopressin, AVP). AVP is synthesized in the hypothalamus and released from the posterior pituitary gland. Increased osmotic pressure is a signal for releasing of this hormone. A major effector of AVP is the water channel aquaporin-2 (AQP2), the chief regulator of water reabsorption in kidney collecting tubules and collecting ducts (Han et al., 1994). AQP2 is abundantly expressed in the principal cells of this section of the nephron. Abundance and cellular localization of AQP2 is regulated by AVP but also through other signaling molecules (Nielsen et al., 1993).

When circulating AVP reaches the principal cells of the collecting duct, it binds to vasopressin receptor type 2 (V2R) and increases the water permeability of the cells. In particular AVP induces translocation of AQP2 from intracellular reservoir of vesicles to the plasma membrane. The membrane insertion is described as the short-term regulation of AQP2 (Jung and Kwon, 2016). Once AQP2 is inserted into the plasma membrane water can pass from the tubular lumen into the interstitium following the osmotic gradient. On the basolateral side of the plasma membrane, AQP3 and AQP4 provide an exit pathway for the water (Figure 2)(Bockenhauer and Bichet, 2014).

At the molecular level, AVP binds to the G protein coupled receptor V2R, located on the basolateral plasma membrane of renal collecting duct principal cells (Figure 2). Binding of AVP to V2R activates the stimulatory G protein, Gs. This leads to the activation of two adenylyl cyclases (ACs), AC3 and AC6, which in turn convert ATP to cyclic adenosine monophosphate (cAMP). This elevation of cAMP leads to the activation of protein kinase A (PKA). In the basal state, PKA is a tetramer consisting of two regulatory subunits (RIα, RIβ, RIIα or RIIβ), each binding to one catalytic subunit (Cα, Cβ, Cγ or PrKX). A subpool of PKA is tethered to a perinuclear AQP2-bearing vesicles by A-kinase anchoring proteins (AKAPs). The binding of four cAMP molecules to a dimer of R subunits induces a conformational change, whereby the C subunits are released. Free, and thus active C subunits, phosphorylate targets nearby including AQP2. AQP2 is phosphorylated in the intracellular C-terminus at Ser256 (Troger et al., 2012; Vukicevic et al., 2016).

Long-term regulation plays an important role in water balance disorders (see below 2.6), but also in the state of water deprivation for 24 h or longer. The response to a prolonged water deprivation is an increase in AVP levels and consequently AQP2 abundance (Brond et al., 2004; Verbalis, 2006). AVP activates AQP2 in a cAMP-dependent manner, which leads to the stimulation of AQP2 transcription (Yasui et al., 1997).

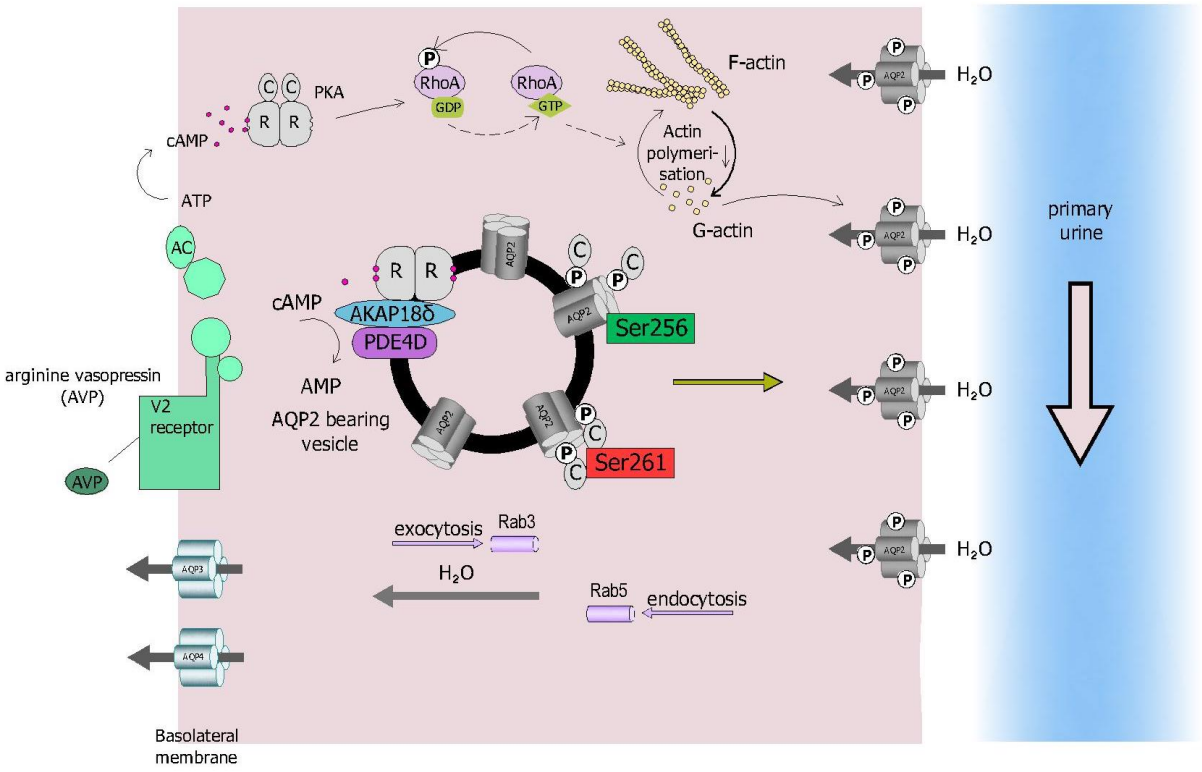

Figure 2. AVP-stimulated translocation of AQP2 from intracellular vesicles into the plasma membrane. Binding of AVP to V2R mediates PKA activation. PKA phosphorylates AQP2 at Ser256, which triggers AQP2 redistribution to the plasma membrane. Insertion of AQP2 into the plasma membrane facilitates the water reabsorption from primary urine. Water exits the cells through AQP3 and AQP4 in the basolateral plasma membrane.

2.3 The role of PKA in the trafficking and phosphorylation of AQP2

The phosphorylation of AQP2 at Ser256 was long thought to be the key trigger for the exocytosis-like redistribution from its location on intracellular vesicles into the plasma membrane. However, several studies reported, that AQP2 is contributing to phosphorylation at Ser256, independent of stimulation by AVP or forskolin (FSK) (Christensen et al., 2000; Hoffert et al., 2007; Yui et al., 2013). These reports indicated that phosphorylation at Ser256 may not be the main checkpoint of AQP2 control.

In addition to the phosphorylation of Ser256, AVP controls the phosphorylation of three further C-terminal residues of AQP2, Ser261, Ser264 and Ser269 (Figure 3) causing increase in phosphorylation of Ser256 (Nishimoto et al., 1999), Ser264 (Fenton et al., 2008) and Ser269 (Hoffert et al., 2008a), while decreasing the phosphorylation at Ser261 (Nedvetsky et al., 2010).

The phosphorylation of Ser264 and Ser269 mediate membrane retention of AQP2, most likely because this phosphorylation reduces the rate of internalization (Hoffert et al., 2008b; Moeller et al., 2009b). In both mice and in Madin-Darby canine kidney cells expressing an S256A mutant, phosphorylation of AQP2 at Ser269 did not occur when Ser256 was replaced by an

unphosphorylatable amino acid. This indicated that Ser269 phosphorylation of the AQP2 depends upon phosphorylation at Ser256 (Hoffert et al., 2008b). New insight provides evidence that AVP-induced Ser269 phosphorylation reduces signal-induced proliferation-associated 1 like 1-(SIPA111)-mediated AQP2 endocytosis (Wang et al., 2017).

AQP2 at Ser261 is highly phosphorylated under resting condition. Upon AVP stimulation is dephosphorylated (Nedvetsky et al., 2009). This is associated with a decrease in p38 mitogen-activated protein kinase (p38MAPK) activity (Nedvetsky et al., 2010; Tamma et al., 2010). Increased phosphorylation at Ser261 is associated with an increased polyubiquitiniation and proteosomal degradation of AQP2. It was also reported that phosphorylation of AQP2 at Ser261 does not affect AQP2 trafficking (Lu et al., 2008). Recent studies show that reduced phosphorylation at Ser261 occurs when Ser256 and Ser269 of AQP2 are phosphorylated (Yui et al., 2016).

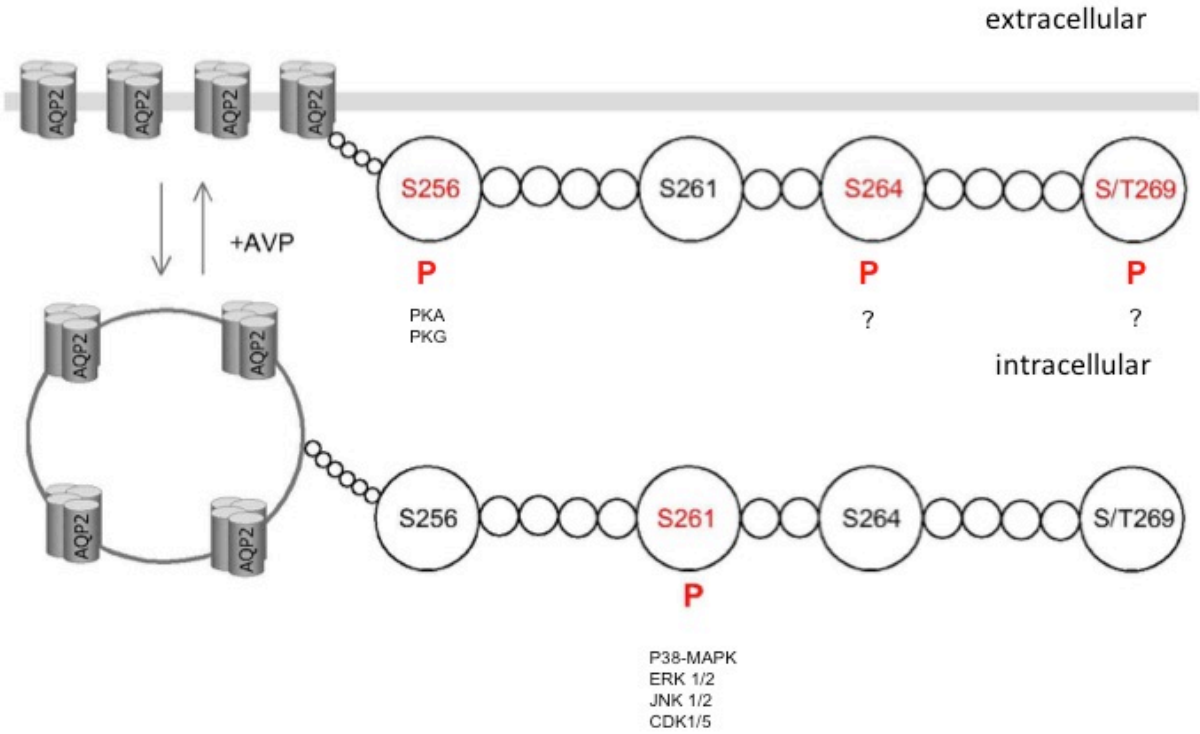

Figure 3. AQP2 phosphorylation. The C-terminus of AQP2 contains the AVP regulated region with four serine residues at Ser256, Ser261, Ser264 and Ser269. These sites have different roles in the content of the AQP2 localization. The phosphorylation of AQP2 at Ser256 is catalysed by PKA (Kamsteeg et al., 2000; Nishimoto et al., 1999) and PKG (Bouley et al., 2000; Brown et al., 2008). Phosphorylation at Ser261 could be regulated by P38-MAPK (Nedvetsky et al., 2010), extracellular signal-regulated kinases (ERK 1/2)(Hoffert et al., 2006), jun amino-terminal kinases (JNK 1/2)(Nielsen et al., 2008; Rinschen et al., 2010) and cyclin-dependent kinases (CDK 1/5)(Rinschen et al., 2010).

As for many proteins, the function and the trafficking of AQP2 is modulated by a balance of reversible phosphorylation and dephosphorylation. Proteomic analysis of inner medulla of collecting ducts identified protein phosphatase 2A (PP2A) as a possible phosphatase, which may be involved in cellular events triggered by AVP (Tamma et al., 2001; Tamma et al., 2014). A recent study showed that specifically the inhibition of PP1/PP2A plays an important role for the AQP2 apical plasma membrane localization and phosphorylation status (Ren et al., 2016).

2.4 AQP2 endocytosis and recycling

The plasma membrane insertion of AQP2 involves the soluble N-ethylmaleimide sensitive factor attachment protein receptor machinery (SNARE) (Liebenhoff and Rosenthal, 1995). Vesicle-associated membrane protein 8 (VAMP8) co-localizes with AQP2 on the intracellular vesicles, and it interacts with the plasma membrane t-SNARE proteins. This suggests that VAMP8 mediates the regulated fusion of AQP2-positive vesicles with the plasma membrane (Procino et al., 2008).

Membrane localization of AQP2 in the presence of AVP correlates with the decreased interaction of phosphorylated AQP2 at Ser256 with several proteins which are involved in the endocytosis, including heat shock protein HSP70, dynamin and clathrin (Moeller et al., 2010). AQP2 recycles constitutively between intracellular vesicles to the plasma membrane and this process is in equilibrium. AQP2 is located in clathrin-coated pits in the apical plasma membrane (Sun et al., 2002). Upon the removal of AVP, AQP2 is retrieved from the plasma membrane back to the cell cytoplasm where it is recycled or sorted by lysosomes for degradation *via* clathrin-mediated endocytosis (Brown et al., 2012).

2.5 Regulators of AQP2 trafficking

2.5.1 The role of the actin cytoskeleton in AQP2 trafficking

The actin cytoskeleton acts as a physical barrier hindering AQP2-bearing vesicles to reach the plasma membrane. In CD8 cells, actin depolymerisation by okadaic acid, an inhibitor of phosphatase 1 (PP1), induced actin depolymerisation and promoted AQP2 translocation to the plasma membrane, whereby similar findings were supported by the effect of FSK (Valenti et al., 2000). Okadaic acid enabled AQP2 trafficking even when CD8 cells were pre-incubated with the PKA inhibitor H89 (Valenti et al., 2000). This implicates that reorganization of the actin cytoskeleton plays an important role in AQP2 trafficking independent of PKA.

The GTP-binding proteins Rab3a and Rab5 are markers for exo- and endocytic vesicles, respectively. AQP2-bearing vesicles are co-enriched with Rab3a (Liebenhoff and Rosenthal, 1995) (Figure 2).

The small GTPase RhoA belongs to a family of small GTP-binding proteins that also includes Rac1 and Cdc42. These proteins have a variety functions such as cytoskeletal organization, cell

migration, trafficking, cell division and cell adhesion (Tamma et al., 2003a). Rho switches between an active, GTP-bound state and an inactive, GDP-bound state. RhoA is phosphorylated on Ser188 by a number of kinases (Tong et al., 2016). Phosphorylation at Ser188 by PKA results in a decrease in the binding of RhoA to Rho kinase and thus essentially in its inhibition (Dong et al., 1998).

Active RhoA inhibits the AQP2 redistribution to the plasma membrane (Tamma et al., 2003b). In resting IMCD cells, RhoA promotes the polymerization of cortical F-actin, hindering trafficking of AQP2-bearing vesicles to the plasma membrane. AVP stimulation inhibits RhoA and thereby causes depolymerisation of cortical F-actin (Klussmann et al., 2001; Tamma et al., 2003b).

In IMCD cells, inhibition of RhoA with clostridum toxin depolymerises the actin cytoskeleton resulting in AQP2 translocation to the plasma membrane despite the absence of AVP. *Vice versa*, transfection of these cells with constitutively active RhoA mutant promoted stress fibers formation and prevented cAMP-induced AQP2 trafficking (Jung et al., 2015). The inhibition of the downstream effectors of RhoA, Rho kinases, also induced the translocation of AQP2 to the plasma membrane (Tamma et al., 2001).

Taken together, RhoA inhibition through RhoA phosphorylation is a crucial event for the actin depolymerisation that controlls cAMP-induced AQP2 translocation.

RhoA regulates actin cytoskeleton dynamics *via* the downstream effectors LIM kinase 1 (LIMK1) and LIMK2. GTP-bound RhoA activates ROCK, which in turn phosphorylates LIMKs (Riento and Ridley, 2003). Phosphorylation and thus activation of LIMK occurs at threonine residue Thr-508 in LIMK1 and Thr-505 in LIMK2 (Maekawa et al., 1999; Ohashi, 2015).

Cofilin, as another downstream effector of RhoA, together with LIMKs also plays an important role in actin cytoskeleton reorganization (Ivanovska et al., 2013; Manetti, 2012). Phosphorylated LIMK deactivates cofilin activity *via* phosphorylation at Ser3. Cofilin binds monomeric actin (G-actin), as well as filamentous actin (F-actin), and when is active, causes depolymerisation of filaments. Therefore, if cofilin is not phosphorylated, it prevents reassembly of G-actin to F-actin (Ohashi, 2015).

However, whether LIMK and cofilin are connected to AQP2 trafficking is unknown.

2.5.2 Microtubuli

AQP2-bearing vesicles redistribute to the plasma membrane along the F-actin cytoskeleton, while for the endocytic retrieval from the plasma membrane to the perinuclear position, AQP2 is transported mainly *via* microtubules (Brown et al., 2012; Vossenkamper et al., 2007).

In primary cultured IMCD cells, perinuclear localization of AQP2 was abolished, and AQP2 was translocated to the plasma membrane in response to nocodazole, a microtubule inhibitor. The AQP2 redistribution was accompanied with reorganization of microtubules and the redistribution of the small GTPase Rab11. AQP2 is perinuclearly co-localized with Rab11 under resting conditions. AVP induces AQP2 redistribution with Rab11 to the plasma membrane (Vossenkamper et al., 2007).

2.5.3 The role of MLC in AQP2 trafficking

Myosins comprise a large family of ATP-dependent molecular motor proteins that interact with actin filaments (Sellers, 2000). In non-muscle cells, myosin II forms contractile bundles in stress fibers. Myosin II is regulated by phosphorylation of its myosin light chain (MLC) by the MLC kinase (MLCK).

Knepper and colleagues have identified many components in this pathway, such as MLCK, MLC, and the IIA and IIB isoforms of the non-muscle MLC, in IMCD cells. AVP induces phosphorylation of MLC and the inhibition of MLCK, and this interaction is predominantly associated with the plasma membrane localization of AQP2 (Chou et al., 2004).

On the basis of these data, a role of non-muscle myosin II in AQP2 trafficking has been revealed (Valenti et al., 2000; Vukicevic et al., 2016).

2.5.4 Prostaglandins and cytochrome P450 metabolites

Arachidonic acid can be metabolized by cytochrome P450 epoxygenase to a various forms of epoxyeicosatrineoic acids (EETs) and prostaglandins, particularly prostaglandin E_2 (PGE_2) (Figure 4) (Boone and Deen, 2008; Flores et al., 2012). PGE_2 is synthesised and released in the collecting duct, where all four prostaglandin receptors ($EP_{1\text{-}4}$) are expressed (Olesen et al., 2011a). PGE_2 is produced after stimulation with various factors that exhibit natriuretic and diuretic effects, including EETs, ATP and endothelin (Breyer and Breyer, 2000; Flores et al., 2012).

The EP_4 receptor in renal collecting ducts plays an important role in regulating urinary concentrating ability. Similar to the V2R, EP_2 and EP_4 couple to Gα, whereby stimulation of the EP_4 receptor induces cAMP signalling, which causes water reabsorption from primary urine (Alexander et al., 2011). The stimulation of EP_2 and EP_4 receptors facilitates phosphorylation of AQP2 at Ser264 (Olesen et al., 2011b). However, only EP_2 signalling, independent of AVP, increases the cytosolic cAMP concentration (Breyer and Breyer, 2001) and facilitates

phosphorylation of AQP2 at Ser256 and Ser269 (Olesen et al., 2011b). It may be possible that EP_2 and EP_4 act *via* different signalling pathways (Olesen et al., 2011b). Available findings raise the question whether EP_2 is expressed in the collecting duct at all (Breyer et al., 1996; Hao and Breyer, 2008; Jensen et al., 2001; Morath et al., 1999; Regan, 2003; Sugimoto et al., 1994), while it is known that EP_4 is highly abundant in the collecting duct (Sugimoto and Narumiya, 2007). Activation of EP_4 could promote AQP2 trafficking, without affecting cytosolic cAMP levels (Olesen et al., 2011b) as a consequence of PKA phosphorylation of EP_4 due to promiscuous G protein coupling (Fujino and Regan, 2006).

In contrast to EP_2 and EP_4, the activation of EP_1 and EP_3 receptors in the collecting duct reduces cAMP production (Pearce et al., 2015; Tamma et al., 2003c). EP_3-signaling also stimulates RhoA (Tamma et al., 2003b). This is probably mediated by the $G\alpha_{12/13}$-dependent activation of Rho guanine nucleotide exchange factors (GEFs) (Wells et al., 2002; Yamaguchi et al., 2000), which directly activate RhoA and thus attenuate AQP2 membrane trafficking (Klussmann et al., 2001; Tamma et al., 2001). The long-term effect of PGE_2 on EP_1 and EP_3 receptors is the down-regulation of the AVP-regulated Na-K-Cl co-transporter. PGE_2 inhibits AQP2 trafficking in rat inner medullary principal cells, presumably *via* cAMP- and Ca^{2+}-independent RhoA activation (Jensen et al., 2010; Lauridsen et al., 2010).

EETs have been shown repeatedly to inhibit the Na-K-Cl co-transporter activity, including inhibition of PGE_2 formation stimulation (Pearce et al., 2015; Sakairi et al., 1995).

A number of compounds have been identified that selectively inhibit epoxygenase activity and the production of EETs (Figure 4), such as the antimycotic agents miconazole, fluconazole ketoconazole, and clotrimazole. They can reduce the formation of EETs by renal and hepatic microsomes by 70 % and can prevent the vasodilator response. At concentrations of 10 µM, they completely inhibit epoxygenase activity while reducing the formation of 20-hydroxyeicosatetrenoic acid (20-HETE) by 50 % (Roman et al., 2002).

The production of the ω-hydroxylation product 20-HETE is negatively regulated by the EETs. The inhibitor *N*-hydroxy-*N*9-(4-butyl-2methylphenyl)formamidine (HET-0016) or 20-HETE antagonists block the formation of 20-HETE. Blockage of the formation of 20-HETE attenuates the vascular responses to angiotensin II, endothelin and norepinephrine (Park et al., 2014). In the kidney, these stimuli enhance the formation of 20-HETE, whereby 20-HETE contributes to the vasoconstrictor and natriuretic actions of these peptides (Roman, 2002). Recent findings provide evidence for an AVP-dependent increase in solubile epoxyde hydrolase (sEH) biosynthesis and enzyme activity in renal collecting ducts of Brattleboro rats, resulting in a decreased EET level (Boldt et al., 2016).

Although the physiological relevance of EETs and the products of P450 systems in reabsorption of salts and water is largely unknown, these products in addition to prostaglandins in collecting ducts may be involved in the control of AQP2.

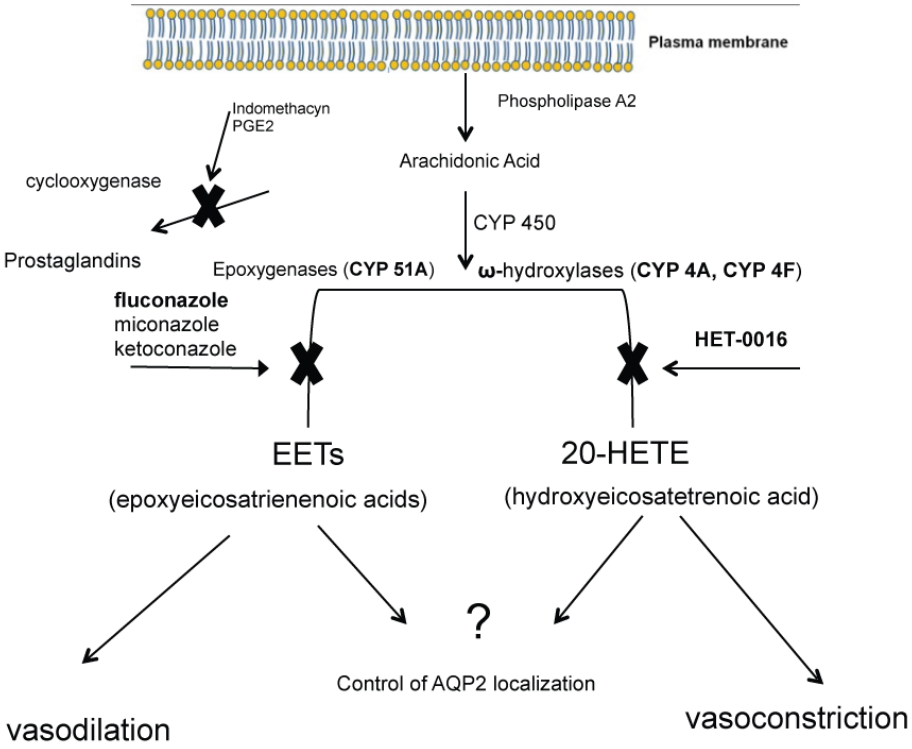

Figure 4. Pathway for arachidonic acid metabolism. Examples of agents available to induce or inhibit various pathways for the metabolism of arachidonic acid (fluconazole, HET-0016); Arachidonic acid is metabolized *via* the cyclooxygenase, lipoxygenase, and cytochrome P-450 (CYP) enzymes to prostaglandins (PG), prostacyclin (PGI_2), thromboxane A_2 (TxA_2), or a series of hydroxyeicosatetraenoic acids (HETEs), epoxyeicosatrienoic acids (EETs).

2.6 AQP2 associated water balance disorders

The dysregulation of AQP2 is implicated in several human diseases. A hallmark of several diseases, such as the syndrome of inappropriate antidiuretic hormone secretion (SIADH), late stage heart failure, and liver cirrhosis are characterized by elevated levels of AVP, which leads to hyponatremia with or without hypervolemia. Excessive AVP production causes water retention through a predominant localization of AQP2 into the plasma membrane and increases circulating blood volume. The final result is a diluted plasma with hyponatremia, an electrolyte disorder defined as a serum sodium level of less than 135 mEq per L. The most frequent cause of hyponatremia is SIADH. It accounts for approximately one-third of all cases (Ishikawa, 2015).

The plasma membrane abundance of AQP2 is increased in SIADH underlining the important role of AQP2 in water retention (Kortenoeven et al., 2013).
The non-osmotic release of AVP is associated with an increase in water permeability in the cells of the renal collecting duct, which leads to an increase in the circulatory plasma volume, and therefore it is consequently linked to the mentioned diseases.
Defects of AQP2 membrane localization cause polyuria, which is a result of diabetes insipidus (Radin et al., 2012).

2.6.1 Diabetes insipidus

Patients suffering from diabetes insipidus have an inability to concentrate urine resulting in polyuria and polydipsia (Bockenhauer and Bichet, 2015; Knoers, 1993). The inability of the kidney to concentrate urine leads to severe dehydration, hypernatremia, and hyperchloremia (Multari et al., 2001; Qureshi et al., 2014).
There are different types of diabetes insipidus, inherited or acquired forms. Mutations in the gene encoding AVP lead to a central diabetes insipidus (CDI), whereas congenital nephrogenic diabetes insipidus (NDI) is caused by mutations in the genes encoding the V2R and AQP2 (Deen et al., 1994; Peters et al., 2007).
The hereditary form of NDI usually becomes apparent within a few months after birth. Approximately 90 % of all congenital NDI forms mutations are in the V2R gene (X-chromosome, Xq28) and they lead to a dysfunctional V2R, causing X-linked NDI (Heinke and Labudde, 2012). AQP2 does not translocate into the plasma membrane and it is down-regulated owning to the lack of a functional V2R gene (Seibold et al., 1992). The X-linked inheritance is more apparent in males due to the lack of a second X chromosome. Even after administration of dDAVP (vasopressin) male patients do not show signs of improvement (Knoers and Deen, 2001).
Approximately, the remaining 10 % of the persons are with congenital NDI carry mutations in the AQP2 gene by inherited autosomal forms. To date 40 mutations in the AQP2 gene have been reported (Figure 5) (Loonen et al., 2008; Savelkoul et al., 2009). Autosomal-recessive NDI is associated exclusively with 32 mutations, and 8 mutations cause autosomal-dominant NDI. Almost all mutations in recessive NDI lead to a misfolded proteins that are trapped in the endoplasmic reticulum and targeted for degradation. In autosomal-dominant NDI all mutations are in the cytosolic C terminus of AQP2.
Up to 55 % of the patients suffering from depression or bipolar disorders, which are treated with lithium, can develop a variable degree of NDI (Bonfrate et al., 2015; Li et al., 2011). It is estimated that 5 in 1000 of the Western population currently are on a lithium treatment (Moeller et al., 2013). Lithium enters the cells *via* epithelial sodium channels and causes

perinuclear accumulation of AQP2. Hypercalcemia (Kamath et al., 2013; Khairallah et al., 2007), hypokalemia (Celik et al., 2014), secondary hyperaldosteronism (Lee et al., 2010; Qureshi et al., 2014), and ureteral obstruction (Jensen et al., 2009) can also cause acquired NDI.

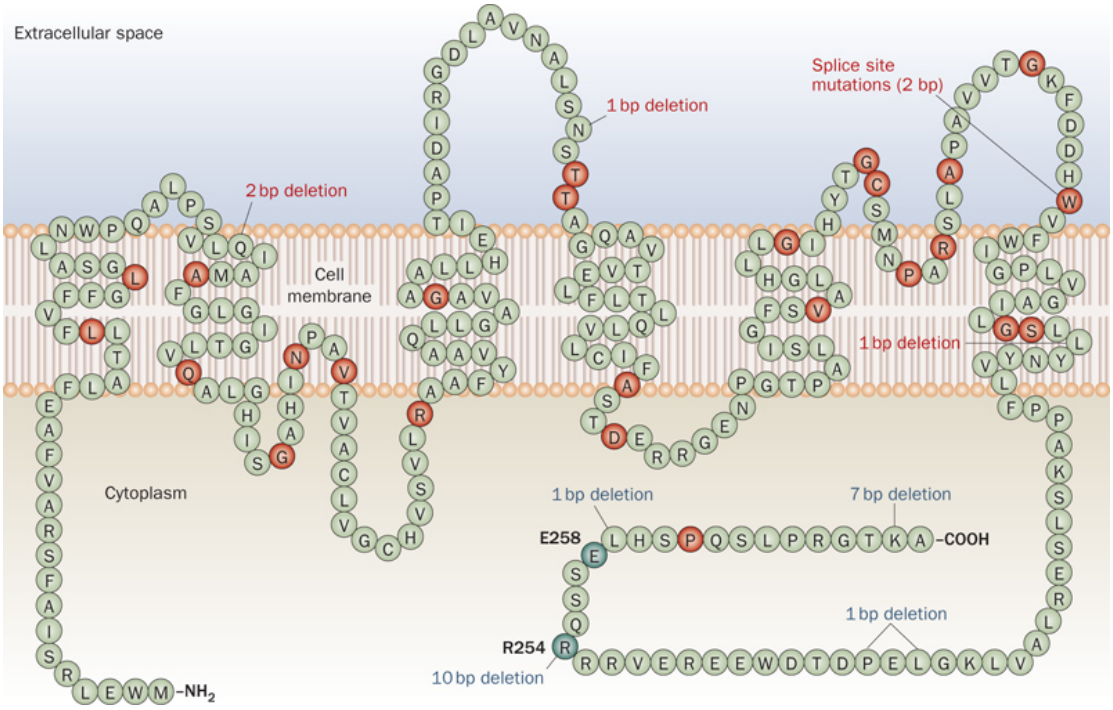

Figure 5. Structure of AQP2 and mutations that cause nephrogenic diabetes insipidus. In red are shown amino acid mutations and AQP2 deletions, which cause autosomal-recesive form of NDI. In blue are presented amino acid mutations and AQP2 deletions, which can cause autosomal-dominant NDI. Abbreviation: bp-base pare. (Adapted from (Noda et al., 2010)).

Gestational DI is another rare DI form that manifests during pregnancy in the third trimester and in an early postpartum period. Placental abruption can release placental vasopressinase into the bloodstream where it degrades AVP. This could be the main reason for the acute postpartum DI, which may cause pregnancy complications such as preeclampsia and the HELLP syndrome (Hemolysis, Elevated Liver enzymes and Low Platelets). Gestational DI can be treated with dDAVP because it is resistant to degradation by vasopressinase (Kortenoeven and Fenton, 2014; Qureshi et al., 2014).

2.7 Pharmacological interference with AQP2 trafficking for the treatment of water balance disorders

An option for the treatment of diseases with a defect in the AVP-induced redistribution of AQP2 is to induce it with drugs. Several regimes have recently emerged for the treatment of NDI. The

current strategy for preventing inappropriate water reabsorption through AQP2 is by blocking V2R.

2.7.1 Statins

Statins, the lipid-lowering drugs, can affect the polymerization state of the actin cytoskeleton causing its depolymerisation (Wade, 2011). The final effects of downregulation of RhoA activity on the AQP2 are both increased exocytosis and decreased endocytosis (Li et al., 2011; Procino et al., 2010; Procino et al., 2011; Procino et al., 2014).

In general, statins inhibit the conversion of mevalonate into isoprenoid intermediates, such as fanesyl pyrophosphate and geranyl-geranyl pyrophosphate (Figure 6)(Verhulst et al., 2004). These isoprenoid products act as a lipid anchors, which are required for membrane tethering and activation of heterotrimetric G proteins and small GTPases, amongst them RhoA (Li et al., 2011). Consequently, statins cause RhoA inactivation and thus AQP2 can translocate to the plasma membrane.

Simvastatin increases AQP2 translocation to the plasma membrane in a dose-dependent manner in LLC-AQP2 and MCD4 cells, which was associated with the inhibition of endocytosis (Procino et al., 2012). Short-term exposure to simvastatin produced no change in cholesterol plasma membrane levels, but increased AQP2 accumulation in the apical plasma membrane of principal cells in kidney sections from Brattleboro rats, along with increased water reabsorption and urinary concentration *in vivo* (Bonfrate et al., 2015; Li et al., 2011). Additionally, *in vitro* and *in vivo* experiments in mice indicated that fluvastatin increases AQP2 plasma membrane accumulation by the changes in the prenylation status of the key proteins regulating AQP2 trafficking in collecting duct such as RhoA (Procino et al., 2011).

This data suggests that statins induce AQP2 trafficking and offer a possibility for the treatment of NDI because of their non-lipid pleiotropic effect due to the inhibition of RhoA and it might affect additional GTPases Rac1 and Cdc42.

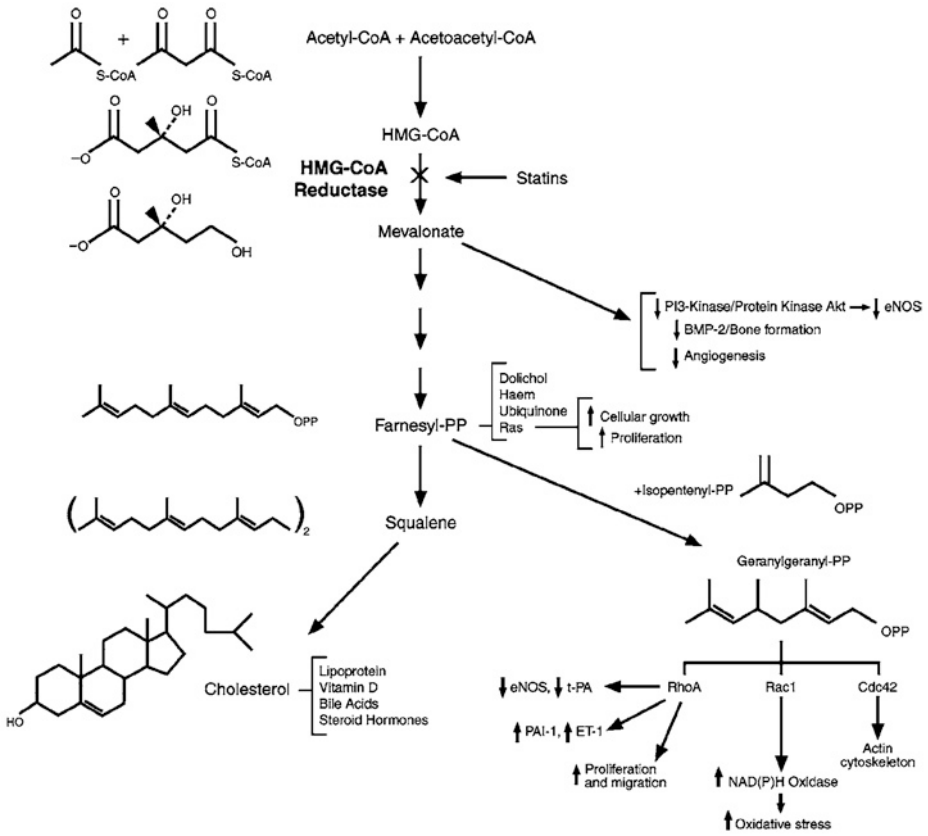

Figure 6. Pathway of cholesterol synthesis. The statin-mediated inhibition in the cholesterol biosynthetic pathway (catalyzation of HMG-CoA to mevalonate) leads in turn to the inhibition of isoprenoid intermediates. A decrease in isoprenylation could decrease activity of small GTPases such as Ras, Rho, and Rac, what leads to modulation of various signaling pathways. BMP-2: bone morphogenetic protein-2; eNOS: endothelial nitric oxide synthase; t-PA: tissue-type plasminogen activator; ET-1: endothelin-1; PAI-1: plasminogen activator inhibitor-1 (adapted from (Liao and Laufs, 2005)).

2.7.2 Diuretics

Thiazides are diuretics. Paradoxically, patients suffering from NDI are often treated with thiazides to decrease urine volume (Kim et al., 2004). The mechanism underlining this paradoxical effect most likely includes the reabsorption of sodium and chloride in the distal collecting duct which is facilitated by AVP, and thus increased osmolality of the urine (Bockenhauer and Bichet, 2014).

Hydrochlorothiazide (HCTZ) combined with amiloride is the main therapy in patients with lithium-induced NDI (Sinke et al., 2014). Treatment with thiazides is associated with the potential risks related to the decreased glomerular filtration rate that causes a reduced excretion of lithium, resulting in lithium intoxication. However, amiloride interferes with lithium uptake through epithelial sodium channels, and that is the reason for combining both drugs (Kishore et al., 2015). A combination of HCTZ with indomethacin reduces the volume of the

urine output more effectively than the administration of thiazide diuretic alone (Kortenoeven and Fenton, 2014).

2.7.3 Prostaglandins

It has been proposed that prostaglandins could be effective in the treatment of water balance disorders such as diabetes insipidus. Butaprost improved symptoms of NDI in a rat model by stimulating EP_2 and EP_4 receptors, and subsequently increasing AQP2 trafficking (Gao et al., 2015; Olesen et al., 2011b). In rat models where the V2R was blocked, symptoms of NDI were greatly improved upon the administration of an EP_2 agonist. EP_2 agonists are available for the treatment of dysmenorrhea (Moeller et al., 2013). Moreover, selective EP_4 agonists improved the symptoms of the NDI which developed in V2R gene-deficient mice (Bockenhauer and Bichet, 2013). The EP_4 receptor agonist, ONO-AE-329 (ONO) effectively increased urine osmolality and ameliorated polyuria in the X-linked NDI mouse model.
One of the possible strategies for the treatment of NDI might be the stimulation of EP_2 and/or EP_4, along with blocking of EP_3 (Pearce et al., 2015; Tamma et al., 2003c).
Patients treated with lithium have increased levels of PGE_2 in the urine (Kim et al., 2008). Mice and rats treated with COX-2 inhibitors relieved the lithium-associated polyuria. Indomethacin in lithium-treated mpkCCD cells, blocked the production of prostaglandin (Kortenoeven et al., 2011). Additionally, mice deficient in PGE_2 synthase-1 (mPGES-1) are not prone to develop lithium-associated polyuria (Baggaley et al., 2010; Jia et al., 2009; Kjaersgaard et al., 2014). Still, in clinical praxis, non-steroidal anti-inflammatory drugs (NSAIDs) remain the best option for the treatment of lithium-induced NDI due to their effective inhibition of prostaglandin synthesis (Kortenoeven et al., 2012).

2.7.4 PDE inhibitors

Among phosphodiesterases (PDEs), PDE5, PDE1 and PDE4 are detected in the principal cells of the collecting duct (Dousa, 1999). cGMP activates protein kinase G (PKG), which can phosphorylate AQP2 at Ser256 and induce its redistribution into the plasma membrane. PDE5 hydrolyses cGMP and thereby prevents cGMP/protein kinase G (PKG) signalling.
One of the PDE5 inhibitors, sildenafil (Viagra), is widely used for the treatment of erectile dysfunction, and has found its place as a therapeutic agent for pulmonary hypertension and subarachnoid hemorrhage. By the activating NO/cGMP pathway, sildenafil causes AQP2 plasma membrane accumulation in LLC-PK_1 (Bouley et al., 2000). Sodium nitroprusside (SNP,

NO donor), L-arginine (a precursor of NO), and atrial natriuretic factor (ANF) induce plasma membrane accumulation of AQP2 *in vitro*, and ANF also *in vivo* (Brown et al., 2012). Mice deficient in NO synthase isoforms can develop NDI (Morishita et al., 2005). PDE5 inhibitors in combination with ANP cause natriuresis and decreased urine output (Bouley et al., 2005) (Assadi and Ghane Sharbaf, 2015). Sildenafil increases urine osmolality and decreases urine output independently of AVP, and since it bypasses the V2R/cAMP, sildenafil should be considered as an alternative agent in the treatment of X-linked NDI (Sanches et al., 2012).

The PDE4 family of enzymes (PDE4A, PDE4B, PDE4C and PDE4D) encode more than 20 isozymes (Houslay, 2010; Klussmann, 2015). Rolipram, a pan-inhibitor of the PDE4 family isoforms, enhances the AVP-induced accumulation of cAMP and induces the translocation of AQP2 into the plasma membrane in IMCD cells (Stefan et al., 2007). Rolipram increased urine osmolality in mice suffering from autosomal dominant NDI (Sohara et al., 2006). Despite this, the clinical trial with rolipram failed (Bichet et al., 1990). Rolipram did not reach the market because of its intolerable side effects, mainly nausea and vomiting.

The non-selective inhibitors of PDE4A-D, roflumilast and apremilast, are available on the market. Roflumilast is approved for the treatment of chronic obstructive pulmonary disease (COPD) and apremilast is used in the therapy of psoriatic arthritis (Klussmann, 2015). These new PDE4 inhibitors could be considered as a novel therapy in the treatment of X-linked NDI.

2.7.5 Vaptans

Vaptans, also called aquaretics, comprise a family of V2R antagonists. They include intravenously administered conivaptan and other oral vaptans, such as tolvaptan, lixivaptan, and satavaptan (Narayen and Mandal, 2012). The aquaretic effect is accomplished by an enhanced free-water clearance without the induction of natriuresis, kaliuresis or changes of the glomerular filtration rate (Graziani et al., 2014). They are approved for therapy of hypervolemic (heart failure, hepatic cirrhosis, SIADH) and normovolemic hyponatremia, and since recently tolvaptan was approved for the treatment of autosomal polycystic kidney disease (ADPKD) (Lin et al., 2014).

Tolvaptan is the most widely used vaptan. It selectively inhibits the binding of AVP to the V2R with an almost 2 times greater affinity than AVP (Torres et al., 2011). Patients treated with tolvaptan have increased AQP2 levels in the urine (Sato et al., 2014). Despite better safety profile compared to other vaptans, tolvatan can cause an excessive and detrimental loss of water in both cases heart failure and ADPKD.

2.8 Aim of the thesis

The water channel aquaporin-2 (AQP2) is attracting attention as a potential therapeutic target in the treatment of cardiovascular and renal diseases associated with the aberrant localization, and the increased and decreased levels of AQP2. Defects preventing the insertion of AQP2 into the plasma membrane of renal collecting duct principal cells in response to AVP cause diabetes insipidus, a disease characterized by a severely impaired urine-concentrating ability. *Vice versa*, the presence of elevated AVP levels, as in the syndrome of inappropriate antidiuretic hormone secretion (SIADH), late stage heart failure, or in liver cirrhosis, results in a predominant localization of AQP2 in the plasma membrane and therefore causes excessive water retention (Vukicevic et al., 2016).
A high-throughput screening of 17,700 small molecules yielded 17 modulators for the cAMP-induced translocation of AQP2 into the plasma membrane, amongst them triazolpropenon (Bogum et al., 2013). Triazolpropenon possesses structural similarity to the antimycotic drug fluconazole.

The main focus and aim of this thesis is to elucidate how fluconazole and triazolpropenon affect the localization of AQP2, and also to elucidate the mode of action. Prospectively, identification of how fluconazole and triazolpropenon affect the localization of AQP2 may pave the way to new insights for the treatment of AQP2-induced water disorders, and possibly even to repurposing of fluconazole.

3 MATERIAL AND METHODS

3.1 Material

3.1.1 Equipment and software

Table 1: Equipment

Equipment	Description	Supplier
Basic equipment		
Beckmann Coulter Centrifuge	Large scale centrifuge	Beckmann Coulter GmbH (Krefeld, DE)
Centrifuge Universal 320 R	Centrifuge	Hettich (Tuttlingen, D)
Duomax 1030	Rocker switch	Heidolph Instruments (Schwabach, DE)
ED124S	Analytical balance	Sartorius AG (Göttingen, DE)
Enspire® 2300	Microplate reader	PerkinElmer (Rodgau, DE)
Eppendorf Research pro	Multichannel pipette	Eppendorf AG (Wesseling-Berzdorf, DE)
IKA® MS 3 basic	Small shaker	IKA (Wilmington, US)
MicroCentrifuge 2	Microscale centrifuge	NeoLab (Heidelberg, DE)
Micromat Duo	Microwave	AEG (Nürnberg, DE)
PipetBoy acu IBS	Pipettor	Integra Biosciences/ Ibs (Fernwald, DE)
Pipettes 2,5/ 10/ 20/ 200/ 1000/ 5000 µl	Pipettes	Eppendorf (Hamburg, DE)
PTR 35	Eppi rotator	Gran Instruments Ltd (Cambridgeshire, UK)
RCT standard	Magnetic stirrer	IKA®-Werke GmbH & Co.KG (Staufen, DE)
RS-TR05	Falcon rotor	Phoenix Intruments (Garbsen, DE)
SBC 52	Electronic balance	Scaltec Instruments GmbH (Göttingen, DE)
Seven Easy ™	pH meter	Mettler Toledo (Gießen, DE)
Sonopuls HD 2070	Ultrasound homogeniser	Bandelin electronic GmbH& Co. KG (Berlin, DE)
Thermomixer Compact	Shaking heater	Eppendorf (Hamburg, DE)
Titramax 100	Plate shaking device	Heidolph Instruments (Schwabach, DE)
Cell culture		
Cryo-container 5100-0001	Freezing container	Thermo Fisher Scientific/NALGENE (Bonn, DE)
GFL 1072	Waterbath	Gesellschaft für Labortechnik mbH (Burgwedel, DE)
Incubator CB210	Cell incubator	Binder (Tuttlingen, DE)
Safe 2020	Sterile bench	Thermo Electron LED GmbH (Langenselbold, DE)
Scepter™ 2.0	Cell counting	Merck Millipore (Schwalbach, DE)

Disposal		
6 well plate 92006	6 well cell culture plate	TPP (Trasadingen, CH)
96 Well Microplate 655101	96 well microplate	Greiner bio-one (Solingen, DE)
Cryo-vials E309.1	Cryoconservation of cells	Carl Roth GmbH & Co KG (Karlsruhe, DE)
Filtertop 99505	Filtertop 500 ml	TPP (Trasadingen, CH)
PVDF membranes T830.1	Western Blotting membranes	Carl Roth GmbH & Co KG (Karlsruhe, DE)
Scepter™ Sensors 60 µM PHCC60050	Cell counting	Merck Millipore (Schwalbach, DE)
T75 cell culture flask	Cell culture flask	TPP (Trasadingen, CH)

Software	**Purpose**	**Vendor/URL**
EndNote X7	Reference manager	endnote.dom
Excel 2011	Spreadsheet	Microsoft (Redmond, US)
GraphPad Prism 5	Statistical analysis	GraphPad Software, Inc. (La Jolla, US)
Illustrator	Graphics, drawing	Adobe Systems, Inc. (San Jose, US)
Image J	Image processing	rsb.info.nih.gov/ij/
Image Studio Ver 2.0	Western Blot analysis	LI-COR Biosciences (Bad-Homburg, DE)
Photoshop	Image processing	Adobe Systems, Inc. (San Jose, US)
Power Point	Presentations	Microsoft (Redmond, US)
ZEN 2011	Confocal microscopy, image acquisition and analysis	Carl Zeiss MicroImaging GmbH (Jena, DE)
Word 2011	Word processing	Microsoft (Redmond, US)

3.1.2 Antibodies

Table 2: Antibodies used for Western blotting (WB) or Immunofluorescence (IF)

Primary antibody	**Origin**	**Supplier**
Aquaporin-2 (AQP2) (C17) (WB)	Goat	Santa Cruz; #9882
AQP2 H27 (IF)	Rabbit	Custom-made (Kenan Maric et al., 1998)
AQP2-pSer256	Rabbit	Abcam; #ab111346
AQP2-pSer261	Rabbit	Abcam; #ab110418
AQP2-Ser269	Rabit	Eurogenetic ZDE12148_0783
CYP51A1	Goat	Santa Cruz; #sc-160263
HSP90	Mouse	Stressgen (Victoria, CA); #SPA-830
Pan-Cadherin	Mouse	Abcam; #ab6528
RhoA	Mouse	Santa Cruz; #sc-418
CYP3A	Mouse	Santa Cruz; #sc-365415
Cofilin	Rabbit	Cell signaling 5175# D3F9
LIMK1	Rabbit	Santa Cruz; #sc-5576

Primary antibody	Origin	Supplier
Myosin light chain 2	Rabbit	Cell signaling #3672
P-cofilin (Ser3)	Rabbit	Cell signaling 3313# 77G2
P-LIMK1/2 (Thr508/505)	Rabbit	Santa Cruz; #sc-28409
P-myosin light chain 2 (Ser19)	Rabbit	Cell signaling #3671
Rab3a	Rabbit	Synaptic system 1071111
Rab5	Rabbit	Abcam; 18211
P-RhoA (Ser188)	Rabbit	Abcam; 41435
Secondary antibody		
Cy3-anti-Rabbit IgG	Mouse	Jackson ImmunoResearch Laboratories; #211-165-109
Peroxidase (POD)-anti-goat IgG	Donkey	Jackson ImmunoResearch Laboratories; #705-035-147
POD-anti-mouse IgG	Donkey	Jackson ImmunoResearch Laboratories; #715-035-151
POD-F(ab')2-anti-rabbit IgG	Donkey	Jackson ImmunoResearch Laboratories; #711-036-152
CY5-anti-goat IgG	Donkey	Dianova 705-175-147

3.1.3 Chemicals and fluorescent dyes

Table 3: Chemicals and fluorescent dyes

Substance	Supplier; article number (#)
4', 6-Diamidine-2'-phenylindole dihydrochloride (DAPI)	Roche Diagnostics GmbH (Mannheim, DE); #10236276001
Alexa Fluor 647 Phalloidin	Invitrogen (Darmstadt, DE); #A22287
Complete mini EDTA-free	Roche Diagnostics (Mannheim, DE); #REF0693159001
EZ-Link™ Sulfo-NHS-SS-Biotin (Biotin)	Thermo Fisher Scientific (Bonn, DE); #21328
Forskolin (FSK)	Biaffin GmbH & Co KG Life Sciences Institute (Kassel, DE); #PKE-FORS-050
HyperLadder I (HyperLadder™ 1kp)	BioLine GmbH (Luckenwalde, DE); #BIO33053
HyperLadder II (HyperLadderTM 50bp)	BioLine GmbH (Luckenwalde, DE); #BIO33054
ImmobilonTM Western Chemiluminescent HRP substrate	Merck Millipore (Schwalbach, DE); #WBKLS0500
Immu-MountTM	Thermo Fisher Scientific (Bonn, DE); #99-904-12
PhosSTOP EASY pack	Roche Diagnostics (Mannheim, DE); #REF04906837001
Precision Plus Protein Standard Dual Color	Bio-Rad Laboratories GmbH (München, DE)
Fluconazole infusion	B.Braun, Melsungen AG
SpectraTM Multicolor High Range Protein Ladder	Thermo Fisher Scientific (Bonn, DE); #26625
Streptavidin agarose beads	Invitrogen (Darmstadt, DE), #15942-050
Tolvaptan tablets	Otsuka Phamaceutical Co.,Ltd
Coomassie PlusTM Protein Assay Reagent	Thermo Fisher Scientific (Bonn, DE); #1856210

Table 4: Buffers and solutions

Buffer/solution	Composition
Biotinylation buffer	500 µg Biotin (Table 3) per well; 10 mM triethanolamine; 150 mM NaCl; 1 mM $MgCl_2$; 0.1 mM $CaCl_2$; pH 8.0
Bio Quenching buffer	50 mM NH_4Cl in PBS
Bio Lysis buffer 1	SLB; 0.5 % Triton X-100; 0.2 % BSA; Complete mini EDTA-free (Table 3)
Bio Lysis buffer 2	SLB; 0.5 % Triton X-100; Complete mini EDTA-free (Table 3)
Blocking buffer (IF)	1x PBS; 0.27 % fish skin gelatine
Blocking buffer (Western blot)	1x TBS-T; 3 % bovine serum albumine (BSA)
Lysis buffer	SLB; PhosSTOP EASY (Table 3); Complete mini EDTA-free (Table 3)
Phosphate-buffered saline (PBS)	137 mM NaCl; 2.7 mM KCl; 1.5 mM KH_2PO_4; 8.1 mM Na_2HPO_4; pH 7.4
Rhotekin lysis buffer	50 mM Tris, pH 7.2; 1 % (w/v) Triton X-100 ; 0.5 % sodium deoxycholate; 500 mM NaCl; 10 mm $MgCl_2$; PhosSTOP EASY (Table 3), Complete mini EDTA-free (Table 3)
Sample buffer	40 % glycerine; 8 % SDS; 0.4 % bromophenol blue; 312.5 mM Tris-HCl; 200 mM DTT; pH 6.8
SDS-polyacrylamide gel electrophoresis (PAGE) running buffer	25 mM Tris; 192 mM glycine; 0.1 % SDS
Separating gel buffer (SDS-PAGE)	0.625 M Tris-HCl; pH 6.8
Standard lysis buffer (SLB)	10 mM K_2HPO_4; 150 mM NaCl; 5 mM EDTA; 5 mM EGTA; 0.5 % Triton X-100; pH 7.4; 0.2 % sodium deoxycholate
Stacking gel buffer (SDS-PAGE)	0.75 M Tris-HCl; pH 8.8
Tank blot buffer	20 mM Tris; 150 mM glycin; 10 % methanol, 0.02 % SDS
TBS + Tween (TBS-T)	1x TBS; 0.05 % Tween-20
Tris-acetate-EDTA (TAE) buffer	40 mM Tris; 1 mM EDTA; 1.14 % (v/v) glacial acetic acid
Tris-buffered saline (TBS)	10 mM Tris-HCl, pH 7.4; 150 mM NaCl
Trypsin-EDTA	Biohrom AG (Berlin, DE); #L2153

3.1.4 Eukaryotic cells

Table 5: Eukaryotic cell lines and primary cells

Cell lines	Description	Culture medium	Supplier, article number (#)
MCD4	Mouse collecting duct cell line, stably expressing human AQP2 (Iolascon et al., 2007)	DMEM/F-12-GlutaMAX ™ (Life Technologies GmbH, Darmstadt, DE; #31331028); 5 % FCS, 5 µM dexamethasone	G. Valenti, Dipartimento di Fisiologa Generale ed Ambientale, (Bari, IT)
Primary cells			
IMCD	Inner medullary collecting duct cells from rats	DMEM- GlutaMAX™ (Life Technologies GmbH, Darmstadt, DE; #21885108); 1 % non-essential amino acids (Biochrom AG; Berlin, DE; #C2-22;) 1 %	Primary cells; made inhouse (Faust et al., 2013; K. Maric et al., 1998)

Cell lines	Description	Culture medium	Supplier, article number (#)
		ultroser G (Cytogen GmbH, Sinn, DE; #15950-017); 500 µM DBcAMP, 20 U/ml nystatin (Sigma Aldrich; #N4014); 0.25 µg/ml gentamicin (Life Technologies GmbH (Darmstadt, DE; #15710); 4.5 g/l glucose; 100 mM NaCl; 100 mM urea	

3.2 Methods

3.2.1 Animal experimental work

Wild type mice BALB/C6 were housed and maintained according recommendations of the Federation of European Laboratory Animal Science Associations (FELASA) in a specific pathogen-free environment in the animal facilities of the Max-Delbrück-Zentrum für Molekulare Medizin (MDC) in Berlin-Buch. All procedures were carried out in accordance with ethical guidelines of the Landesamt für Gesundheit und Soziales (LaGeSo), Berlin. Fluconazole and tolvaptan analysis were approved by license. Mice were water-deprived for 24 h in metabolic cages. Seven-week old mice were sacrificed by cervical dislocation and kidneys were harvested.

3.2.2 Cell and tissue lysis

Confluent eukaryotic cells were washed twice with ice-cold PBS and covered with lysis buffer. In a 1.5 ml reaction tube, cells were disrupted by eight ultrasound impulses (65 % amplitude) at 4 °C, using Sonoplus HD 2070. Isolated inner medullae from mice or whole kidneys were homogenized with douncer or plastic pistil in lysis buffer. Lysates were centrifuged at 14,000 g for 45 min at 4 °C. Cell debris was removed and supernatant was used for Bradford assays and Western blotting analysis.

3.2.3 Bradford assay

Coomassie Plus Bradford protein assay (Table 3) was used to determine the concentration of proteins in cells lysates according to the manufacturer`s protocol. The color change from brown to blue is due to the binding of proteins to Comassie in an acidic system and represents a colorimetric method. Measured is the absorption maximum shift from 465 nm to 595 nm. Sample lysate of 5 µl of or protein standards (defined concentration of 0.125 - 2 mg/ml) was added per well in a 96 well microplate and 250 µl Coomassie PlusTM Protein Assay Reagent was mixed and incubated for 10 min at room temperature in the dark. Absorbance at 595 nm was

measured using the Enspire®2300 microplate reader. According to the readout of the standards, protein concentration of samples was determined. Lysates were adjusted to the desired concentrations by addition of appropriate lysis buffer.

3.2.4 Western blotting

Protein samples were denatured for 5 min at 95°C, separated by SDS-PAGE, and transferred from the polyacrylamide gel to polyvinylidene fluoride (PVDF) membranes using TankBlot (110 V for 120 min) and Tank blot buffer. Membranes were blocked for 60 min at room temperature (1 % BSA in TBS-T as blocking buffer for cells and 3 % in TBS-T as blocking buffer for inner medullae and kidney lysates) and agitated with primary antibody diluted in blocking buffer at 4 °C overnight. Membranes were washed 3x 10 min in TBS-T and incubated with peroxidase (POD)-labelled secondary antibodies, diluted in blocking buffer, for 60 min at room temperature. Membranes were washed 3x 10 min in TBS-T, and proteins were detected by Immobilon® Western Chemiluminescent HRP substrate (Table 3). Signals were visualized using the Odyssey Imager. Image processing and densitometric analysis was performed with the Image Studio Lite Ver. 5.2.5.

3.2.5 Rhotekin-pulldown assay

After treatment of IMCD cells or mice, the homogenized IMCD cells or inner medullae from mice were incubated for 10 min in Rhotekin lysis buffer at 4 °C, and scraped into a 1.5 ml tubes. Cell debris was removed by centrifugation (5 min, 15,000x g, 4 °C). The supernatant was incubated with 400 µl of Rho binding domain (RBD) beads (provided by Bärbel Pohl (MDC)) for 1 h at 4 °C, with a gentle agitation (Klussmann et al., 2001; Sander et al., 1999; Tamma et al., 2001). Beads were washed 3x with Rhotekin lysis buffer without disturbing the beads pellets, resuspended in sample buffer and analysed by SDS-PAGE. RhoA from the pulldown (PD) fraction was related to the input of RhoA, which was related to the loading of input (HSP90).

3.2.6 Immunofluorescence microscopy

IMCD or MCD4 cells were grown on 12 mm diameter cover slides. Medium was aspirated and the cells were fixed with 10 % trichloroacetic acid (TCA) for 10 min at room temperature. Cells were washed three times with 1x PBS and were permeabilised with 0.1 % Triton X-100 for 5 min at room temperature. Unspecific binding was inhibited by blocking with fish skin gelatin (0.27 %) for 60 min at 37 °C. Cells were incubated with a anti-AQP2 antibody H27 (1:300

dilution of H27, stored in glycerol 1:1; resulting in a final dilution of 1:600) for 45 min at 37 °C, and washed three times with 1x PBS. Cells were incubated with a secondary anti-rabbit antibody (1:300), 1x DAPI and Alexa Fluor 647-Phalloidin for 45 min at 37 °C and finally were washed with 1x PBS three times. Using Immu-MountTM, cells were fixed on microscope slides and stored at 4°C overnight.

3.2.7 Preparation of paraffin-embedded kidney sections

Tissues were fixed in PBS containing 4 % paraformaldehyde for 1 h at 4°C, dehydrated and embedded in Tissue-Tek O.C.T. Compound (Sakura Finetek) for cryosectioning. Primary antibodies were incubated overnight at 4 °C.

3.2.8 Laser scanning microscope LSM 780

Mounted cell slides and tissue sections were analyzed with a Laser Scanning Microscope (LSM) 780 confocal laser scanning microscope at 63x magnification. Three channels were recorded: DAPI, using a 405 nm laser and filter for 415-495 nm, Cy3, using a 561 nm laser and filter for 566-631 nm and Alexa Fluor 647-Phalloidin using a 633 nm laser and filter for 638-740 nm. Pinholes were set to 40-70 µm, digital gain remained 1.00 and master gain was adjusted to approximately 650 for all channels.

3.2.9 Bitionylation of the cell surface proteins

The assay was performed as previously published (Bogum et al., 2013). Cells were washed twice with ice-cold PBS (without Ca and Mg salts) and were incubated with biotinlyation buffer for 60 min at 4 °C. After two washing steps with biotinylation buffer, cells were incubated for 10 min with biotinylation quenching buffer at 4 °C to remove the unbound biotin. Lysates were prepared using biotinylation lysis buffer 1. Lysates were sonicated and incubated for 20 min at 37 °C. Cell debris was removed by centrifugation (30 min, 15,000x g, 4 °C). Lysates were incubated with 80 µl washed streptavidin agarose beads at 4 °C overnight. Beads were washed 3x with biotinylation lysis buffer 1 and 2. Proteins were eluted using sample buffer, denaturated, and analyzed by SDS-PAGE.

3.2.10 Phosphatase activity assay

For para-Nitrophenylphosphate (pNPP)-based evaluation, cells were lysed in lysis buffer without phosphatase inhibitors, and aliquot in amount of 100 µg in triplicates were diluted in Colorimetric Assay Buffer (containing 10 mM pNPP) as described previously (McAvoy and

Nairn, 2010). After 30 min of incubation at 30 °C, the absorbance was determined at 405 nm with an xMark™Microplate Absorbance Spectrophotometer (Bio-Rad, Hercules, USA), and phosphatase activity was then calculated.

3.2.11 PKA activity assay

The PKA activity assay is based on phosphorylation of a PKA substrate peptide (PepTag A1 peptide). By addition of the phosphate group, the peptide obtains a negative charge compared to a positive one before the reaction, and can thus be separated from the non-phosphorylated peptide by an agarose gel electrophoresis. The peptide substrate is labelled fluorescently. The PKA activity assay was conducted according to the manufacturer's protocol and as previously published (Bogum et al., 2013). Medium was removed and lysates were prepared. PepTag A1 peptide (56 ng/µl) was incubated with 15 µl of cleared supernatant in PepTag PKA reaction buffer (final volume 25 µl) at 30 °C for 10 min. Samples were denatured for 10 min at 95 °C. Peptides were separated by 0.8 % agarose gel electrophoresis. Images were taken with the Lumi Imager F1 and bands were analyzed densitometrically.

3.2.12 Cell culture

3.2.12.1 Culturing of rat primary inner medullary collecting duct (IMCD) cells

IMCD cells were prepared as described previously (Faust et al., 2013). In brief, 10 to 12 weeks old rats (Wistar Han, Charles River Laboratories International, Inc., Sulzfeld, DE) were anesthetised and decapitated. Inner medullae were dissected and digested enzymatically with hyaluronidase and collagenase. Cells were resuspended in fully supplemented medium (Table 5) and seeded in collagen type IV (BD Biosciences, Heidelberg, DE; #356233)-coated dishes. 24 h before starting the experiment, cells were incubated in a medium without dbcAMP and nystatin in order to increase the perinuclear location of AQP2.

3.2.12.2 Culturing of mammalian cells

MCD4 cells were grown in appropriate medium (Table 5). When confluent, cells were washed with ice-cold PBS and detached with 1x Trypsin-EDTA for 5 min at 37 °C. Trypsinization was stopped by serum-containing medium. A defined volume of cell suspension was transferred into a new cell culture flask with freshly added medium. By repeating the process the cell passage increased by factor of one.

3.2.12.3 Cell counting

Cells were detached from plastic surfaces of culture dishes by trypsinization. The cell suspension was diluted 1:10 in a 1.5 ml reaction tube using PBS. Using the ScepterTM 2.0 pipette with 60 µM tips, cells of 9-21 µM size were counted.

3.2.12.4 Freezing and thawing of mammalian cells lines

When confluent, MCD4 cells were trypsinized and centrifuged (2 min, 300x g, room temperature). The pellet was resuspended in 3 ml of appropriate medium (Table 5) (T75 cell culture flask). The equal volume of FCS containing 20 % DMSO was added. The cell suspension was aliquoted in 3x 2 ml vials, which were stored at -80 °C in a Cryo-container to achieve a cooling rate of 1 °C/min. After a minimum of 3 h, the cell-containing vials were transferred to liquid nitrogen.
To re-culture cells, frozen vials were thawed by slight agitation in a water bath at 37 °C. With a sterile Pasteur pipette, cells of one vial were slowly transferred into a T75 cell culture flask, containing 15 ml medium. After 2-4 days cells were grown confluent.

3.3 Statistical analysis

GraphPad Prism 7 was used to perform statistical analysis. Unpaired t-test or one-way ANOVA with posthoc Bonferonni were applied. Significant differences are indicated as $p \leq 0.05$ = *, $p \leq 0.01$ = **, $p \leq 0.001$ = ***, $p \leq 0.0001$ = ****. Mean plus standard error of mean (SEM) are plotted.

4 RESULTS

4.1 Fluconazole promotes the AQP2 redistribution to the plasma membrane in primary IMCD cells

4.1.1 Fluconazole induces redistribution of AQP2

In mouse collecting duct cells stably expressing human AQP2 (MCD4 cells) and resting primary cultured rat inner medullary collecting duct (IMCD) cells AQP2, is located mainly intracellularly. Forskolin (FSK) mimicks the effect of AVP by elevating cAMP levels. In the presence of FSK, AQP2 redistributes from a mainly perinuclear location to the plasma membrane (Faust et al., 2013).

In a high-throughput screening of 17,700 small molecules 17 inhibitors of the cAMP-induced translocation of AQP2 into the plasma membrane were identified, amongst them triazolpropenon (Bogum et al., 2013). Despite promising inhibitory effect observed in MCD4 and IMCD cells (see 4.3), triazolpropenon in concentration of 34 µM was close to its 50 % lethal concentration.
Fluconazole possesses a structural similarity to triazolpropenon. Both substances contain triazole rings and both are commercially available. Fluconazole is registered as a drug and is widely used in clinical praxis for the treatment of fungal infections.

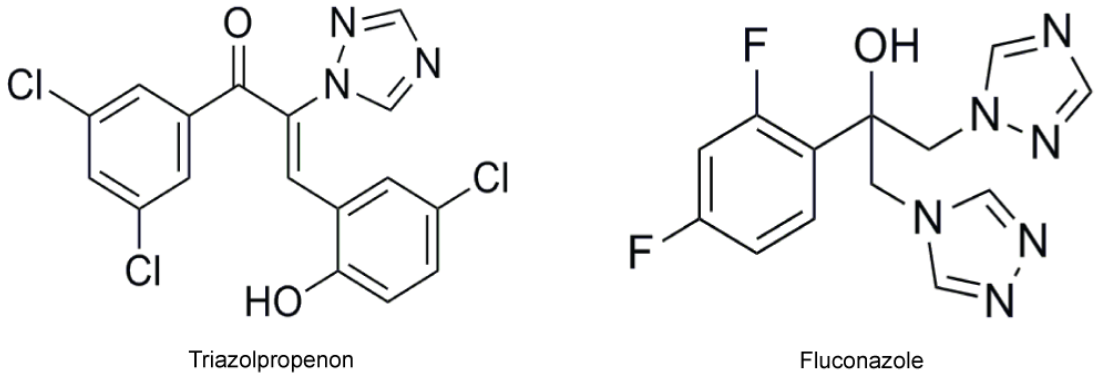

Figure 7. Triazolpropenon and fluconazole have structural similarity due to the triazole ring.

Although it has a structural similarity to triazolpropenon (Figure 7), fluconazole has an opposite effect on the localization of AQP2. To evaluate the localization of AQP2 at the plasma membrane, immunofluorescence images were analysed and fluorescence signal

intensity arising from AQP2 was expressed as the ratio of fluorescence signal intensity at the plasma membrane to intracellular signal intensity. Immunofluorescence microscopic images showed that fluconazole induces an AVP-independent AQP2 translocation to the plasma membrane. Since a similar additive effect is observed with AVP and also with FSK (Figure 8) in immunofluorescence microscopic images and in quantification of these images, further experiments were performed, in combination with FSK, in order to achieve supra-physiological PKA activity in IMCD cells *via* direct activation of adenylyl cyclase (Faust et al., 2013).

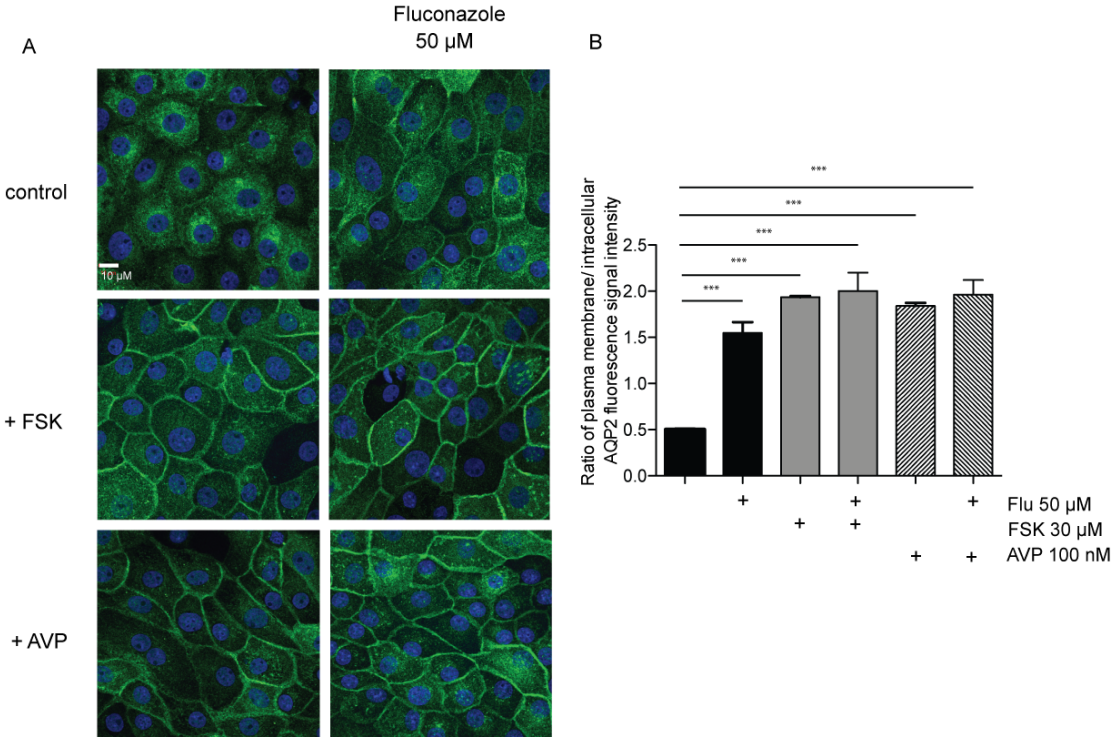

Figure 8. Fluconazole (Flu) induces the redistribution of AQP2 from intracellular vesicles to the plasma membrane in IMCD cells. IMCD cells were left untreated (control) or stimulated with forskolin (FSK 30 µM, 30 minutes) or with AVP (100 nM, 30 minutes) or with fluconazole (50 µM) alone or in combination with forskolin or AVP for 1 h. A) AQP2 was detected by immunofluorescence microscopy using specific primary antibodies (H27) and Cy3-coupled anti-rabbit secondary antibodies (green). Nuclei were stained with DAPI (blue). Shown are representative images from one of three independent experiments. B) The intensities of intracellular and plasma membrane immunofluorescence signals arising from AQP2 were determined and related to perinuclear signal intensities (mean ± SEM; three independent experiments). The ratios of plasma membrane to intracellular fluorescence signal intensities were calculated. Ratios < 1 indicate a predominant intracellular localization, ratios > 1 a predominant plasma membrane location of AQP2. Values significantly different from FSK and AVP-treated cells are indicated (mean± SEM, ***p<0.001).

As an independent biochemical approach, cell-surface biotinylation assays were used to quantify the effect of fluconazole on the AQP2 plasma membrane localization. Biotinylation is a method for the quantification of the AQP2 abundance and it shows a portion of AQP2 inserted into the plasma membrane (Bogum et al., 2013). Cell-surface proteins were biotinylated and precipitated with streptavidin-agarose beads. As expected, in FSK stimulated IMCD cells, the AQP2 abundance in the plasma membrane

was increased when compared to basal condition. IMCD cells were treated with fluconazole (10 μM and 50 μM) alone and in combination with FSK. Bands representing complex glycosylated (cg), high mannose glycosylated (hm) and non-glycosylated (ng) of AQP2 were observed. Densitometric analysis confirmed that fluconazole (50 μM), in combination with FSK significantly increases the abundance of AQP2 in the plasma membrane compared to the FSK-treated controls (Figure 9). Fluconazole alone did not alter the plasma membrane abundance although immunofluorescence analysis showed an increase of AQP2 at the plasma membrane. Since the biotinylation method detects biotinylated proteins only at the surface of the cell, it appears that the fraction of AQP2 present in the plasma membrane is below the detection level as in mice fluconazole AQP2 was inserted into the plasma membrane (Figure 19).

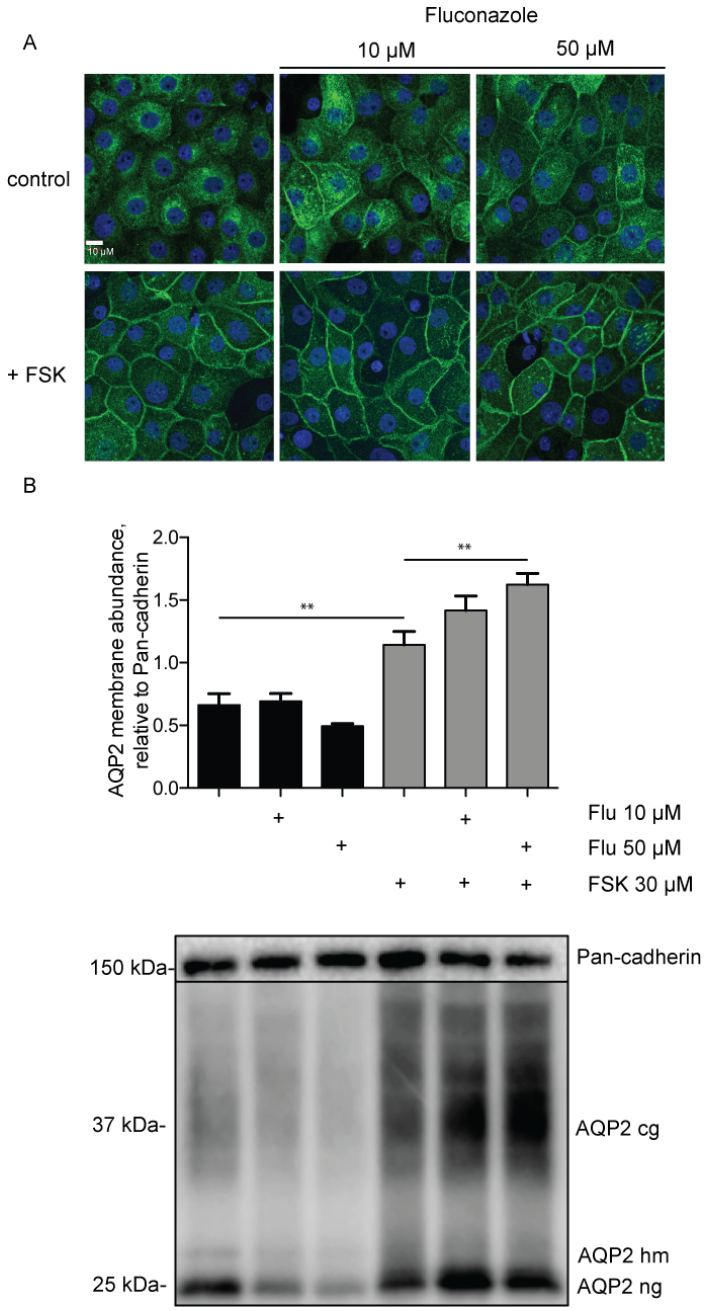

Figure 9. Fluconazole (Flu) exhibits enhanced effect of forskolin (FSK) on AQP2 insertion into the plasma membrane in IMCD cells. IMCD cells were left untreated or stimulated with forskolin (30 µM, 30 minutes), or with fluconazole alone in indicated concentrations or in combination with forskolin for 1 h. A) AQP2 was detected by immunofluorescence microscopy using specific primary antibodies (H27) and Cy3-coupled anti-rabbit secondary antibodies (green). Nuclei were stained with DAPI (blue). Shown are representative images from one of three independent experiments. B) Lower panel. Cell-surface biotinylation assays were carried out to quantify the effect of fluconazole on the localization of AQP2 into the plasma membrane. In order to detect AQP2 on the surface of the cells, surface proteins were precipitated with streptavidin agarose beads. AQP2 and Pan-cadherin as loading control were detected by Western blotting (five independent experiments). Upper panel. The signals emerging from the complex glycosylated (cg), high manose (hm) and non-glycosylated (ng) forms of AQP2 were semi-quantitative analysed and the sums statistically compared. Statistically significant differences are indicated (mean± SEM, **p<0.01).

4.1.2 Fluconazole increases AQP2 abundance and modulates critical phosphorylations of AQP2 in IMCD cells

To elucidate the molecular mechanisms underlying the fluconazole-induced AQP2 trafficking, the cAMP/PKA signaling pathway was investigated. As previously showed, FSK increases the AQP2 abundance compared to the basal state. Fluconazole alone also increases the level of AQP2 abundance (Figure 10-under A). The phosphorylation of Ser256 increases in response to FSK and fluconazole (Figure 10-under B). Since fluconazole increases the phosphorylation of Ser256 and the amount of phosphorylated AQP2 is related to increased AQP2 abundance, this yields an unchanged ratio. In other words, the higher the AQP2 abundance the more AQP2 would be phosphorylated. This goes along with data obtained from immunofluorescence microscopic analysis.

Fluconazole (10 μM and 50 μM) significantly decreases the phosphorylation at Ser261 of AQP2, related to both total AQP2 and to HSP90, compared to basal levels. This is in line with the redistribution of AQP2 towards the plasma membrane. As expected, upon stimulation with FSK alone, or in combination with fluconazole (10 μM and 50 μM) the phosphorylation at Ser261 is decreased compared to the untreated control (Figure 10-under C).

FSK increases the phosphorylation at Ser269 of AQP2. Fluconazole alone has a trend towards the increase in phosphorylation of Ser269. However, this is not statistically significant when related to both AQP2 abundance and to HSP90. Fluconazole (50 μM) in the presence of FSK markedly increases the phosphorylation at Ser269 of AQP2 compared to basal condition and to FSK as well (Figure 10-under D).

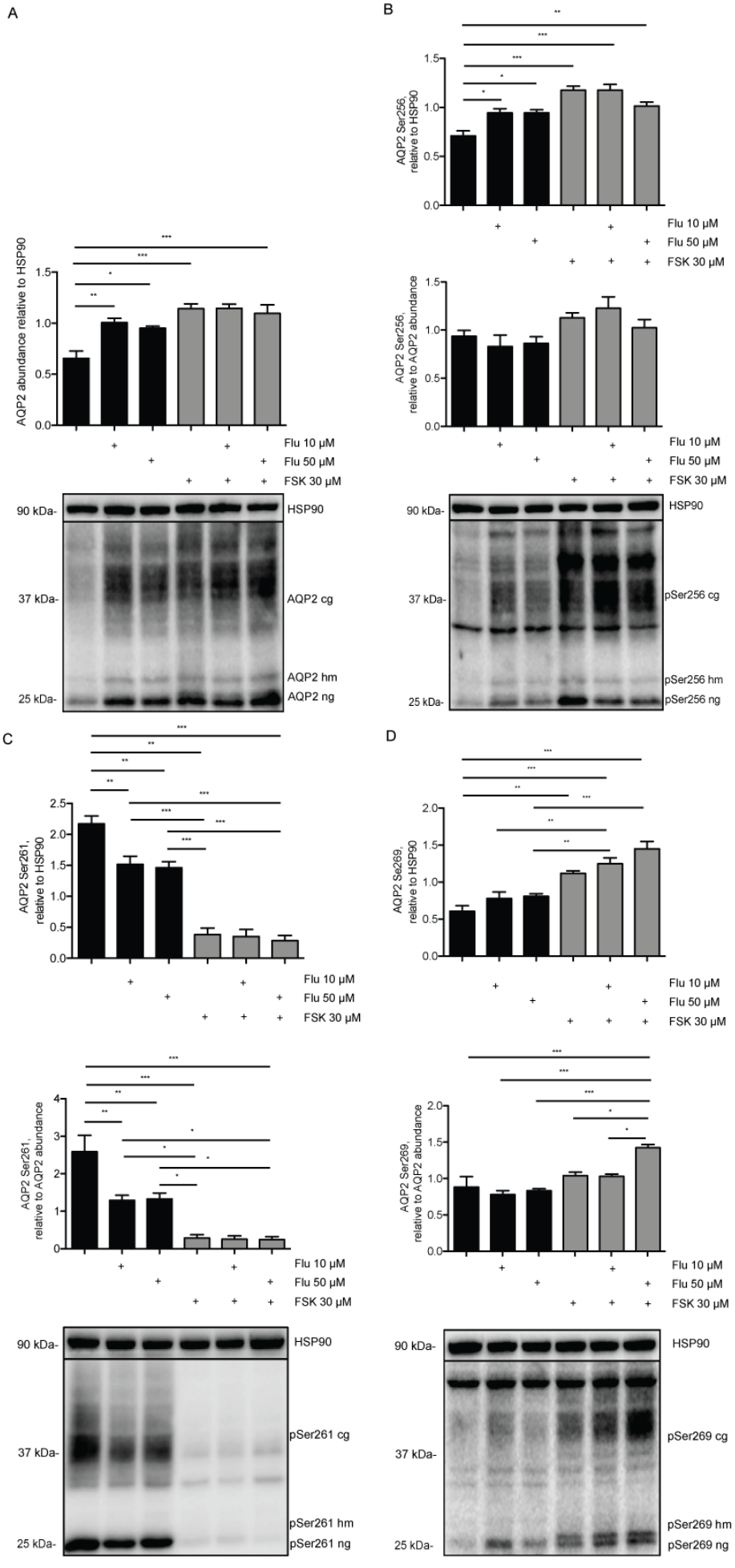
A
AQP2 abundance relative to HSP90
Flu 10 µM
Flu 50 µM
FSK 30 µM
90 kDa-
HSP90
37 kDa-
AQP2 cg
AQP2 hm
25 kDa-
AQP2 ng
B
AQP2 Ser256, relative to HSP90
AQP2 Ser256, relative to AQP2 abundance
pSer256 cg
pSer256 hm
pSer256 ng
C
AQP2 Ser261, relative to HSP90
AQP2 Ser261, relative to AQP2 abundance
pSer261 cg
pSer261 hm
pSer261 ng
D
AQP2 Se269, relative to HSP90
AQP2 Ser269, relative to AQP2 abundance
pSer269 cg
pSer269 hm
pSer269 ng

Figure 10. Fluconazole (Flu) increases AQP2 abundance and changes phosphorylation status of AQP2 in IMCD cells. IMCD cells were left untreated or stimulated with forskolin (FSK 30 µM, 30 minutes), or with fluconazole alone in indicated concentrations or in combination with forskolin for 1 h. Lower panels. Lysates were prepared and proteins were separated with SDS-PAGE. A) AQP2 B) pSer256-AQP2 C) pSer261-AQP2 D) pSer269-AQP2 and HSP90 as loading control for all blots were detected by Western blotting. Shown are representative blots from one of four independent experiments. Upper panels. The signals emerging from the complex glycosylated (cg), high manose (hm) and non-glycosylated (ng) forms of AQP2 were semi-quantitative analysed and the sums statistically compared. Statistically significant differences are indicated (mean± SEM, *p<0.05; **p<0.01; ***p<0.001).

4.1.3 Fluconazole promotes the AQP2 redistribution without globally affecting PKA and phosphatase activity

To gain insight into the effects of fluconazole on the PKA signaling pathway, a potential influence of fluconazole on global PKA activity was assessed (Figure 11) with a PKA assay (Bogum et al., 2013). In this assay the ability of PKA to phosphorylate a substrate peptide PepTag A1 is determined. After treatment of cells with the compounds of interest, PKA activity is compared with the amounts of phosphorylated peptides. Addition of a cAMP-solution to each sample, as a positive control, showed the maximum PKA activity that can be achieved in a given sample, hence representing the total amount of PKA present. As expected, FSK alone increases global PKA activity compared to basal state. Fluconazole alone did not affect global PKA activity.

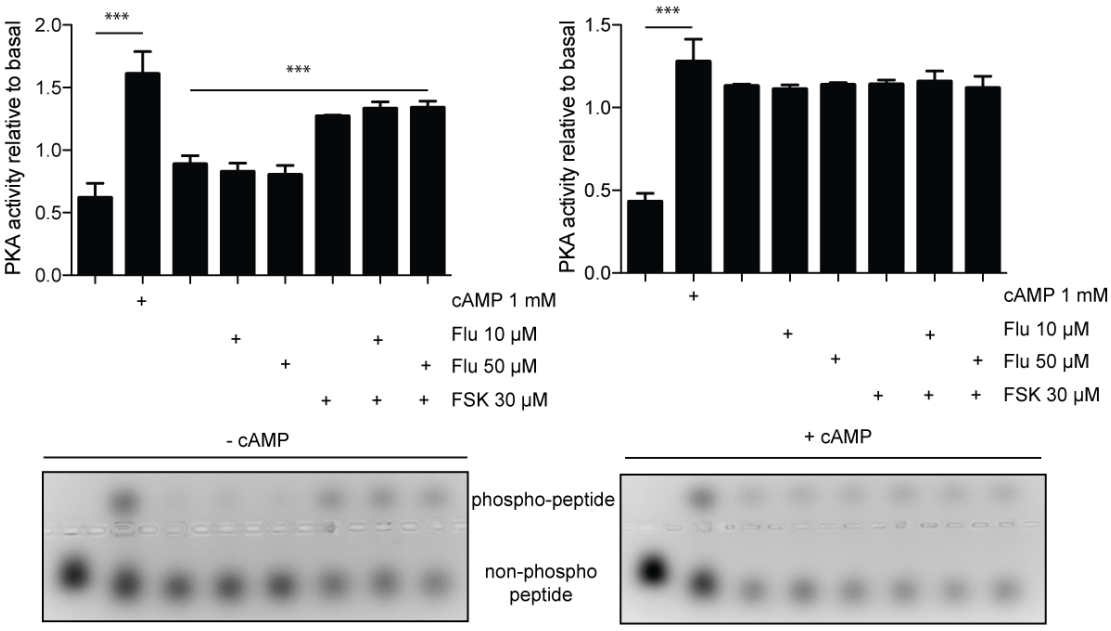

Figure 11. Fluconazole (Flu) does not affect global PKA activity in IMCD cells. IMCD cells were left untreated or stimulated with forskolin (FSK 30 µM, 30 minutes), or with fluconazole alone in indicated concentrations or in combination with forskolin for 1 h. Lower panels. Cell lysates were prepared and PKA activity was determined by measuring its ability to phosphorylate the substrate peptide PepTag A1. In positive controls and where indicated cAMP (1 mM) was added to induce maximal PKA activity. PKA activity is expressed as the ratio of phosphorylated to non-phosphorylated PepTag A1 peptides. Agarose gels from one of three representative experiments show PKA-phosphorylated and non-phosphorylated PepTag A1

peptide. Upper panels. The amounts of phosphorylated and non-phosphorylated PepTag A1 peptides were semi-quantitative analysed. Statistically significant differences are indicated (mean ± SEM, ***p<0.001).

To investigate the potential influence of fluconazole on phosphatase activity, IMCD cells were treated with fluconazole alone (10 μM and 50 μM), and in combination with FSK for 1 h or 24 h (Figure 12). Phosphatase activity is measured by taking advantage of the p-Nitrophenylphosphate (pNPP) solution colorimetric assay as described in (McAvoy and Nairn, 2010). The results indicated that fluconazole does not affect global phosphatase activity in IMCD cells.

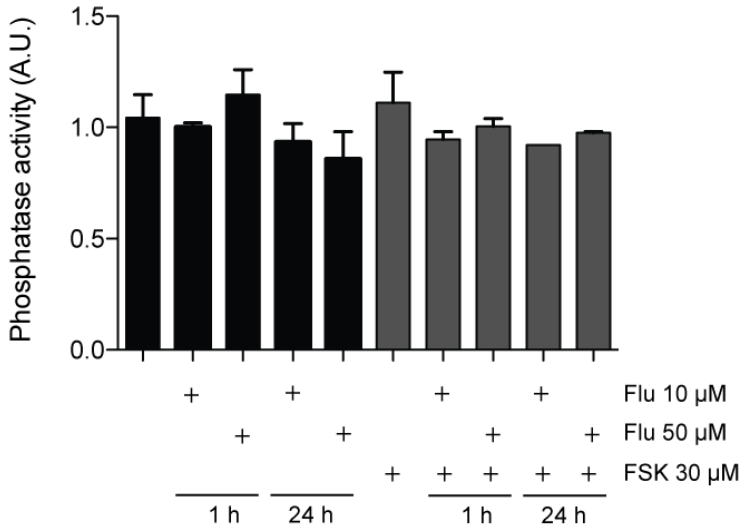

Figure 12. Fluconazole (Flu) does not affect global phosphatase activity in IMCD cells. IMCD cells were left untreated or stimulated with forskolin (FSK 30 μM, 30 minutes), or with fluconazole alone in indicated concentrations or in combination with forskolin for 1 h or 24 h. Lysates were prepared without phosphatase inhibitors and amounts of 100 μg of proteins were loaded (each sample in triplicates in 96-well plate). 10 mM pNPP substrate solution was added to each sample for 30' at 37 °C and absorbance was measured at 405 nm. Samples comprised also the positive control, one negative and one blank, all in triplicates. The molar extinction coefficient for pNPP is 18,000 $M^{-1}cm^{-1}$. The blank was subtracted to account for any phosphate release occurring in the absence of phosphatase. Shown are results from three independent experiments. There are no statistically significant differences (mean ± SEM).

4.1.4 Fluconazole reduces F actin-containing stress fibers in IMCD cells

Similarly to statins, fluconazole could decrease RhoA activity by blocking the conversion of mevalonate to farnezyl-pyrophosphate (FPP). Isoprenoid intermediates such as FPP and geranylgeranyl-PP act as lipid anchors required for membrane tethering and activation of small GTP-ases, amongst them RhoA. Active RhoA controls the cellular localization of AQP2 *via* F-actin cytoskeleton polymerization. Inhibition of RhoA causes depolymerisation of F-actin cytoskeleton.

Thus, it was examined whether fluconazole affects the F-actin cytoskeleton. IMCD cells were treated with fluconazole for 1 h or 24 h, and then stained with phalloidin to detect F-actin (Figure 13). Since it had already been shown that RhoA activity is decreased in IMCD cells upon increased levels of cAMP (Klussmann et al., 2001), FSK served as a control. F-actin-containing stress fibers were reduced upon FSK stimulation compared to the basal conditions, and dot-like structures, most likely, G-actin had appeared.

Fluconazole alone, and in combination with FSK, after 1 h dramatically decreased F-actin-containing stress fibers, as was confirmed by microscopic inspection. Especially in cells treated with fluconazole and stimulated with FSK for 1 h, F-actin-containing stress fibers had almost completely disappeared, including the dotted structures. Fluconazole alone and in combination with FSK had a similar effect on F-actin-containing stress fibers after 24 h.

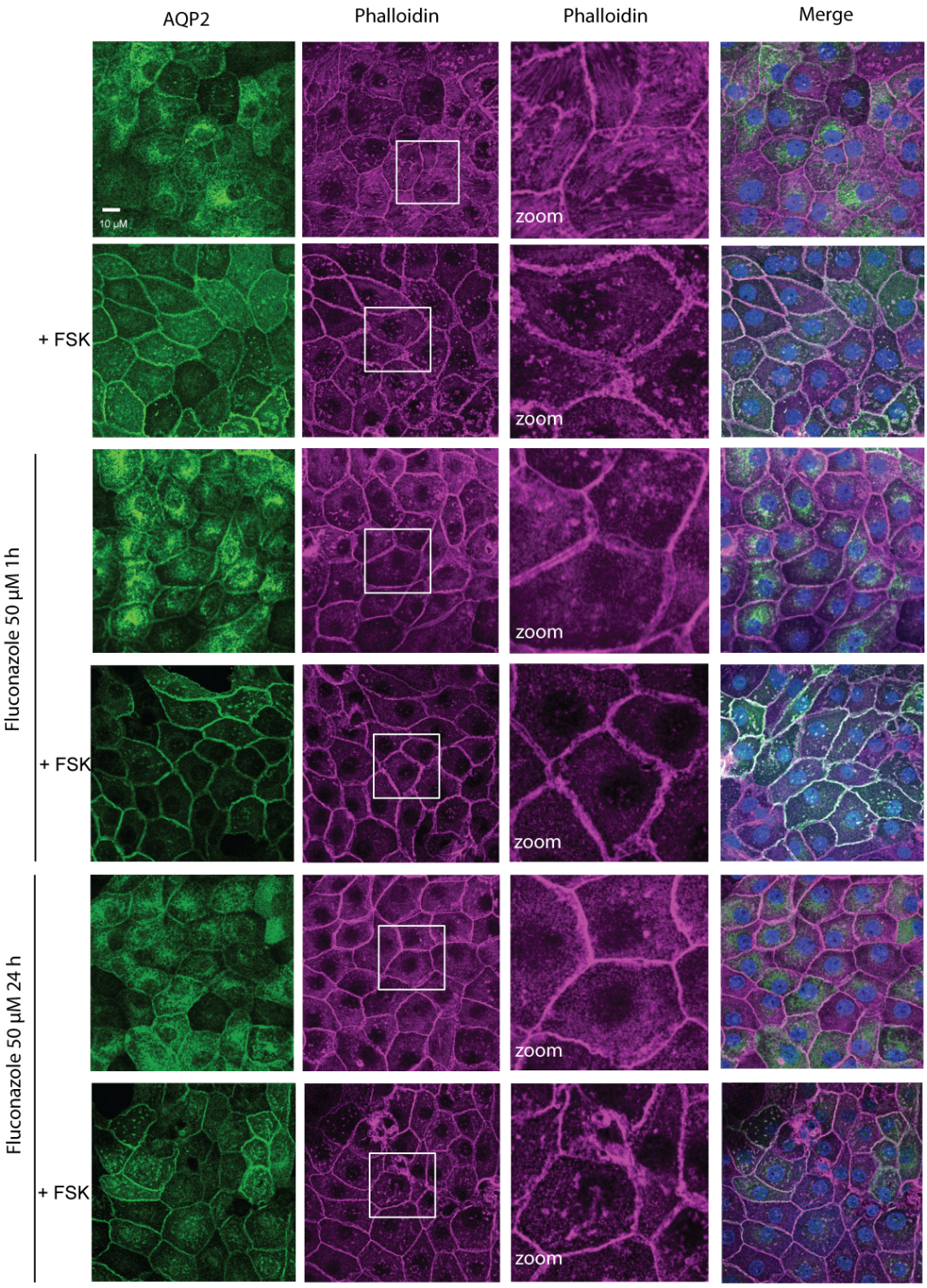

Figure 13. Fluconazole decreases F-actin-containing stress fibers in IMCD cells. IMCD cells were left untreated or stimulated with forskolin (FSK 30 µM, 30 minutes) or with fluconazole (50 µM) alone or in combination with forskolin for 1 h or 24 h. AQP2 was detected by immunofluorescence microscopy using specific primary antibodies (H27) and Cy3-coupled anti-rabbit secondary antibodies (green) and F-actin was detected by using Alexa Fluor 647 Phalloidin (red). Nuclei were stained with DAPI (blue). The magnified views (zoom) of F-actin are from the indicated squares. Shown are representative images from one of three independent experiments.

4.1.5 Fluconazole decreases RhoA activity in IMCD cells

Since active RhoA promotes the formation of F-actin filaments, and after treatment with fluconazole F-actin filaments were disassembled, the next step was to determine the fraction of active RhoA in IMCD cells by using a rhotekin assay. The assay uses the Rho-binding domain (also called the RBD) of the Rho effector, rhotekin. The RBD motif binds specifically to the GTP-bound form of Rho, and was employed for affinity purification of the GTP-Rho from cell lysates. Western blotting was used to compare total RhoA to the GTP-loaded form of the GTPase (Sander et al., 1999). IMCD cells treated with FSK served as a positive control for reduced total RhoA activity (Tamma et al., 2003c). IMCD cells treated with fluconazole (50 µM) showed significantly reduced RhoA activity compared to basal condition (Figure 14). A similar effect was observed in combination with FSK. An additional effect of fluconazole and FSK was not observed. The attenuation of Rho activity would favour depolymerization of the F-actin cytoskeleton and would allow the translocation of AQP2 into the cell membrane.

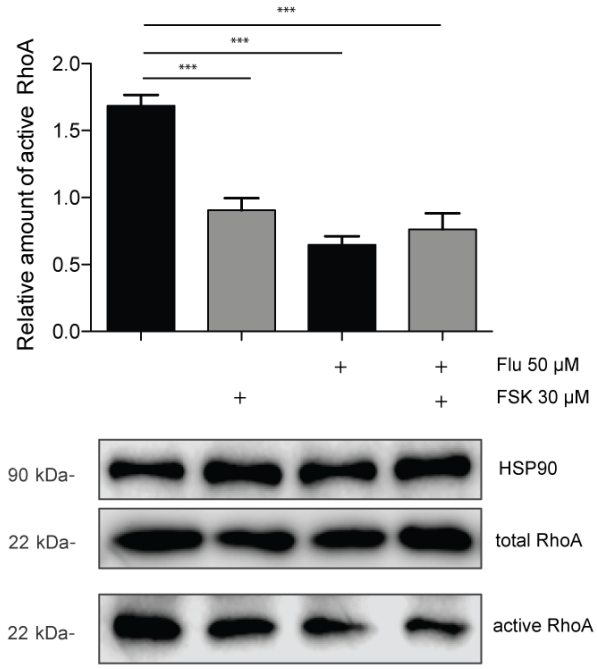

Figure 14. Fluconazole (Flu) decreases RhoA activity in IMCD cells. IMCD cells were left untreated or stimulated with forskolin (FSK 30 µM, 30 minutes), or with fluconazole alone in indicated concentration or in combination with forskolin for 1 h. Lower panels. Lysates were prepared and active RhoA was precipitated with RBD-sepharose beads. Input and pulldown fractions were separated by SDS-PAGE and RhoA and HSP90 were detected using specific antibodies. HSP90 served as loading control for the input. The amount of active RhoA is related to normalised RhoA (total RhoA to HSP90 (Input)). Shown are representative blots from one of five independent experiments. Upper panel. Blots were semi-quantitative analysed and statistically compared. Statistically significant differences are indicated (mean± SEM, ***p<0.001).

4.1.6 Fluconazole decreases the phosphorylation and thus activity of LIMK1 but does not modify the cofilin phosphorylation status which activates actin polymerization in IMCD cells

LIMK1 and cofilin are downstream effectors of RhoA. Active RhoA, activates ROCK which in turns activates LIMK1 *via* phosphorylation. Phosphorylation of LIMK1 associates with deactivation of cofilin. Reduced RhoA activity could activate cofilin, which when active, plays an essential role in actin reorganization by depolymerisation and severing actin filaments (Kobayashi et al., 2006). The decrease in F-actin-containing stress fibers by flucaonazole and FSK may involve cofilin dephosphorylation.

Fluconazole (50 µM) decreased the phosphorylation of LIMK1 at Ser508 related to total LIMK1. As expected, FSK alone and with fluconazole reduced phosphorylation at this position (Figure 15).

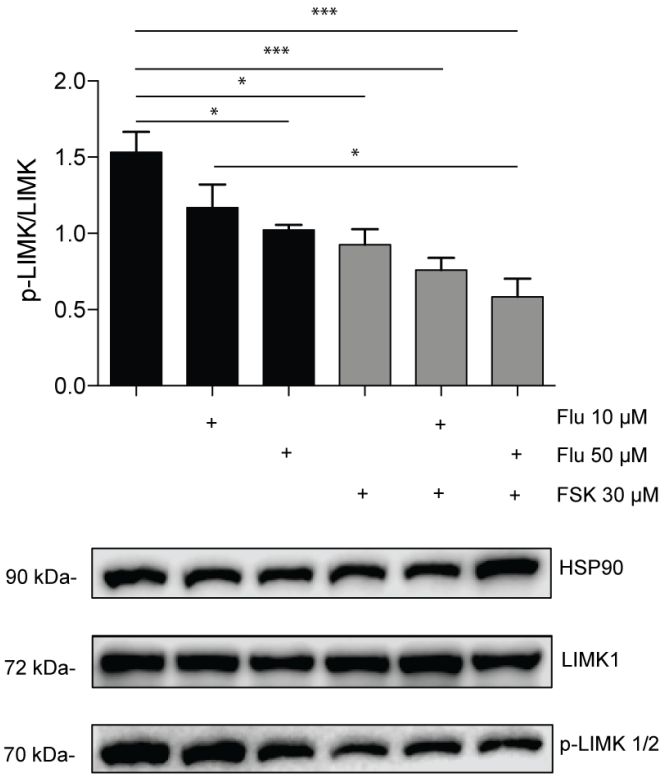

Figure 15. Fluconazole (Flu) decreases the phosphorylation of LIMK1 in IMCD cells. IMCD cells were left untreated or stimulated with forskolin (FSK 30 µM, 30 minutes), or with fluconazole alone in indicated concentrations or in combination with forskolin for 1 h. Lower panels. Lysates were prepared and proteins were separated by SDS-PAGE. LIMK1, p-LIMK 1/2 and HSP90 as a loading control were detected by Western blotting. Representative blots from one of five independent experiments are shown. Upper panel. Blots were semi-quantitative analysed and statistically compared. Statistically significant differences are indicated (mean± SEM, *p<0.05, ***p<0.001).

It has been already demonstrated that cofilin activity was suppressed by PKA (Havekes et al., 2016) but so far cofilin activity and consequent activation was never related to AQP2 trafficking. A potential effect of fluconazole or FSK on phosphorylation of Ser3 of cofilin in IMCD cells was assessed. As expected, FSK stimulation decreases phosphorylation of cofilin at Ser3. The ratio of p-cofilin/cofilin was dramatically decreased compared to basal condition (Figure 16). Similarly, in combination with fluconazole a similar effect was observed. Despite dephosphorylation of LIMK1 and an expected increase in cofilin activity, fluconazole alone caused no change in the cofilin phosphorylation status. Changes of the phosphorylation status of cofilin upon treatment with FSK are possibly related to increased level of cAMP and activation of PKA upon FSK stimulation.

The changes in cofilin phosphorylation upon FSK stimulation may involve members of the Slingshot phosphatases (Niwa et al., 2002). Haloacid dehalogenase chronophin (CIN), PP1, and PP2A dephosphorylate cofilin (Gohla et al., 2005). However no changes in total phosphatase activity upon treatment with fluconazole or FSK stimulation was observed (Figure 12).

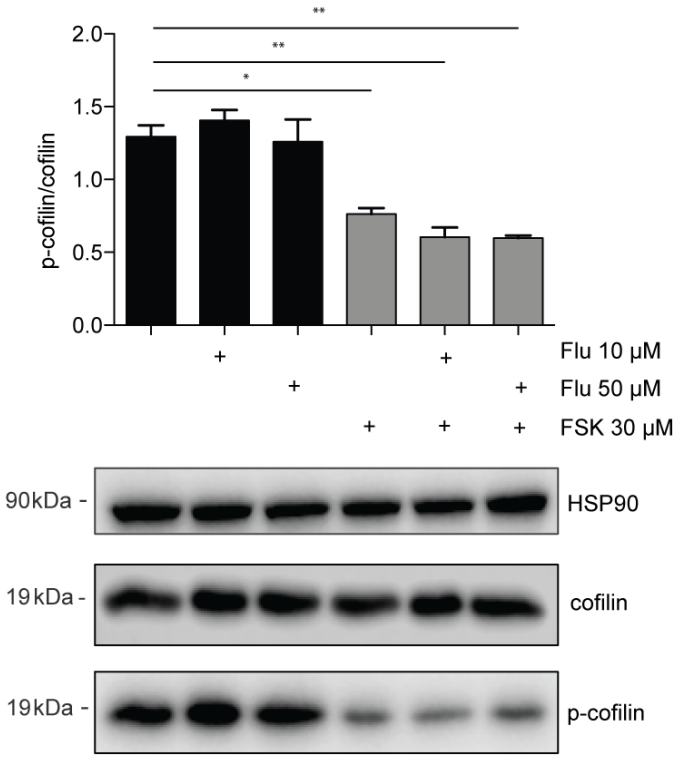

Figure 16. Fluconazole (Flu) causes no change in the phosphorylation of cofilin in IMCD cells. IMCD cells were left untreated or stimulated with forskolin (FSK 30 µM, 30 minutes), or with fluconazole alone in indicated concentrations or in combination with forskolin for 1 h. Lower panels. Lysates were prepared and

proteins were separated by SDS-PAGE. Cofilin, p-cofilin and HSP90 as a loading control were detected by Western blotting. Representative blots from one of three independent experiments are shown. Upper panels. Blots were semi-quantitative analysed and statistically compared. Statistically significant differences are indicated (mean± SEM, *p<0.05, **p<0.01).

4.1.7 Fluconazole increases phosphorylation of MLC

AVP increases the phosphorylation of MLC (Chou et al., 2004). Phosphorylation of MLC is associated with predominant plasma membrane localization of AQP2.

In IMCD cells, FSK stimulated an increase in the phosphorylation of MLC at Ser19. Consequently, the ratio of p-MLC/MLC was increased compared to basal state. Fluconazole alone (50 µM) also increased the ratio p-MLC/MLC (Figure 17). Fluconazole did not add to the effect of FSK.

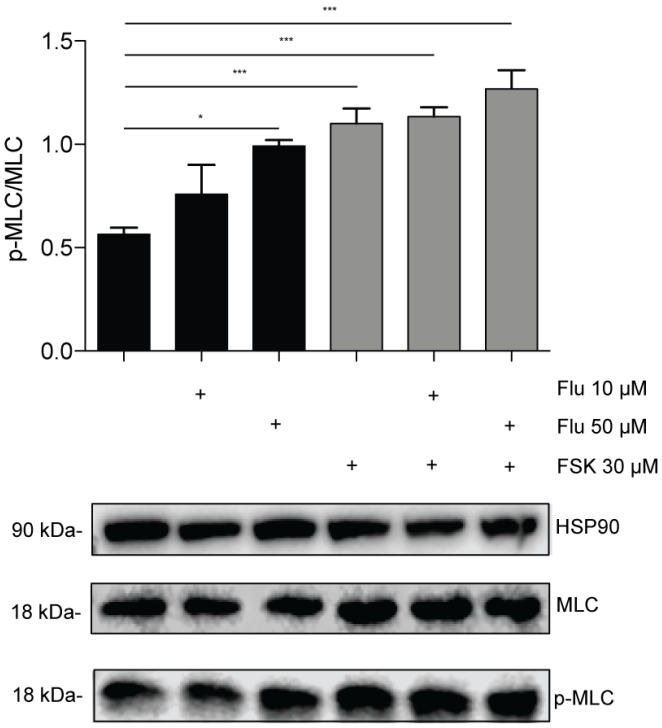

Figure 17. Fluconazole (Flu) increases the phosphorylation of MLC in IMCD cells. IMCD cells were left untreated or stimulated with forskolin (FSK 30 µM, 30 minutes), or with fluconazole alone in indicated concentrations or in combination with forskolin for 1 h. Lower panels. Lysates were prepared and proteins were separated by SDS-PAGE. MLC, p-MLC and HSP90 as a loading control were detected by Western blotting. Representative blots from one of five independent experiments are shown. Upper panels. Blots were semi-quantitative analysed and statistically compared. Statistically significant differences are indicated (mean± SEM, *p<0.05, ***p<0.001).

4.2 Fluconazole promotes the redistribution of AQP2 in wild-type mice

4.2.1 Fluconazole increases the AQP2 abundance at the plasma membrane of collecting duct principal cells

Due to the obvious effect in primary cells, it was investigated whether fluconazole would act similarly in a whole organism. As reported previously, fluconazole plasma concentration in humans ranged from 20 up to 50 mg/L or up to 70 mg/L for high-dose therapy (800 mg/day) (Santos et al., 2010). On the other hand, fluconazole ranged from 4.6 mg/L to 9 mg/L at low-dose therapy (200-400 mg daily). In humans for effective pharmacotherapy of candidiasis, fluconazole must reach 4.0 mg/L plasma levels at low-dose intravenous therapy with 100 mg daily doses (Cousin et al., 2003). In a recent study, neutropenic five-week old murine pathogen-free male mice of the strain Udea: ICR (CD-2) were subcutaneously treated every 3 to 6 h with doses ranging from 1 to 128 mg/kg per day (Gonzalez et al., 2015). In *candida albicans*-infected neutropenic mice, the dose administered subcutaneously was in a range between 6.25 mg/kg to 100 mg/kg and the peak levels in the blood ranged between 5.2 mg/L and 100 mg/L (Lepak et al., 2006).

For further experiments doses were chosen based on previous studies on mice (Gonzalez et al., 2015; Khan et al., 2015; Lepak et al., 2006). Experiments with mice were performed in collaboration with Dr. med. Christian Hinze and Prof. Dr. Kai M. Schmidt-Ott. To achieve in the blood of mice a concentration of 50 µM of fluconazole that effectively induced the AQP2 redistribution in primary cells, seven-week old wild type BALB/C6 mice were treated with different doses of the drug (20, 40, 80 and 100 mg/kg) and the concentration in the blood was determined. The mice were treated with single intraperitoneal (i.p.) injections and concentrations of the drug were determined (Lab 28 Berlin). Moreover, the initial attempt to detect the desired concentration of fluconazole in the blood after a single i.p. injection failed. This may be due to the fact that mice are fast metabolizers and that single injection is not enough. The experiment was repeated and mice were treated with fluconazole in two concentrations 40 mg/kg and 80 mg/kg every 24 h over 96 h. Mice were sacrificed 7 h after the last injection. In these regimes fluconazole in the blood was detected: 40 mg/kg was equivalent to 12.32 mg/L (40 µM)

and 80 mg/kg was equivalent to 15.4 mg/L (50 μM). In further experiments mice received fluconazole i.p. injections of 80 mg/kg or 0.9 % NaCl (saline) as a negative control every 24 h over a period of 96 h.

AVP levels increase during water deprivation (Oliverio et al., 2000). In order to achieve an elevation of AVP, an additional groups of mice during the last 24 h of the 96 h of treatment with fluconazole, or 0.9 % NaCl, were placed in metabolic cages and were water-deprived. At the end of the treatment, mice were sacrificed.

Kidneys were harvested; left kidneys were subjected to immunofluorescence microscopic analysis and right kidneys to the preparation of kidney lysates. In control animals treated with 0.9 % NaCl, AQP2 is localized mainly intracellularly (Figure 18). The localization and signal intensity of AQP2 in kidney sections suggested that fluconazole enhanced the AQP2 signal intensity and promoted AQP2 accumulation to the plasma membrane. The effect of fluconazole on the AQP2 localization was confirmed by semi-quantitative analysis (Figure 18-under B). Remarkably, the effect of fluconazole on the AQP2 localization and signal intensity was even stronger in water-deprived animals treated with fluconazole in comparison to their water-deprived control littermates (Figure 18-under C). This was better visible on longitudinal sections (Figure 18-under D).

In parallel, in fluconazole-treated mice and their controls were measured urine parameters. Water deprivation served as a positive control for eventual additive effect of fluconazole in water-deprivation, as seen with biotinylation assay in IMCD cells. Water deprivation decreases urine output and increases urine osmolality, as expected. Fluconazole treatment in water-deprived mice (n=15) compared to water-deprived controls (n=15) led to a dramatic decrease of urine output (reduction by nearly 40 %) accompanied by a striking increase in urine osmolality (increased by nearly 30 %). This was similar in terms of urine osmolality (increased by nearly 40 %) in groups of mice, which were not water-deprived but treated with fluconazole (n=5) compared to 0.9 % NaCl (n=5) treated controls. Since this group was not water deprived, and mice were not placed into the metabolic cages, urine production was not measured (Figure 19).

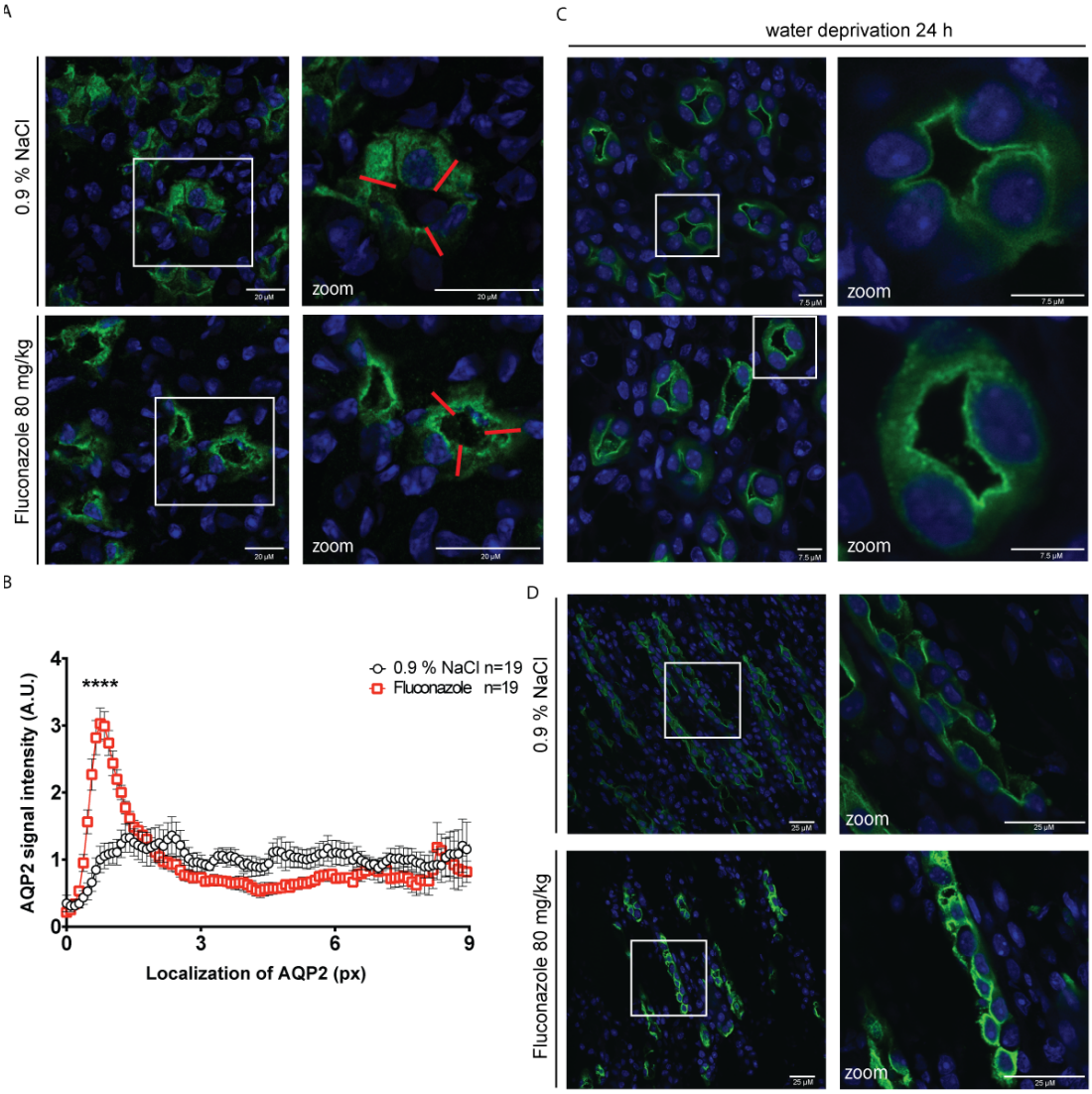

Figure 18. Fluconazole increases the AQP2 abundance at the plasma membrane of collecting ducts principal cells in wild type BALB/C6 mouse. Mice were treated with fluconazole i.p. injections (80 mg/kg) to achieve a concentration of 15.4 mg/L in the blood or with 0.9 % NaCl every 24 h over a period of 96 h. A) Tissue sections from left kidneys were subjected to immunofluorescence microscopic analysis of AQP2. AQP2 was detected by immunofluorescence microscopy using specific primary antibodies (H27) and Cy3-coupled anti-rabbit secondary antibodies (green). Nuclei were stained with DAPI (blue). Shown are representative images from one of three independent experiments. The magnified views (zoom) of collecting ducts are from the indicated squares. B) Semi-quantitative analysis of AQP2 localization in mouse collecting ducts. Collecting ducts from three different animals were analysed. Plotted is the AQP2 signal intensity versus the localization of AQP2 along the red line superimposed onto the cells as indicated. The peak in fluconazole signals corresponds to the plasma membrane of the cells facing the collecting duct. Red: animals treated with fluconazole (n=19) Black: animals treated with 0.9 % NaCl (n=19). Statistically significant differences are indicated (mean± SEM, ****p<0.0001). C) Mice were treated with fluconazole i.p. injections (80 mg/kg) to achieve a concentration of 15.4 mg/L in the blood or with 0.9 % NaCl every 24 h over a period of 96 h and last 24 h water-deprived. Tissue sections from left kidneys were subjected to immunofluorescence microscopic analysis of AQP2. AQP2 was detected by immunofluorescence microscopy using specific primary antibodies (H27) and Cy3-coupled anti-rabbit secondary antibodies (green). Nuclei were stained with DAPI (blue). Shown are representative images from one of three independent experiments. The magnified views (zoom) of collecting ducts are from the indicated squares. D) Mice were treated in same regime as under C) and presented are longitudinal tissue sections with the same staining as under C).

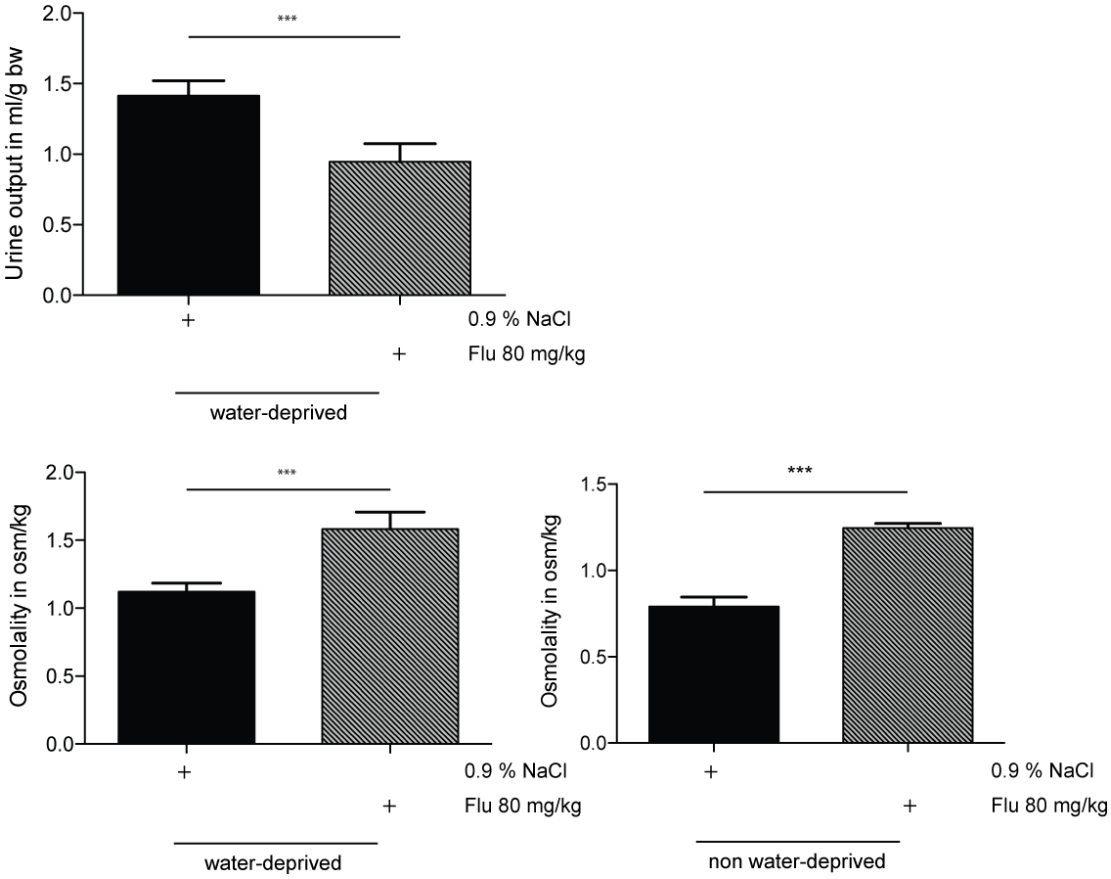

Figure 19. Fluconazole (Flu) decreases urine output and increases urine osmolality in water-deprived and non-water-deprived wild type BALB/C6 mice. Mice were treated with fluconazole i.p. injections (80 mg/kg) to achieve a concentration of 15.4 mg/L in the blood or with 0.9 % NaCl every 24 h over a period of 96 h or treated in the same regime and additionally last 24 h water deprived. 24 h urine osmolality and output were monitored (n=15 for each of water-deprived groups). In experiment without water deprivation only urine osmolality was monitored (n=5 for each of non-water-deprived groups). Statistically significant differences are indicated (mean± SEM, ***p<0.001)(abbreviation bw-body weight).

4.2.2 Fluconazole increases AQP2 abundance and changes phosphorylation sites of AQP2 in wild type mice

Fluconazole alone increases the amount of AQP2 abundance compared to 0.9 % NaCl control treated mice (Figure 20-under A). In addition, fluconazole increases the phosphorylation of AQP2 at Ser256 (Figure 20-under B) and reduces phosphorylation at Ser261 (Figure 20-under C) compared to 0.9 % NaCl control treated mice. Fluconazole does not show any effect on the phosphorylation at Ser269 of AQP2 (Figure 20-under D).

Moreover, in water-deprived mice treated with fluconazole, the abundance of a marker of exocytic vesicles, Rab3, was significantly increased when compared to the control water-deprived animals (Figure 21-under A). Rab5 and RhoA abundance was not changed (Figure 21-under B and C).

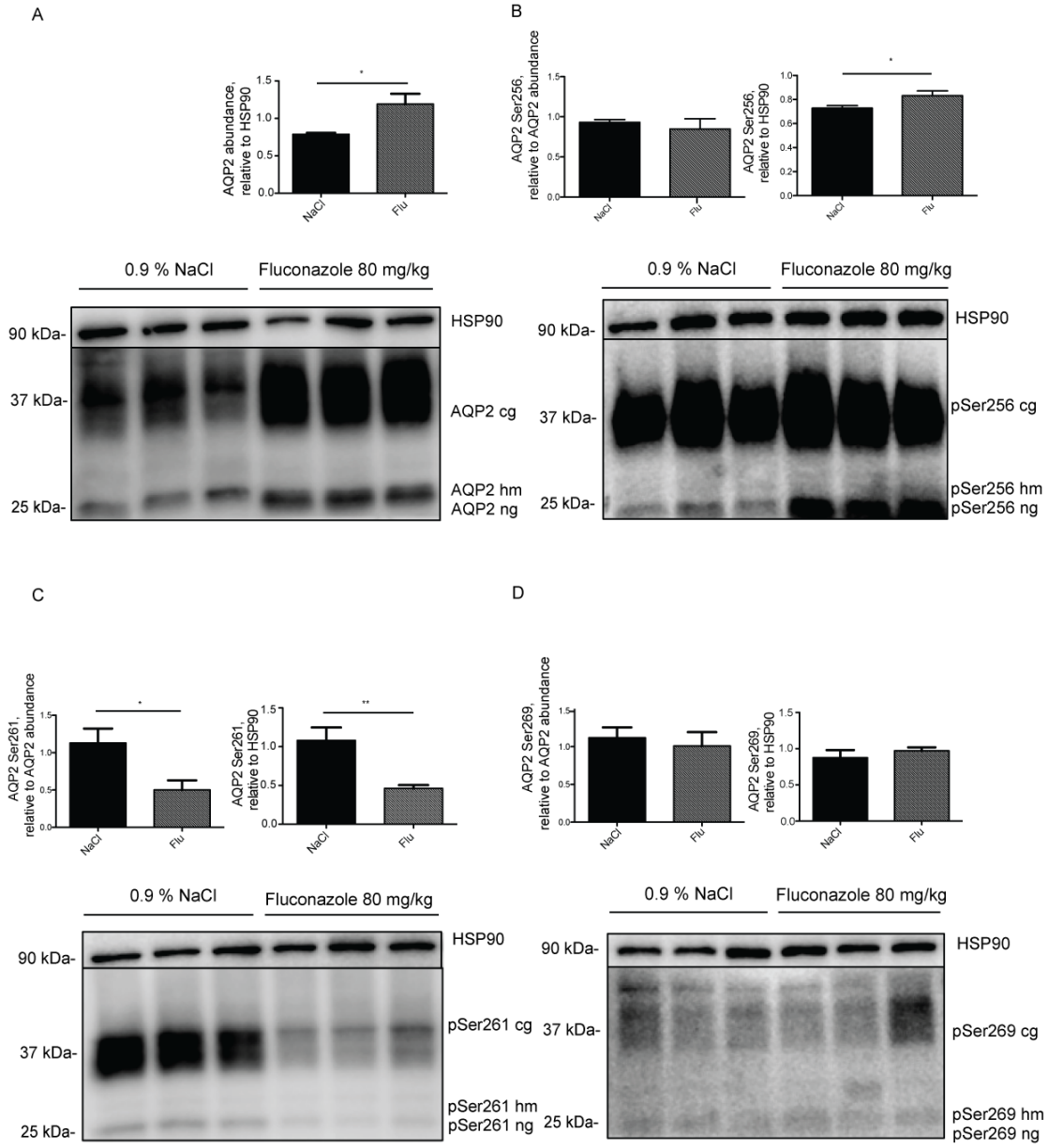

Figure 20. Fluconazole increases AQP2 abundance and modulates critical phosphorylations of AQP2 in wild type BALB/C6 mice. Mice were treated with fluconazole i.p. injections (80 mg/kg) to achieve a concentration of 15.4 mg/L in the blood or with 0.9% NaCl every 24 h over a period of 96 h. Lower panels. Lysates were prepared of inner medullae (n=5 per each condition) and proteins were separated by SDS-PAGE. A) AQP2 B) pSer256-AQP2 C) pSer261-AQP2 D) pSer269-AQP2 and HSP90 as loading control for all blots were detected by Western blotting. Upper panels. The signals emerging from the complex glycosylated (cg), high manose (hm) and non-glycosylated (ng) forms of AQP2 were semi-quantitative analysed and the sums statistically compared. Statistically significant differences are indicated (mean± SEM, *p<0.05, **p<0.01).

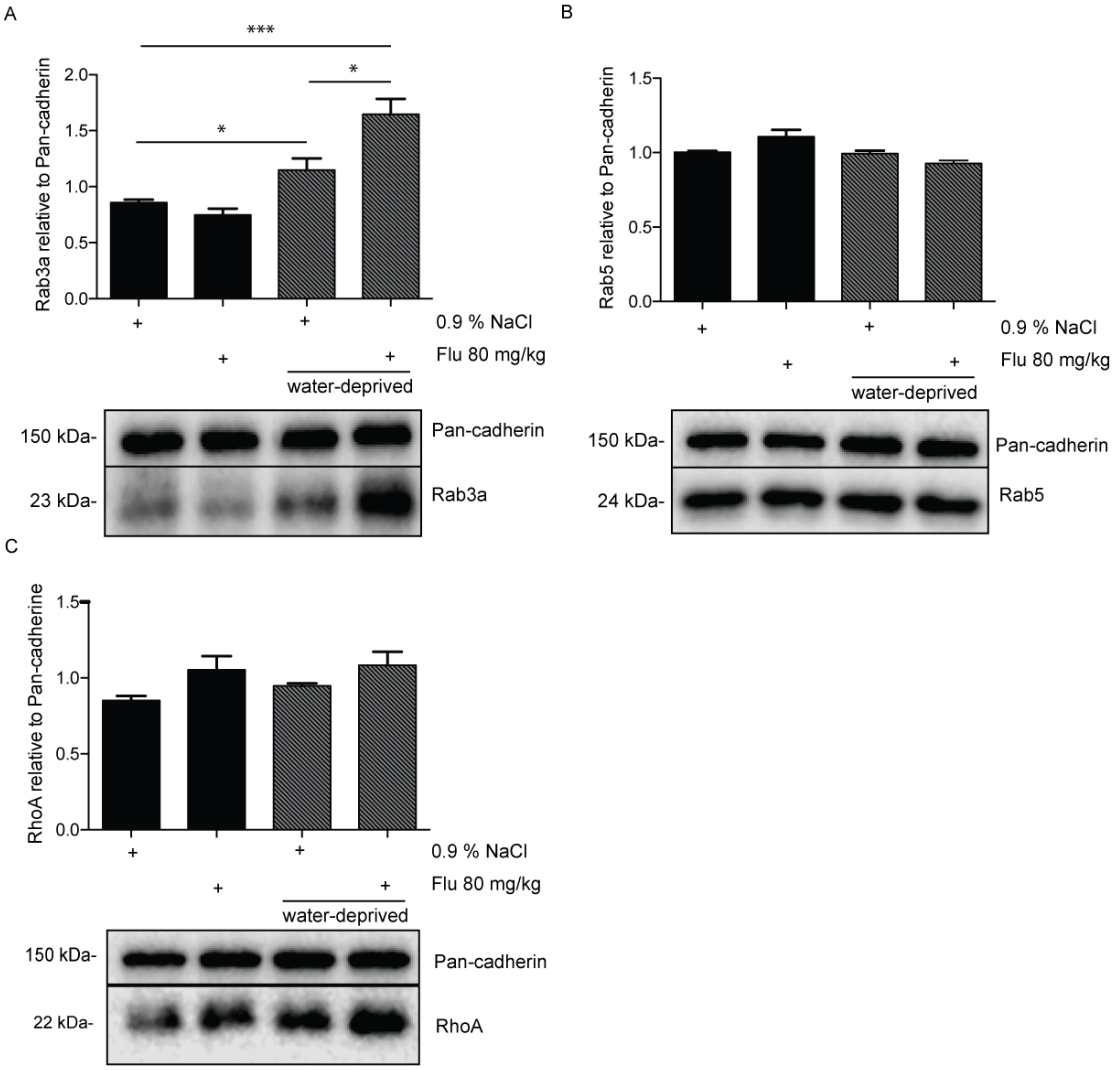

Figure 21. Fluconazole (Flu) increases the level of a marker of exocytic vesicles Rab3 in water-deprived wild type BALB/C6 mice. Mice were treated with fluconazole i.p. injections (80 mg/kg) to achieve a concentration of 15.4 mg/L in the blood or with 0.9 % NaCl every 24 h over a period of 96 h or treated in the same regime with 0.9 % NaCl and fluconazole and additionally last 24 h water deprived. Lower panels. Lysates were prepared from whole right kidneys and proteins separated by SDS-PAGE. A) Rab3, B) Rab5, C) RhoA and Pan-cadherin as a loading control for all blots were detected by Western blotting. Representative blots from one of three independent experiments are shown. Upper panels. Blots were semi-quantitative analysed and statistically compared. Statistically significant differences are indicated (mean± SEM, ***p<0.001, *p<0.05).

4.2.3 Fluconazole deacreses RhoA activity in wild type mice

Since in IMCD cells the F-actin-containing stress fibers content was decreased upon treatment with fluconazole (Figure 13), the level of active RhoA in kidney inner medullae from mice treated with fluconazole or with 0.9 % NaCl was investigated. The lysates were combined with agarose beads, conjugated with Rho-binding domain of Rhotekin, to pull down the active, GTP-bound RhoA, as described above (4.1.4). Quantification of the data from five pull-down experiments revealed a significant

decrease in RhoA activity in fluconazole-treated mice in comparison to 0.9 % NaCl-treated mice (Figure 22). Therefore, the reduction in RhoA-activity most likely inhibits the actin-barrier formation and it permits the membrane accumulation of AQP2.

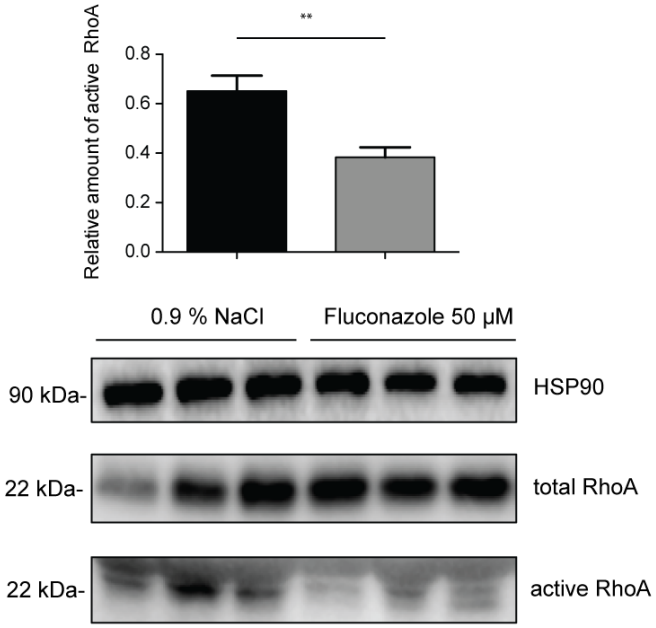

Figure 22. Fluconazole decreases RhoA activity in wild type BALB/C6 mice. Mice were treated with fluconazole i.p. injections (80 mg/kg) to achieve a concentration of 15.4 mg/L in the blood or with 0.9 % NaCl every 24 h over a period of 96 h. Lower panels. Lysates were prepared of inner medullae (n=5, per each condition) and active RhoA was precipitated with RBD-sepharose beads. Input and pulldown fractions were separated by SDS-PAGE and HSP90 and RhoA were detected using specific antibodies. HSP90 served as loading control for the input. Upper panel. The amount of active RhoA is related to normalised RhoA (total RhoA to HSP90 (Input)). Blots were semi-quantitative analysed and statistically compared. Statistically significant differences are indicated (mean± SEM, **p<0.01).

AVP activation raises the level of intracellular cAMP, resulting in the activation of PKA, that is able to phosphorylate RhoA at Ser188 (Dong et al., 1998). Since reduced RhoA activity in mice treated with fluconazole was observed, next the phosphorylation of RhoA at Ser188 was investigated.

In mice treated with fluconazole, the phosphorylation of RhoA at Ser188 was significantly increased, confirming the reduced activity of RhoA (Figure 23.)

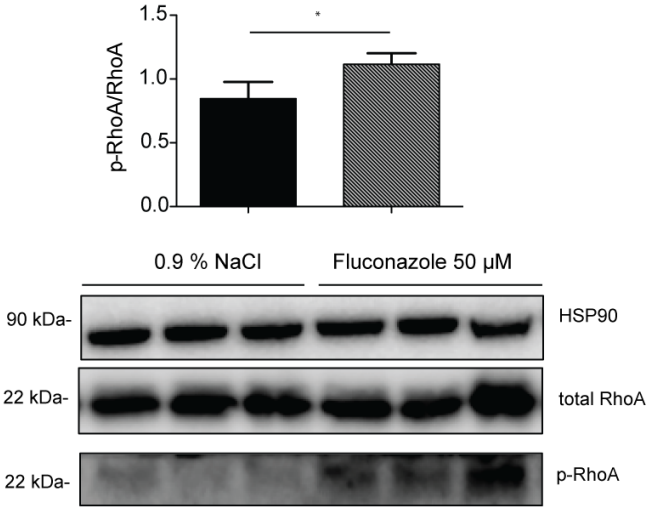

Figure 23. Fluconazole increases phosphorylation of RhoA in wild type BALB/C6 mice. Mice were treated with fluconazole i.p. injections (80 mg/kg) to achieve a concentration of 15.4 mg/L in the blood or with 0.9 % NaCl every 24 h over a period of 96 h. Lower panels. Lysates were prepared of inner medullae (n=5 per each condition) and separated by SDS-PAGE. RhoA, p-RhoA and HSP90 as a loading control were detected by Western blotting. Upper panels. Blots were semi-quantitative analysed and statistically compared. Statistically significant differences are indicated (mean± SEM, *p ≤ 0.05).

4.2.4 Fluconazole causes dephosphorylation of Cofilin at Ser3 in water-deprived mice

Increased cofilin activity is associated with F-actin reorganization and a decrease in F-actin-containing stress fibers. Fluconazole in water-deprived mice, causes dephosphorylation at Ser3 of cofilin compared to 0.9 % NaCl control treated mice and fluconazole-treated mice, whereas water deprivation had no effect on cofilin dephosphorylation (Figure 24).

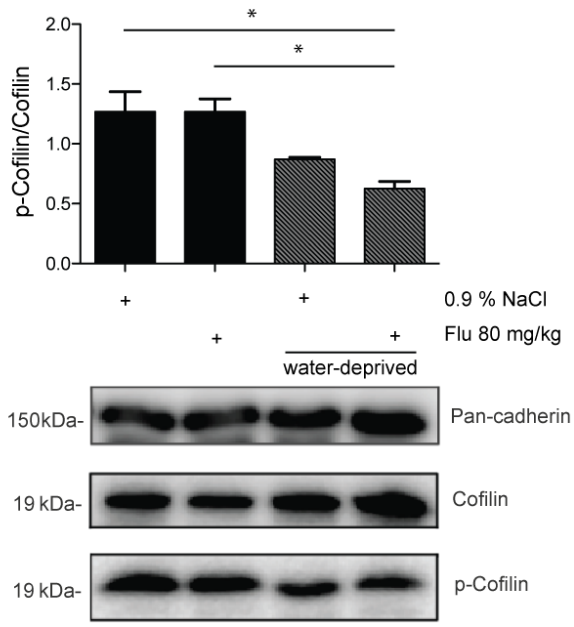

Figure 24. Fluconazole (Flu) causes dephosphorylation of cofilin at Ser3 in water-deprived wild type BALB/C6 mice. Mice were treated with fluconazole i.p. injections (80 mg/kg) to achieve a concentration of 15.4 mg/L in the blood or with 0.9 % NaCl every 24 h over a period of 96 h or treated in the same regime and additionally last 24 h water deprived. Lower panels. Lysates were prepared from right whole kidney and proteins were separated by SDS-PAGE. Cofilin, p-cofilin and Pan-cadherin as a loading control were detected by Western blotting. Representative blot from one of three independent experiments are shown. Upper panel. Blots were semi-quantitative analysed and statistically compared. Statistically significant differences are indicated (mean± SEM, *$p<0.05$).

4.2.5 Fluconazole decreases urine output and increases urine osmolality in tolvaptan-treated mice

Tolvaptan causes an excessive and detrimental loss of water. Since the presented data indicate that fluconazole causes water retention in an AVP-independent manner, fluconazole may ameliorate the tolvaptan-induced excessive water secretion. To test this hypothesis, mice were treated with tolvaptan alone or in combination with fluconazole. Tolvaptan dosage (20 mg/kg) in mice was established according to previous published experiments (Gankam Kengne et al., 2015).

Tolvaptan alone dramatically increased urine output (nearly 40 %) and reduced urine osmolality (nearly 50 %), compared to 0.9 % NaCl-treated control mice (Figure 25). The urine output was lower (by nearly 20 %) in the mice that were treated with both drugs. Urine osmolality tended to increase (by nearly 15 %) if the combination of fluconazole and tolvaptan was administered. However, this was not statistically significant. Thus, consequently fluconazole may be beneficial as a co-treatment with tolvaptan in reducing the dehydrating effect of heart failure and ADPKD.

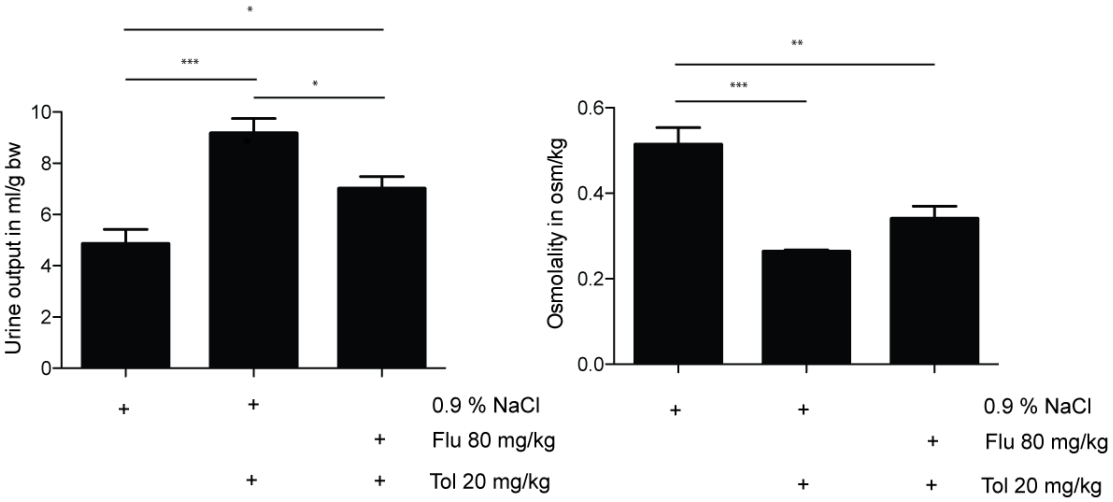

Figure 25. Fluconazole (Flu) decreases urine output in tolvaptan-treated wild type BALB/C6 mice. Mice were treated with fluconazole i.p. injections (80 mg/kg) to achieve a concentration of 15.4 mg/L in the blood or with 0.9 % NaCl (2 groups of mice) every 24 h over a period of 96 h. 24 h prior sacrificing mice were placed into the metabolic cages and single i.p. injection (20 mg/kg) of tolvaptan (Tol) was administered to the one of 0.9 % NaCl-treated mice group and in fluconazole-treated mice group. 24 h urine osmolality and output were monitored (n=5 per each group). Statistically significant differences are indicated (mean± SEM, * $p \leq 0.05$; ** $p \leq 0.01$; *** $p \leq 0.001$).

4.3 The effect of triazolpropenon on the AQP2 redistribution in MCD4 and IMCD cells

4.3.1 Triazolpropenon prevents redistribution of AQP2 into the plasma membrane in both MCD4 and IMCD cells

To examine the effect of previously identified small molecule, inhibitor of the AQP2 redistribution, MCD4 cells were treated with triazolpropenon (0.4 μM and 4 μM) alone or in combination with FSK. FSK alone induces translocation of AQP2 from intracellular vesicles to the plasma membrane and this served as a control (Figure 26). Immunofluorescence microscopic analysis (see 4.1.1) showed that triazolpropenon alone did not alter the plasma membrane abundance of AQP2. Treatment with FSK in presence of triazolpropenon decreased the AQP2 plasma membrane localization in a dose-dependent manner, defining triazolpropenon as inhibitor of the FSK-induced AQP2 redistribution.

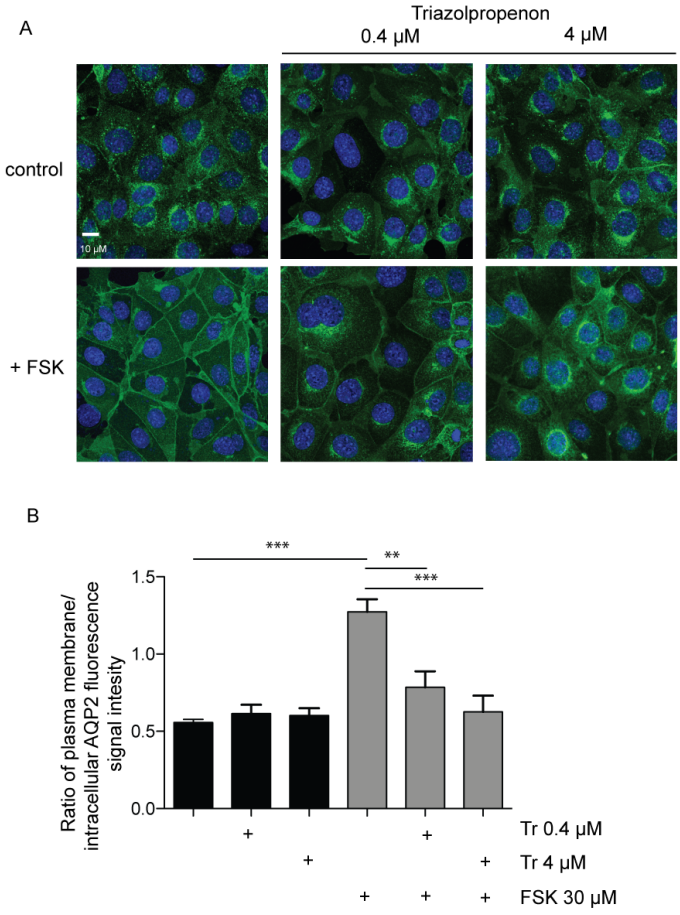

Figure 26. Triazolpropenon (Tr) prevents the forskolin-induced redistribution of AQP2 in MCD4 cells. MCD4 cells were left untreated or stimulated with forskolin (FSK 30 μM, 30 minutes) or with

triazolpropenon alone in indicated concentrations or in combination with forskolin for 1 h. A) AQP2 was detected by immunofluorescence microscopy using specific primary antibodies (H27) and Cy3-coupled anti-rabbit secondary antibodies (green). Nuclei were stained with DAPI (blue). Shown are representative images from one of three independent experiments. B) The intensities of intracellular and plasma membrane immunofluorescence signals arising from AQP2 were determined and related to perinuclear signal intensities (mean ± SEM; three independent experiments). The ratios of plasma membrane to intracellular fluorescence signal intensities were calculated. Ratios < 1 indicate a predominant intracellular localization, ratios > 1 a predominant plasma membrane location of AQP2. Values significantly different from FSK and AVP-treated cells are indicated (**p<0.01; ***p<0.001).

4.3.2 Triazolpropenon increases phosphorylation of AQP2 at Ser261 in a presence of forskolin in MCD4 cells

In order to investigate whether triazolpropenon affects AQP2 abundance and phosphorylations of AQP2 at Ser256 and Ser261, MCD4 cells were treated with triazolpropenon alone and in combination with FSK. Triazolpropenon alone did not alter AQP2 abundance (Figure 27-under A). Triazolpropenon increases phosphorylation of AQP2 at Ser261 (Figure 27-under C), indicating a possible interference with the PKA pathway. The phosphorylation of AQP2 at Ser256 (Figure 27-under B) is expected to increase after stimulation with FSK. This was not observed with the available antibody. Since this antibody does not work in MCD4 cells, potential inhibitory effect on this phosphorylation site could not be completely excluded. The phosphorylation of AQP2 at Ser264 and Ser269 could not be detected, as no phospho-specific antibodies were available for MCD4 cells.

An inhibitory effect of triazolpropenon on the AQP2 trafficking was also confirmed in primary IMCD cells. In addition to immunofluorescence images obtained from IMCD cells upon treatment with triazolpropenon, cell surface biotinylation assays were performed in order to quantify the effect of triazolpropenon on the AQP2 membrane localization (Figure 28). Triazolpropenon reduced the plasma membrane abundance of AQP2 in presence of FSK compared to the appropriate control.

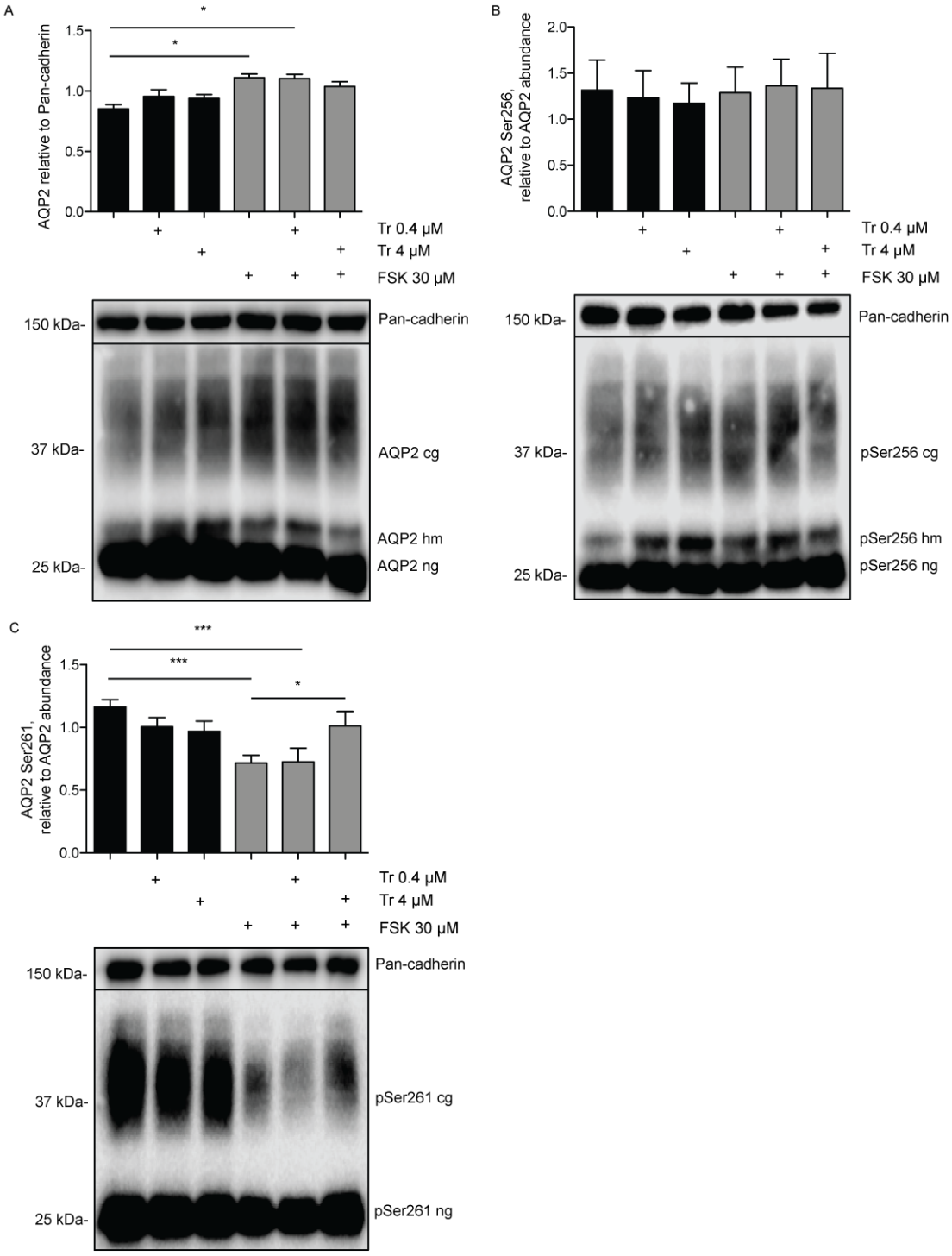

Figure 27. Triazolpropenon (Tr) inhibits the forskolin-induced dephosphorylation of AQP2 at Ser261 in MCD4 cells. MCD4 cells were left untreated or stimulated with forskolin (FSK 30 µM, 30 minutes) or with triazolpropenon alone in indicated concentrations or in combination with forskolin for 1 h. Lower panels. Lysates were prepared and proteins were separated with SDS-PAGE. A) AQP2 B) pSer256-AQP2 C) pSer261-AQP2 and HSP90 as loading control for all blots were detected by Western blotting. Shown are representative blots from one of four independent experiments. Upper panels. The signals emerging from the complex glycosylated (cg), high manose (hm) and non-glycosylated (ng) forms of AQP2 were semi-quantitative analysed and the sums statistically compared. Statistically significant differences are indicated (mean± SEM, *p<0.05; ***p<0.001).

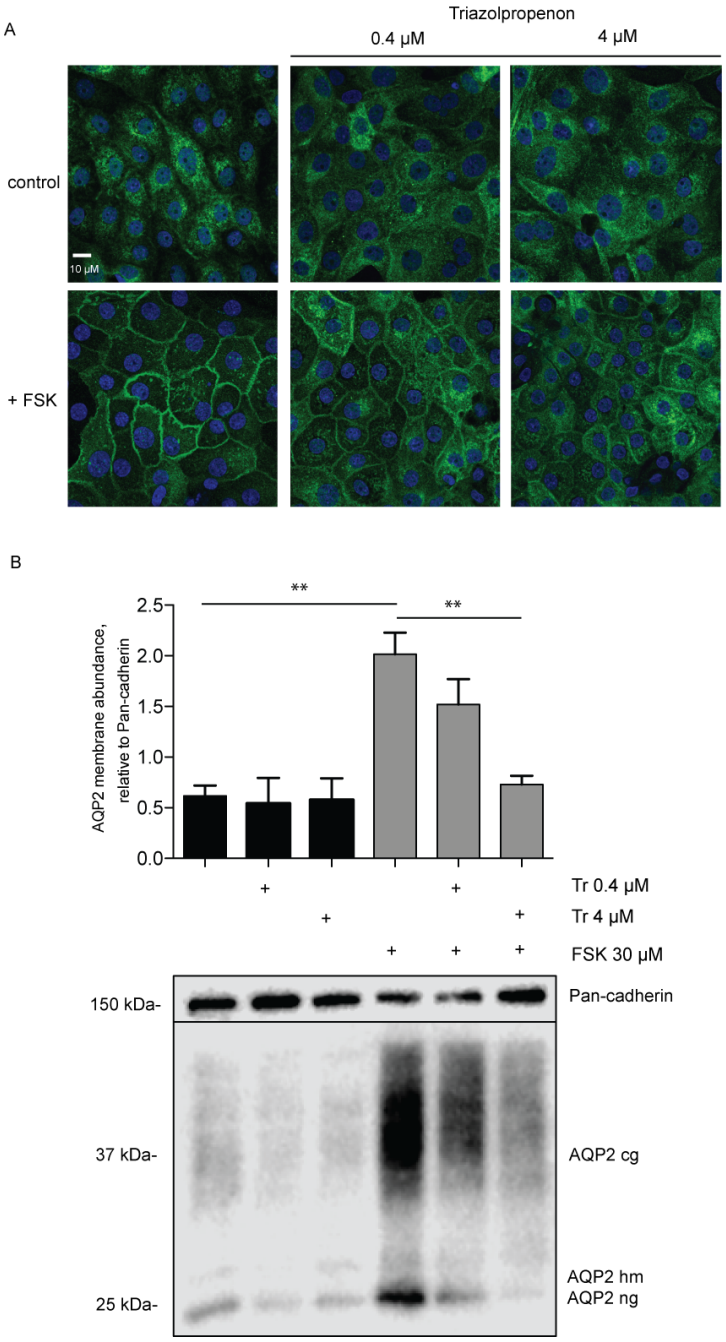

Figure 28. Triazolpropenon (Tr) prevents the forskolin-induced redistribution of AQP2 from intracellular vesicles into the plasma membrane in IMCD cells. IMCD cells were left untreated or stimulated with forskolin (FSK 30 µM, 30 minutes) or with triazolpropenon alone in indicated concentrations or in combination with forskolin for 1 h. A) AQP2 was detected by immunofluorescence microscopy using specific primary antibodies (H27) and Cy3-coupled anti-rabbit secondary antibodies (green). Nuclei were stained with DAPI (blue). Shown are representative images from one of three independent experiments. B) Lower panel. Cell-surface biotinylation assays were carried out to quantify the effect of triazolpropenon on the localization of AQP2 into the plasma membrane. In order to detect AQP2 on the surface of the cells, surface proteins were precipitated with streptavidin agarose beads. AQP2 and Pan-cadherin as loading control were detected by Western blotting (three independent experiments). Upper panel. The signals emerging from the complex glycosylated (cg), high manose (hm) and non-glycosylated (ng) forms of AQP2 were semi-quantitative analysed and the sums statistically compared. Statistically significant differences are indicated (mean ± SEM, **p<0.01).

4.3.3 Forskolin could modulate the formation of epoxyeicosatrineoic acid (EETs) and 20-hydroxyeicosatetraenoic acid (20-HETE)

Fluconazole blocks fungal lanosterol 14α-demethylase (CYP51A1) and thereby inhibits ergosterol biosynthesis, causing membrane defects. Fluconazole is a substrate for elimination and an inhibitor of several other cytochrome P450 enzymes (CYP2C9, CYP2C19, CYP3A4) (Niwa et al., 2005). The inhibitory effect on the AQP2 redistribution is apparently not due to obvious membrane defects, similar to those caused by fluconazole in fungi. According to the human protein atlas CYP2C9 and CYP2C19 are not expressed in the kidney and CYP3A4 only at low level.

CYP51A1, the main target of fluconazole (Strushkevich et al., 2010) is expressed in IMCD and MCD4 cells, also in rat renal inner medullae, and in whole kidney homogenates (Figure 29). In IMCD cells, other CYPs, such as CYP4A1 and CYP4F2, are detected. CYP51A, CYP4A, and CYP4F are involved in the synthesis of cholesterol but also in the synthesis of EETs and 20-HETE, which are derivatives of arachidonic acid.

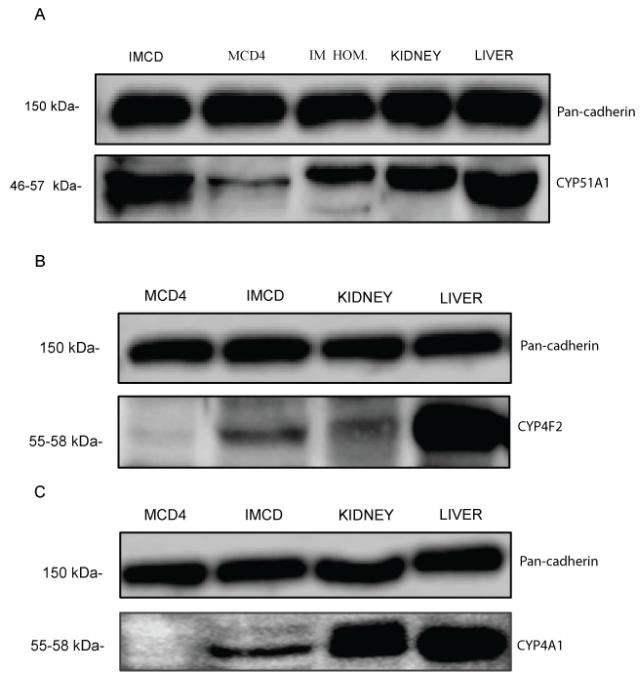

Figure 29. Detection of CYP51A1, CYP4F2 and CYP4A1. Lysates from IMCD cells and MCD4 cells, from mouse inner medullae (IM HOM.), from mouse kidney (KIDNEY) and from rat liver (LIVER) were prepared and proteins were separated with SDS-PAGE. A) CYP51A1, B) CYP4F2 and C) CYP4A1 and Pan-cadherin as a loading control for all blots were detected by Western blotting. Shown are representative blots from one of three independent experiments.

20-HETE is released from phospholipid membranes in response to different vasoconstrictor stimuli such as angiotensin II and bradykinin (Figure 4). Angiotensin II releases 20-HETE into the urine of rabbits. In kidneys, EETs induces a vasodilator response and 20-HETE, a vasoconstrictor response, and this response is associated with decreased urine output. Miconazole, econazole, clotrimazole and ketoconazole, the azole group of drugs, to which fluconazole belongs, reduce EETs level up to 70 %. FSK induces vasoconstriction *via* angiotensin II receptors in rabbit isolated femoral artery (Randall et al., 1996). Similarly to vasoconstrictors and azoles, FSK might be able to induce production of 20-HETE and to decrease the level of EETs in IMCD cells. In this sense blockage of 20-HETE formation upon FSK treatment could also attenuate AQP2 redistribution to plasma membrane.

To test the hypothesis that FSK could induce production 20-HETE and that blocking of 20-HETE could prevent AQP2 redistribution to the plasma membrane, IMCD cells were left untreated or treated with FSK and additionally treated with the inhibitor of 20-HETE formation, HET-0016 in the presence of FSK. As proposed, the inhibitor of 20-HETE production, HET-0016, prevents the AQP2 redistribution into the plasma membrane in the presence of FSK (Figure 30). Biotinylation indicated the concentration-dependent inhibitory effect of HET-0016 on the AQP2 redistribution in the presence of FSK.

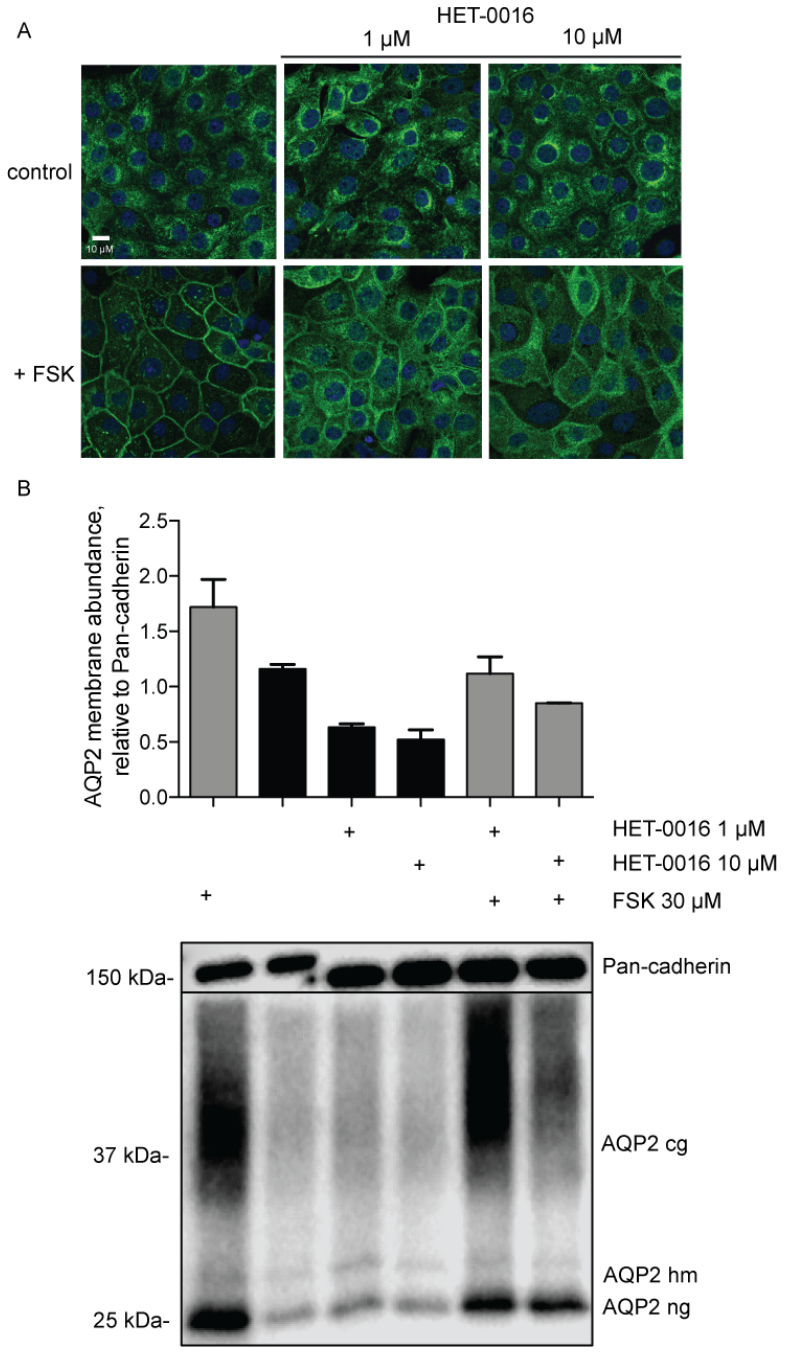

Figure 30. HET-0016 prevents the forskolin-induced redistribution of AQP2 from intracellular vesicles into the plasma membrane in IMCD cells. IMCD cells were left untreated or stimulated with forskolin (FSK 30 µM, 30 minutes) or with HET-0016 alone in indicated concentrations or in combination with forskolin for 1 h. A) AQP2 was detected by immunofluorescence microscopy using specific primary antibodies (H27) and Cy3-coupled anti-rabbit secondary antibodies (green). Nuclei were stained with DAPI (blue). Shown are representative images from one of three independent experiments. B) Lower panel. Cell-surface biotinylation assays were carried out to quantify the effect of HET-0016 on the localization of AQP2 into the plasma membrane. In order to detect AQP2 on the surface of the cells, surface proteins were precipitated with streptavidin agarose beads. AQP2 and Pan-cadherin as loading control were detected by Western blotting (two independent experiments). Upper panel. The signals emerging from the complex glycosylated (cg), high manose (hm) and non-glycosylated (ng) forms of AQP2 were semi-quantitative analysed.

5 DISCUSSION

5.1 Fluconazole promotes the redistribution of AQP2 from intracellular vesicles into the plasma membrane of renal collecting duct principal cells

Here for the first time, a previously unidentified effect of the widely used drug fluconazole is reported. It promotes an AVP-independent redistribution of AQP2 into the plasma membrane of primary IMCD cells and in wild type mice of renal collecting duct principal cells.

On the molecular level AVP increases AQP2 membrane abundance. Upon challenge with AVP, the membrane location of AQP2 is dictated by the phosphorylation of three C-terminal residues of AQP2, Ser261, Ser264 and Ser269. AVP causes an increase in phosphorylation of Ser256 (Nishimoto et al., 1999), Ser264 (Fenton et al., 2008) and Ser269 (Hoffert et al., 2008a), and a decrease in the phosphorylation at Ser261 (Nedvetsky et al., 2010). The administration of fluconazole results in a pattern of phosphorylation similar to the one induced by AVP in both IMCD cells and in wild type mice. Fluconazole increases AQP2 abundance and the PKA-dependent phosphorylation of AQP2 at Ser256. This phosphorylation is the key trigger for the membrane insertion of AQP2. Although similar end points are induced by fluconazole and AVP, this effect cannot be explained by a global activation of PKA activity since fluconazole does not affect total cellular PKA activity in IMCD cells. However, PKA could be activated locally. In addition to phosphorylation at Ser256, fluconazole decreases phosphorylation of AQP2 at Ser261, which was associated with a decreased polyubiquitination and proteasomal degradation (Nedvetsky et al., 2010). The effect of the Ser261 residue phosphorylation/dephosphorylation on AQP2 trafficking is not clear (Hoffert et al., 2007; Lu et al., 2008). In the presence of FSK, fluconazole (50 μM) markedly increases phosphorylation of AQP2 at Ser269, leading to an exclusive localization of AQP2 at the plasma membrane (Hoffert et al., 2008a; Moeller et al., 2009a; Wang et al., 2017). Phosphorylation of Ser269 of AQP2 resulted in a reduced rate of AQP2 internalization from the apical plasma membrane (Moeller et al., 2010). Taken together, these results indicate that Ser256 and Ser261, along with AQP2 abundance are critical for the fluconazole-mediated AQP2 membrane accumulation.

Fluconazole increases the phosphorylation of AQP2 at Ser256 without affecting not only global PKA activity, but also without affecting global phosphatase activity in IMCD cells. However, fluconazole could change phosphatase activity locally. Phosphatase inhibitors promote the AQP2 redistribution to the plasma membrane *via* the nitric oxide/cGMP pathway (Bouley et al., 2000). Calyculin (PP1 and PP2A inhibitor) increased the phosphorylation of AQP2 at Ser256 and Ser264 (Ren et al., 2016). Several studies have predicted that Ser256 of AQP2 may potentially be phosphorylated by stimuli other than PKA (Bouley et al., 2000; Brown et al., 2008) suggesting that an unidentified kinase or stimuli activates fluconazole-induced phosphorylation of AQP2 at Ser256 by another means. Some of the alternative stimuli are a promising starting point for bypassing the defective V2R receptor in 90 % of cases of NDI.

5.2 Fluconazole reduces F actin-containing stress fibers and allows AQP2-bearing vesicles to reach the plasma membrane

The fluconazole-induced translocation of AQP2 to the plasma membrane is associated with a decrease in RhoA activity, in both IMCD cells and in wild type mice, and a decrease in F-actin-containing stress fibers in IMCD cells. These results corroborate previous findings that active RhoA in resting IMCD cells maintains F-actin as a physical barrier for the prevention of AQP2-bearing vesicles reaching the plasma membrane. Attenuation of RhoA signaling causes F-actin depolymerization and a decrease in F-actin-containing stress fibers, and facilitates the membrane insertion of AQP2 in the presence of AVP (Klussmann and Rosenthal, 2001; Klussmann et al., 2001; Tamma et al., 2001). cAMP-induced AQP2 translocation is associated with RhoA phosphorylation by PKA at Ser188 and an increased interaction with RhoA-GDI (GDP dissociating inhibitor) (Tamma et al., 2003a). However, fluconazole acts independent of AVP and increases phosphorylation of RhoA at Ser188 in wild type mice, suggesting that an unidentified kinase activates fluconazole-induced phosphorylation of RhoA at Ser188.

Fluconazole blocks CYP51A1, a cytochrome P450 enzyme that is involved in the synthesis of sterols (Strushkevich et al., 2010), which was identified in IMCD cells. Azoles, to which fluconazole belongs, are involved not only in attenuation of cholesterol synthesis, but also in the synthesis of epoxyeicosatrineoic acid (EETs) and 20-hydroxyeicosatetraenoic acid (20-HETE), which are derivatives of arachidonic acid (Roman, 2002). PGE_2, an arachidonic acid derivate, antagonizes the AVP-induced redistribution of AQP2 through stimulation of the EP_3 receptor (Tamma et al., 2003c).

Boldt et *al.* reported that the decrease in EET levels in response to AVP could be crucial for sodium retention and consequently water retention. Notably, they identified a mechanism for the regulation of EET levels in response to AVP, which centrally involves the function of sEH. Further studies are needed to identify the physiological relevance of EETs and the products of P450 systems in the reabsorption of salts and water, and to answer the question of whether these products may be involved in the control of localization of AQP2 in addition to prostaglandins in the collecting ducts.

Similarly to statins, fluconazole inhibits cholesterol synthesis by blocking the conversion of mevalonate to the isoprenoid product farnezyl-PP. Previous findings suggest that the isoprenoid products are important for the activity of small GTPases, amongst them RhoA (Li et al., 2011; Wennerberg and Der, 2004). Statins exhibit their pleiotropic effect on AQP2 through inhibition of isoprenoid production, which causes downregulation of RhoA and an inhibition of AQP2 endocytosis. Thus, inhibition of isoprenoid production affects the actin cytoskeleton and promotes the AQP2 redistribution to the plasma membrane (Procino et al., 2016; Wade, 2011).

RhoA downstream effectors play a key role in the actin cytoskeleton polymerization. Active RhoA, activates ROCK, which in turns activates LIMK1 *via* phosphorylation at Thr508 (Ohashi, 2015). Phosphorylation of LIMK1 associates with the deactivation of cofilin *via* its phosphorylation. Reduced RhoA activity could activate cofilin, which when active, plays an essential role in actin reorganization by depolymerisation and severing actin filaments (Kobayashi et al., 2006). Fluconazole (50 µM) decreases the phosphorylation of LIMK1/2 in IMCD cells, whereby an increase in cofilin activity *via* its dephosphorylation was expected. Ultimately, this was not detected. However, FSK decreases LIMK1/2 phosphorylation and consequently cofilin dephosphorylation, which is associated with reduced F-actin-containing stress fibers in IMCD cells. This observation would be a novel link of the RhoA-LIMK1-cofilin pathway to the AQP2 trafficking. Possibly, this phenomenon may potentially solely be related to the increased cAMP levels or increased PKA activity, and since fluconazole acts independently of global PKA, it does not influence RhoA downstream pathway.

Nevertheless, this contradicts other cell systems where increased PKA activity is associated with increased LIMK1 phosphorylation and cofilin dephosphorylation. Sleep deprivation increases PDE4A5 protein levels, causing a reduction in cAMP levels and an attenuation of the PKA-LIMK signaling pathway, resulting in a reduction in the phosphorylation of cofilin in hippocampal area C1 in mice (Havekes et al., 2016). Altered

cell morphology and enhanced migration was observed in mouse embryonic fibroblasts (MEFs) lacking the PKA regulatory subunit Prkar1a. These cells showed an increased phosphorylation of cofilin, a crucial modulator of actin dynamics, and these changes could be mimicked by stimulating the activity of PKA (Nadella et al., 2009). However, in both reports, PKA phosphorylates LIMK1 at Ser596, while phosphorylation at Thr508, observed in IMCD cells, is regulated by the downstream effectors of RhoA, PAK and ROCK. The effect of fluconazole on phosphorylation at Ser596 of LIMK1 was not investigated due to the lack of specific antibody. Perhaps PKA exhibits a different effect when it acts *via* RhoA and its downstream effectors as opposed to when it directly phosphorylates LIMK1.

Fluconazole (50 μM) leads to an increased phosphorylation of MLC in IMCD cells. There is ample evidence that myosins are involved in vesicular trafficking (DePina and Langford, 1999) (Rogers and Gelfand, 2000). MLC phosphorylation was increased in response to dDAVP in IMCD cells (Chou et al., 2004) supporting the notion that fluconazole induces plasma membrane localization of AQP2.

5.3 Fluconazole enhances the effect of forskolin on the AQP2 plasma membrane localization in principal cells and urine-concentrating ability in water-deprived mice

Immunofluorescence microscopic analysis showed that fluconazole induces the AQP2 translocation in an AVP-independent manner in IMCD cells. Cell surface biotinylation assays demonstrated that the effect of fluconazole (50 μM) in combination with FSK on the AQP2 redistribution exhibited a stronger effect as when compared to FSK stimulation alone. Thus, a potential explanation for the observed stronger effect may be due to increased phosphorylation at Ser269 upon fluconazole treatment in a combination with FSK compared to FSK alone. Although a stronger effect of fluconazole and FSK was observed, fluconazole alone did not alter the plasma membrane abundance. The reason for this discrepancy compared to the immunofluorescence images of IMCD cells lays probably in an incomplete insertion of AQP2 into the plasma membrane upon fluconazole treatment. According to a recent study with a biotinylation assay, it was shown that tacrolimus did not alter the plasma membrane abundance in IMCD cells. However, in the same study an increase in phosphorylation of AQP2 at Ser264 in IMCD cells was observed, which was associated with predominant plasma membrane localization of AQP2 (Ren et al., 2016).

Immunofluorescence images show that AQP2 was in the plasma membrane upon treatment with fluconazole in IMCD, similarly to what was observed in wild type mice both without and with water deprivation, which is a condition when the AVP level is elevated. A biotinylation assay in IMCD cells did not show that AQP2 was inserted into the plasma membrane upon fluconazole treatment. However, decreased urine volume and increased urine osmolality in water-deprived and non-water-deprived mice compared with their control littermates clearly show that AQP2 was inserted into the plasma membrane upon treatment with fluconazole. This discrepancy may be additionally due to different cell/animal models (rat IMCD vs. wild type mice) and variable treatment strategies (1 h in cultured IMCD cells vs. 96 h in wild type mice). Indeed, increased Rab3a in water-deprived mice treated with fluconazole possibly explains the enhanced effect of fluconazole in water-deprived mice.

5.4 Fluconazole may be beneficial in reducing the large urine output in nephrogenic diabetes insipidus patients, in tolvaptan-treated polycystic kidney disease and heart failure patients

Fluconazole is the most commonly used first-line drug of the azole family in clinical prophylaxis and in treatment of mucosal and invasive *Candida* infections including vulvovaginal candidiasis (Gao et al., 2016). Fluconazole is also used as integrated therapy for HIV or cryptococcosis infections (Srichatrapimuk and Sungkanuparph, 2016). It is used as an alternative to ketoconazole because it has fewer common side effects, in particular hepatotoxicity (Garcia Rodriguez et al., 1999). While ketoconazole is at least three times more potent as an inhibitor (Ervine et al., 1996), it is extensively hepatically metabolized, heightening the risk of hepatotoxicity. Fluconazole is minimally metabolized in the liver and 80 % excreted with urine unchanged (Como and Dismukes, 1994). Both drugs are strong inhibitors of the CYP450 enzyme system. Fluconazole has recently been reported as alternative to ketoconazole in treatment of Cushing's disease (Burns et al., 2016). It acts by blocking the activities of 11-β-hydroxylase and 17-α-hydroxylase to suppress the human cortisol production in cultured adrenal cortical carcinoma and human adrenal cortical cells, and it also has a higher potency on a reduced cortisol production in comparison to ketoconazole (Burns et al., 2016).

Mutations in the V2R cause NDI. In this case, the proteins for the trafficking of AQP2 are intact. Therefore, the stimulation of a receptor-independent pathway of the AQP2 redistribution could improve or correct the urine concentration defect. In addition, NDI is usually treated with thiazide, amiloride and/or indomethacin combination, alongside salt restriction. However, these therapies are only partially effective. Statins, sildenafil and rosiglitazone also increase urine osmolality and decrease urine output but even so, none of them are approved for the treatment of NDI.

Tolvaptan is already described as an effective drug in producing NDI model as a result of blocking the V2R (Miranda et al., 2014). Urine output and urine osmolality were used to confirm this model. Fluconazole decreased urine output in tolvaptan-treated mice. Urine osmolality showed a tendency to be increased with fluconazole in tolvaptan-treated mice, but this did not reach statistical significance due to a low number of repetitions (n=5).

The fluconazole-induced urine-concentrating effect in tolvaptan-treated mice might be a novel treatment option for patients suffering from NDI. However, drug-drug interactions must be carefully considered as fluconazole is a strong inhibitor of CYP3A4 system and many drugs are metabolized by CYP3A4. In addition, fluconazole may be beneficial as a co-treatment with tolvaptan to reduce the dehydrating effect of this drug in heart failure and ADPKD.

There were also some limitations of this study. The concentration of 50 μM of fluconazole in IMCD cells was equivalent to the accumulating concentration of 15.4 mg/L in mice, which were treated with fluconazole dose of 80 mg/kg every 24 h over a period of 96 h. This regime was in order to ensure the maximal bioavailability of the drug since mice are fast metabolizers. The dose of 80 mg/kg was in the range of higher doses used for candida treatments in humans. However, other research groups treated mice with doses of up to 128 mg/kg of fluconazole (Gonzalez et al., 2015).

Fluconazole, despite the structural similarity to triazolpropenon, exhibits an opposite effect on redistribution of AQP2 of the one seen with triazolpropenon. Although triazolpropenon prevented the redistribution of AQP2 into the plasma membrane in both MCD4 and IMCD cells, further experiments were not performed due to its toxicity near its 50 % lethal concentration.

Collectively, the data presented here demonstrate a novel effect of the antimycotic drug fluconazole. The fluconazole-induced redistribution of AQP2 is AVP/PKA-independent. The mechanism underlying this redistribution involves a decrease in RhoA activity accompanied with depolymerisation of the F-actin cytoskeleton. Additionally,

fluconazole improves the urine concentration ability in wild type and tolvaptan-treated mice, and could be repurposed as a novel treatment of NDI (Figure 31).

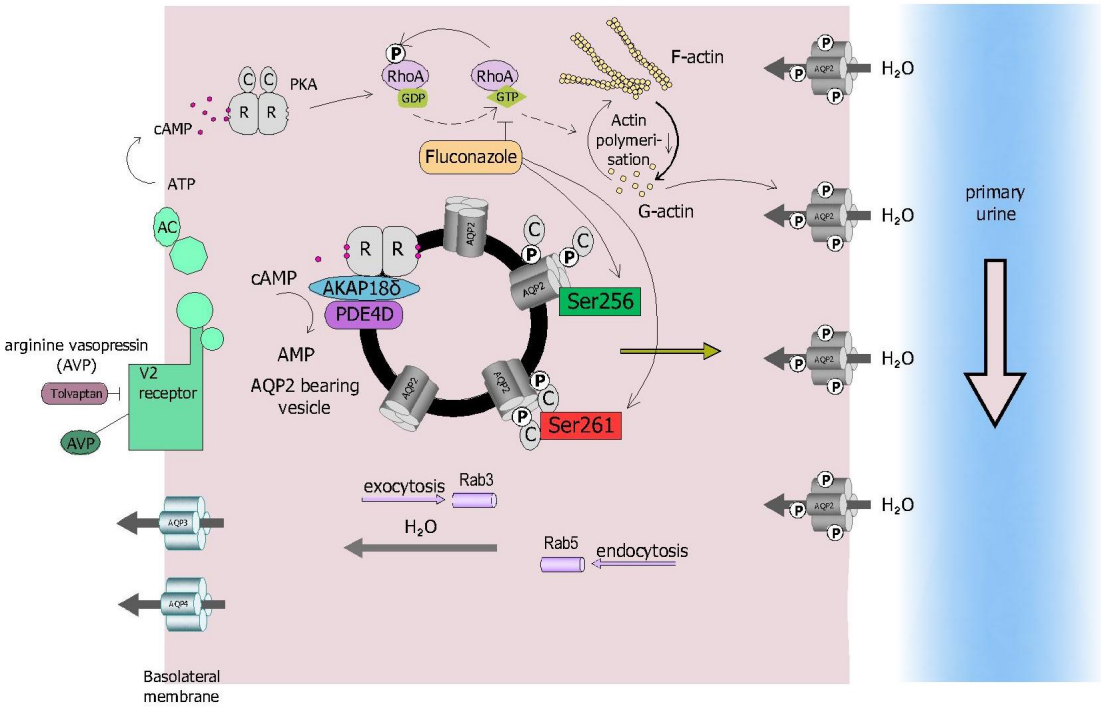

Figure 31. Proposed mechanism for the fluconazole-induced AQP2 translocation from intracellular vesicles to the plasma membrane. Fluconazole increases the phosphorylation of AQP2 at Ser256 and decreases the phosphorylation of AQP2 at Ser261. The fluconazole-induced redistribution of AQP2 involves decrease in RhoA activity, which is associated with depolymerisation of F-actin. Fluconazole promotes the AQP2 redistribution even when V2R receptor is pharmacologically blocked by Tolvaptan.

OUTLOOK

The current study presented in this thesis showed that fluconazole improves urine-concentrating ability in tolvaptan V2R-blocked mice. The use of a V2R KO model would additionally confirm this effect. Several NDI and V2R KO mice models are already available (Efe et al., 2016; Li et al., 2009). Li *et al.* reported that a conditional deletion of V2R causes 70 % reduction in AQP2 abundance. Further investigation is needed to reveal whether fluconazole restores AQP2 abundance and phosphorylation of its serine residues, and whether this result is restored urine-concentrating ability involving the same observed mechanism in wild type mice treated with fluconazole.

Investigation of produced acids upon fluconazole treatment and their further characterization would be of great interest for clarifying their potential involvement in the regulation of AQP2 trafficking.

The data about patients treated with clinically approved drug fluconazole are highly relevant for investigating whether fluconazole promotes AQP2 redistribution also in humans. It would be highly beneficial to translate these results to patients with NDI. Finally, the finding that fluconazole may promote water retention as a part of this mechanism is of vital importance for the consideration of whether it should be used for heart failure patients and with other comorbidities that include aspects of water retention.

SUMMARY

The water channel aquaporin-2 (AQP2) resides on intracellular vesicles of renal collecting duct principal cells. Binding of antidiuretic hormone (arginine-vasopressin, AVP) to vasopressin V2 receptors on the surface of the cells induces the translocation of AQP2 into the plasma membrane and facilitates water reabsorption from primary urine. Defects preventing the insertion of AQP2 into the plasma membrane cause diabetes insipidus (DI), a disease characterized by polyuria and polydipsia. *Vice versa*, a predominant localization of AQP2 in the plasma membrane is also associated with diseases, e.g. the syndrome of inappropriate antidiuretic hormone secretion (SIADH), late stage heart failure or liver cirrhosis. Here a so far unidentified effect of the widely used antimycotic drug, fluconazole, on the trafficking of AQP2 is reported. Fluconazole was identified through an unbiased screening of a small molecule library. Immunofluorescence microscopic analysis showed that it induces the AQP2 translocation in an AVP-independent manner in primary cultured rat inner medullary collecting duct (IMCD) cells. Forskolin mimicks the effect of AVP by elevating cAMP levels. In IMCD cells, fluconazole enhances the forskolin-induced increase in the localization of AQP2 in the plasma membrane. A similar effect of fluconazole on the AQP2 localization was observed in wild type mice without and upon water deprivation, a condition when the AVP level is elevated. These observations are in line with the findings that fluconazole decreases the urine volume and increases urine osmolality in both normal and water-deprived mice compared with their control littermates. At the molecular level, fluconazole increases the key trigger phosphorylation of AQP2 at Ser256, increases AQP2 abundance, and reduces phosphorylation of AQP2 at Ser261. The fluconazole-induced translocation of AQP2 to the plasma membrane is associated with an inhibition of the small GTPase RhoA and a decrease in F-actin-containing stress fibers. Thus, fluconazole removes a physical barrier hindering AQP2-bearing vesicles to reach the plasma membrane. Additionally, fluconazole decreases the urine volume in mice treated with the V2 receptor blocker tolvaptan. These observations may lead to new indications for fluconazole, i.e. treatment of diabetes insipidus for enhancing water reabsorption and as co-medication with tolvaptan to prevent excessive tolvaptan-induced water loss in patients with autosomal polycystic kidney disease.

ZUSAMMENFASSUNG

In Hauptzellen des renalen Sammelrohrs liegt der Wasserkanal Aquaporin-2 (AQP2) auf intrazellulären Vesikeln vor. Die Stimulation das Vasopressin V2 Rezeptor auf Oberfläche renalen Hauptzellen durch Bindung von antidiuretischem Hormon (Arginin-Vasopressin, AVP) induziert die Translokation von AQP2 in die Plasmamembran. Dadurch wird die Wasser-Rückresorption aus dem Primärharn verstärkt. Defekte, die den Einbau von AQP2 in die Membran verhindern, führen zu Diabetes insipidus: ein Krankheitsbild, das von Polyurie und Polydipsie geprägt ist. Umgekehrt ist eine vorwiegende Membranlokalisation ebenso pathologisch und mit Krankheiten wie dem Syndrom der inadäquaten ADH-Sekretion (SIADH), Herzinsuffizienz und Leberzirrhose assoziiert. Diese Arbeit befasst sich mit einem bisher unbekannten Effekt des weitverbreiteten Antimykotikums Fluconazol auf die Umverteilung von AQP2 in Hauptzellen der Niere. Fluconazol wurde im Rahmen eines *Screenings* niedermolekularer Verbindungen identifiziert.

Immunfluoreszenzmikroskopische Untersuchungen von primär kultivierten Sammelrohrzellen der inneren Medulla von Ratten (IMCD-Zellen, *inner medullary collecting duct*) zeigten, dass Fluconazol die AQP2-Umverteilung AVP-unabhängig induziert. Forskolin imitiert die AVP-induzierte Erhöhung des intrazellulären cAMP Spiegels. In IMCD-Zellen erhöht Fluconazol die Forskolin-induzierte Plasmamembran-lokalisation von AQP2. Ein ähnlicher Effekt von Fluconazol auf die AQP2-Lokalisation wurde in Wildtyp-Mäusen mit und ohne Wasserentzug beobachtet. Wasserentzug erhöht den AVP-Spiegel im Blut. Fluconazol-induzierte Umverteilung von AQP2 geht einher mit reduziertem Urinvolumen und erhöhter Urin-Osmolarität der Fluconazol-behandelten Mäuse, sowohl bei Wasserentzug als auch unter Kontrollbedingungen, im Vergleich zu Kontroll-Wurfgeschwistern.

Auf molekularer Ebene erhöht Fluconazol die impulsgebende Phosphorylierung von AQP2 an Ser256, die Gesamtmenge an AQP2 und reduziert die Phosphorylierung von AQP2 an Ser261. Die Fluconazol-induzerte Umverteilung von AQP2 in die Plasmamembran ist mit der Hemmung der kleinen GTPase RhoA und einem Abbau F-Aktin-basierter Stressfasern assoziiert. Auf diese Weise reduziert Fluconazol die F-actin Barriere, die den Transport AQP2-haltiger Vesikel zur Plasmamembran behindert. Des

Weiteren reduziert Fluconazol das Urinvolumen von Mäusen, die mit dem V2-Rezeptor-Blocker Tolvaptan behandelt wurden. Die in dieser Arbeit gewonnenen Erkenntnisse können genutzt werden, um Fluconazol neuen Indikationen zuzuweisen. So könnte es potenziell genutzt werden, um die Wasser-Rückresorption bei Diabetes insipidus-Patienten zu steigern. Als Zusatz-Medikation zu Tolvaptan bei autosomaler polyzystischer Nierenerkrankung könnte es den Tolvaptan-vermittelten Wasserverlust verhindern.

6 BIBLIOGRAPHY

Alexander, S.P., Mathie, A., and Peters, J.A. (2011). Guide to Receptors and Channels (GRAC), 5th edition. Br. J. Pharmacol. *164 Suppl 1*, S1-324.

Assadi, F., and Ghane Sharbaf, F. (2015). Sildenafil for the Treatment of Congenital Nephrogenic Diabetes Insipidus. American journal of nephrology *42*, 65-69.

Baggaley, E., Nielsen, S., and Marples, D. (2010). Dehydration-induced increase in aquaporin-2 protein abundance is blocked by nonsteroidal anti-inflammatory drugs. American journal of physiology. Renal physiology *298*, F1051-1058.

Bichet, D.G., Ruel, N., Arthus, M.F., and Lonergan, M. (1990). Rolipram, a phosphodiesterase inhibitor, in the treatment of two male patients with congenital nephrogenic diabetes insipidus. Nephron *56*, 449-450.

Bockenhauer, D., and Bichet, D.G. (2013). Urinary concentration: different ways to open and close the tap. Pediatric nephrology.

Bockenhauer, D., and Bichet, D.G. (2014). Urinary concentration: different ways to open and close the tap. Pediatric nephrology *29*, 1297-1303.

Bockenhauer, D., and Bichet, D.G. (2015). Pathophysiology, diagnosis and management of nephrogenic diabetes insipidus. Nature reviews. Nephrology *11*, 576-588.

Bogum, J., Faust, D., Zuhlke, K., Eichhorst, J., Moutty, M.C., Furkert, J., Eldahshan, A., Neuenschwander, M., von Kries, J.P., Wiesner, B.*, et al.* (2013). Small-molecule screening identifies modulators of aquaporin-2 trafficking. Journal of the American Society of Nephrology : JASN *24*, 744-758.

Boldt, C., Roeschel, T., Himmerkus, N., Plain, A., Bleich, M., Labes, R., Blum, M., Krause, H., Magheli, A., Giesecke, T.*, et al.* (2016). Vasopressin lowers renal epoxyeicosatrienoic acid levels by activating soluble epoxide hydrolase. American journal of physiology. Renal physiology, ajprenal 00062 02016.

Bonfrate, L., Procino, G., Wang, D.Q., Svelto, M., and Portincasa, P. (2015). A novel therapeutic effect of statins on nephrogenic diabetes insipidus. Journal of cellular and molecular medicine *19*, 265-282.

Boone, M., and Deen, P.M. (2008). Physiology and pathophysiology of the vasopressin-regulated renal water reabsorption. Pflugers Archiv : European journal of physiology *456*, 1005-1024.

Bouley, R., Breton, S., Sun, T., McLaughlin, M., Nsumu, N.N., Lin, H.Y., Ausiello, D.A., and Brown, D. (2000). Nitric oxide and atrial natriuretic factor stimulate cGMP-dependent membrane insertion of aquaporin 2 in renal epithelial cells. J Clin Invest *106*, 1115-1126.

Bouley, R., Pastor-Soler, N., Cohen, O., McLaughlin, M., Breton, S., and Brown, D. (2005). Stimulation of AQP2 membrane insertion in renal epithelial cells in vitro and in vivo by the cGMP phosphodiesterase inhibitor sildenafil citrate (Viagra). American journal of physiology. Renal physiology *288*, F1103-1112.

Breyer, M.D., and Breyer, R.M. (2000). Prostaglandin E receptors and the kidney. American journal of physiology. Renal physiology *279*, F12-23.
Breyer, M.D., and Breyer, R.M. (2001). G protein-coupled prostanoid receptors and the kidney. Ann Rev Physiol *63*, 579-605.
Breyer, M.D., Davis, L., Jacobson, H.R., and Breyer, R.M. (1996). Differential localization of prostaglandin E receptor subtypes in human kidney. Am. J. Physiol. Renal Physiol. *270*, F912-918.
Brond, L., Hadrup, N., Salling, N., Torp, M., Graebe, M., Christensen, S., Nielsen, S., and Jonassen, T.E. (2004). Uncoupling of vasopressin signaling in collecting ducts from rats with CBL-induced liver cirrhosis. American journal of physiology. Renal physiology *287*, F806-815.
Brown, D., Bouley, R., Paunescu, T.G., Breton, S., and Lu, H.A. (2012). New insights into the dynamic regulation of water and acid-base balance by renal epithelial cells. American journal of physiology. Cell physiology *302*, C1421-1433.
Brown, D., Hasler, U., Nunes, P., Bouley, R., and Lu, H.A. (2008). Phosphorylation events and the modulation of aquaporin 2 cell surface expression. Curr Opin Nephrol Hypertens *17*, 491-498.
Burns, K., Christie-David, D., and Gunton, J.E. (2016). Fluconazole in the treatment of Cushing's disease. Endocrinol Diabetes Metab Case Rep *2016*, 150115.
Celik, G., Ozturk, E., Ipekci, S.H., Yilmaz, S., Colkesen, F., Baldane, S., and Kebapcilar, L. (2014). An uncommon presentation of Sjogren's syndrome and brucellosis. Transfusion and apheresis science : official journal of the World Apheresis Association : official journal of the European Society for Haemapheresis *51*, 77-80.
Chou, C.L., Christensen, B.M., Frische, S., Vorum, H., Desai, R.A., Hoffert, J.D., de Lanerolle, P., Nielsen, S., and Knepper, M.A. (2004). Non-muscle myosin II and myosin light chain kinase are downstream targets for vasopressin signaling in the renal collecting duct. The Journal of biological chemistry *279*, 49026-49035.
Christensen, B.M., Zelenina, M., Aperia, A., and Nielsen, S. (2000). Localization and regulation of PKA-phosphorylated AQP2 in response to V(2)-receptor agonist/antagonist treatment. American journal of physiology. Renal physiology *278*, F29-42.
Como, J.A., and Dismukes, W.E. (1994). Oral azole drugs as systemic antifungal therapy. N Engl J Med *330*, 263-272.
Cousin, L., Berre, M.L., Launay-Vacher, V., Izzedine, H., and Deray, G. (2003). Dosing guidelines for fluconazole in patients with renal failure. Nephrology, dialysis, transplantation : official publication of the European Dialysis and Transplant Association - European Renal Association *18*, 2227-2231.
Deen, P.M., Weghuis, D.O., Sinke, R.J., Geurts van Kessel, A., Wieringa, B., and van Os, C.H. (1994). Assignment of the human gene for the water channel of renal collecting duct Aquaporin 2 (AQP2) to chromosome 12 region q12-->q13. Cytogenetics and cell genetics *66*, 260-262.
DePina, A.S., and Langford, G.M. (1999). Vesicle transport: the role of actin filaments and myosin motors. Microsc Res Tech *47*, 93-106.
Dong, J.M., Leung, T., Manser, E., and Lim, L. (1998). cAMP-induced morphological changes are counteracted by the activated RhoA small GTPase and the Rho kinase ROKalpha. The Journal of biological chemistry *273*, 22554-22562.

Dousa, T.P. (1999). Cyclic-3',5'-nucleotide phosphodiesterase isozymes in cell biology and pathophysiology of the kidney. Kidney Int *55*, 29-62.
Efe, O., Klein, J.D., LaRocque, L.M., Ren, H., and Sands, J.M. (2016). Metformin improves urine concentration in rodents with nephrogenic diabetes insipidus. JCI Insight *1*.
Ervine, C.M., Matthew, D.E., Brennan, B., and Houston, J.B. (1996). Comparison of ketoconazole and fluconazole as cytochrome P450 inhibitors. Use of steady-state infusion approach to achieve plasma concentration-response relationships. Drug Metab Dispos *24*, 211-215.
Faust, D., Geelhaar, A., Eisermann, B., Eichhorst, J., Wiesner, B., Rosenthal, W., and Klussmann, E. (2013). Culturing primary rat inner medullary collecting duct cells. J Vis Exp.
Fenton, R.A., Moeller, H.B., Hoffert, J.D., Yu, M.J., Nielsen, S., and Knepper, M.A. (2008). Acute regulation of aquaporin-2 phosphorylation at Ser-264 by vasopressin. Proceedings of the National Academy of Sciences of the United States of America *105*, 3134-3139.
Flores, D., Liu, Y., Liu, W., Satlin, L.M., and Rohatgi, R. (2012). Flow-induced prostaglandin E2 release regulates Na and K transport in the collecting duct. American journal of physiology. Renal physiology *303*, F632-638.
Fujino, H., and Regan, J.W. (2006). EP(4) prostanoid receptor coupling to a pertussis toxin-sensitive inhibitory G protein. Mol. Pharmacol. *69*, 5-10.
Gankam Kengne, F., Couturier, B.S., Soupart, A., and Decaux, G. (2015). Urea minimizes brain complications following rapid correction of chronic hyponatremia compared with vasopressin antagonist or hypertonic saline. Kidney Int *87*, 323-331.
Gao, M., Cao, R., Du, S., Jia, X., Zheng, S., Huang, S., Han, Q., Liu, J., Zhang, X., Miao, Y.*, et al.* (2015). Disruption of prostaglandin E2 receptor EP4 impairs urinary concentration via decreasing aquaporin 2 in renal collecting ducts. Proceedings of the National Academy of Sciences of the United States of America *112*, 8397-8402.
Gao, M., Wang, H., and Zhu, L. (2016). Quercetin Assists Fluconazole to Inhibit Biofilm Formations of Fluconazole-Resistant Candida Albicans in In Vitro and In Vivo Antifungal Managements of Vulvovaginal Candidiasis. Cell Physiol Biochem *40*, 727-742.
Garcia Rodriguez, L.A., Duque, A., Castellsague, J., Perez-Gutthann, S., and Stricker, B.H. (1999). A cohort study on the risk of acute liver injury among users of ketoconazole and other antifungal drugs. Br J Clin Pharmacol *48*, 847-852.
Gohla, A., Birkenfeld, J., and Bokoch, G.M. (2005). Chronophin, a novel HAD-type serine protein phosphatase, regulates cofilin-dependent actin dynamics. Nat Cell Biol *7*, 21-29.
Gonzalez, J.M., Rodriguez, C.A., Zuluaga, A.F., Agudelo, M., and Vesga, O. (2015). Demonstration of Therapeutic Equivalence of Fluconazole Generic Products in the Neutropenic Mouse Model of Disseminated Candidiasis. PloS one *10*, e0141872.
Graziani, G., Pini, D., Oldani, S., Cucchiari, D., Podesta, M.A., and Badalamenti, S. (2014). Renal dysfunction in acute congestive heart failure: a common problem for cardiologists and nephrologists. Heart failure reviews *19*, 699-708.

Han, J.S., Maeda, Y., Ecelbarger, C., and Knepper, M.A. (1994). Vasopressin-independent regulation of collecting duct water permeability. The American journal of physiology *266*, F139-146.
Hao, C.M., and Breyer, M.D. (2008). Physiological regulation of prostaglandins in the kidney. Annu. Rev. Physiol. *70*, 357-377.
Havekes, R., Park, A.J., Tudor, J.C., Luczak, V.G., Hansen, R.T., Ferri, S.L., Bruinenberg, V.M., Poplawski, S.G., Day, J.P., Aton, S.J.*, et al.* (2016). Sleep deprivation causes memory deficits by negatively impacting neuronal connectivity in hippocampal area CA1. Elife *5*.
Heinke, F., and Labudde, D. (2012). Membrane protein stability analyses by means of protein energy profiles in case of nephrogenic diabetes insipidus. Computational and mathematical methods in medicine *2012*, 790281.
Hoffert, J.D., Fenton, R.A., Moeller, H.B., Simons, B., Tchapyjnikov, D., McDill, B.W., Yu, M.J., Pisitkun, T., Chen, F., and Knepper, M.A. (2008a). Vasopressin-stimulated increase in phosphorylation at Ser269 potentiates plasma membrane retention of aquaporin-2. The Journal of biological chemistry *283*, 24617-24627.
Hoffert, J.D., Fenton, R.A., Moeller, H.B., Simons, B., Tchapyjnikov, D., McDill, B.W., Yu, M.J., Pisitkun, T., Chen, F., and Knepper, M.A. (2008b). Vasopressin-stimulated Increase in Phosphorylation at Ser269 Potentiates Plasma Membrane Retention of Aquaporin-2. J. Biol. Chem. *283*, 24617-24627.
Hoffert, J.D., Nielsen, J., Yu, M.J., Pisitkun, T., Schleicher, S.M., Nielsen, S., and Knepper, M.A. (2007). Dynamics of aquaporin-2 serine-261 phosphorylation in response to short-term vasopressin treatment in collecting duct. American journal of physiology. Renal physiology *292*, F691-700.
Hoffert, J.D., Pisitkun, T., Wang, G., Shen, R.F., and Knepper, M.A. (2006). Quantitative phosphoproteomics of vasopressin-sensitive renal cells: regulation of aquaporin-2 phosphorylation at two sites. Proceedings of the National Academy of Sciences of the United States of America *103*, 7159-7164.
Houslay, M.D. (2010). Underpinning compartmentalised cAMP signalling through targeted cAMP breakdown. Trends Biochem Sci *35*, 91-100.
Ishikawa, S.E. (2015). Hyponatremia Associated with Heart Failure: Pathological Role of Vasopressin-Dependent Impaired Water Excretion. Journal of clinical medicine *4*, 933-947.
Ivanovska, J., Tregubova, A., Mahadevan, V., Chakilam, S., Gandesiri, M., Benderska, N., Ettle, B., Hartmann, A., Soder, S., Ziesche, E.*, et al.* (2013). Identification of DAPK as a scaffold protein for the LIMK/cofilin complex in TNF-induced apoptosis. Int J Biochem Cell Biol *45*, 1720-1729.
Jensen, A.M., Bae, E.H., Fenton, R.A., Norregaard, R., Nielsen, S., Kim, S.W., and Frokiaer, J. (2009). Angiotensin II regulates V2 receptor and pAQP2 during ureteral obstruction. American journal of physiology. Renal physiology *296*, F127-134.
Jensen, A.M., Bae, E.H., Norregaard, R., Wang, G., Nielsen, S., Schweer, H., Kim, S.W., and Frokiaer, J. (2010). Cyclooxygenase 2 inhibition exacerbates AQP2 and pAQP2 downregulation independently of V2 receptor abundance in the postobstructed kidney. American journal of physiology. Renal physiology *298*, F941-950.
Jensen, B.L., Stubbe, J., Hansen, P.B., Andreasen, D., and Skott, O. (2001). Localization of prostaglandin E(2) EP2 and EP4 receptors in the rat kidney. Am. J. Physiol. Renal Physiol. *280*, F1001-1009.

Jia, Z., Wang, H., and Yang, T. (2009). Mice lacking mPGES-1 are resistant to lithium-induced polyuria. American journal of physiology. Renal physiology *297*, F1689-1696.
Jung, H.J., Kim, S.Y., Choi, H.J., Park, E.J., Lim, J.S., Frokiaer, J., Nielsen, S., and Kwon, T.H. (2015). Tankyrase-mediated beta-catenin activity regulates vasopressin-induced AQP2 expression in kidney collecting duct mpkCCDc14 cells. American journal of physiology. Renal physiology *308*, F473-486.
Jung, H.J., and Kwon, T.H. (2016). Molecular mechanisms regulating aquaporin-2 in kidney collecting duct. American journal of physiology. Renal physiology *311*, F1318-F1328.
Kamath, C., Govindan, J., Premawardhana, A.D., Wood, S.J., Adlan, M.A., and Premawardhana, L.D. (2013). Nephrogenic diabetes insipidus partially responsive to oral desmopressin in a subject with lithium-induced multiple endocrinopathy. Clinical medicine *13*, 407-410.
Kamsteeg, E.J., Heijnen, I., van Os, C.H., and Deen, P.M. (2000). The subcellular localization of an aquaporin-2 tetramer depends on the stoichiometry of phosphorylated and nonphosphorylated monomers. J. Biol. Chem. *151*, 919-930.
Khairallah, W., Fawaz, A., Brown, E.M., and El-Hajj Fuleihan, G. (2007). Hypercalcemia and diabetes insipidus in a patient previously treated with lithium. Nature clinical practice. Nephrology *3*, 397-404.
Khan, M.A., Aljarbou, A.N., Khan, A., and Younus, H. (2015). Liposomal thymoquinone effectively combats fluconazole-resistant Candida albicans in a murine model. Int J Biol Macromol *76*, 203-208.
Kim, G.H., Choi, N.W., Jung, J.Y., Song, J.H., Lee, C.H., Kang, C.M., and Knepper, M.A. (2008). Treating lithium-induced nephrogenic diabetes insipidus with a COX-2 inhibitor improves polyuria via upregulation of AQP2 and NKCC2. American journal of physiology. Renal physiology *294*, F702-709.
Kim, G.H., Lee, J.W., Oh, Y.K., Chang, H.R., Joo, K.W., Na, K.Y., Earm, J.H., Knepper, M.A., and Han, J.S. (2004). Antidiuretic effect of hydrochlorothiazide in lithium-induced nephrogenic diabetes insipidus is associated with upregulation of aquaporin-2, Na-Cl co-transporter, and epithelial sodium channel. Journal of the American Society of Nephrology : JASN *15*, 2836-2843.
Kishore, B.K., Carlson, N.G., Ecelbarger, C.M., Kohan, D.E., Muller, C.E., Nelson, R.D., Peti-Peterdi, J., and Zhang, Y. (2015). Targeting renal purinergic signalling for the treatment of lithium-induced nephrogenic diabetes insipidus. Acta physiologica *214*, 176-188.
Kjaersgaard, G., Madsen, K., Marcussen, N., and Jensen, B.L. (2014). Lithium induces microcysts and polyuria in adolescent rat kidney independent of cyclooxygenase-2. Physiological reports *2*, e00202.
Klussmann, E. (2015). Protein-protein interactions of PDE4 family members - Functions, interactions and therapeutic value. Cellular signalling.
Klussmann, E., and Rosenthal, W. (2001). Role and identification of protein kinase A anchoring proteins in vasopressin-mediated aquaporin-2 translocation. Kidney Int *60*, 446-449.
Klussmann, E., Tamma, G., Lorenz, D., Wiesner, B., Maric, K., Hofmann, F., Aktories, K., Valenti, G., and Rosenthal, W. (2001). An inhibitory role of Rho in the vasopressin-mediated translocation of aquaporin-2 into cell membranes of renal principal cells. The Journal of biological chemistry *276*, 20451-20457.

Knoers, N. (1993). Nephrogenic Diabetes Insipidus. In GeneReviews(R), R.A. Pagon, M.P. Adam, H.H. Ardinger, S.E. Wallace, A. Amemiya, L.J.H. Bean, T.D. Bird, C.T. Fong, H.C. Mefford, R.J.H. Smith, and K. Stephens, eds. (Seattle (WA)).
Knoers, N.V., and Deen, P.M. (2001). Molecular and cellular defects in nephrogenic diabetes insipidus. Pediatric nephrology *16*, 1146-1152.
Kobayashi, M., Nishita, M., Mishima, T., Ohashi, K., and Mizuno, K. (2006). MAPKAPK-2-mediated LIM-kinase activation is critical for VEGF-induced actin remodeling and cell migration. The EMBO journal *25*, 713-726.
Kortenoeven, M.L., and Fenton, R.A. (2014). Renal aquaporins and water balance disorders. Biochimica et biophysica acta *1840*, 1533-1549.
Kortenoeven, M.L., Schweer, H., Cox, R., Wetzels, J.F., and Deen, P.M. (2011). Lithium reduces aquaporin-2 transcription independent of prostaglandins. Am J Physiol Renal Physiol.
Kortenoeven, M.L., Schweer, H., Cox, R., Wetzels, J.F., and Deen, P.M. (2012). Lithium reduces aquaporin-2 transcription independent of prostaglandins. American journal of physiology. Cell physiology *302*, C131-140.
Kortenoeven, M.L., Sinke, A.P., Hadrup, N., Trimpert, C., Wetzels, J.F., Fenton, R.A., and Deen, P.M. (2013). Demeclocycline attenuates hyponatremia by reducing aquaporin-2 expression in the renal inner medulla. American journal of physiology. Renal physiology *305*, F1705-1718.
Lauridsen, T.G., Vase, H., Starklint, J., Graffe, C.C., Bech, J.N., Nielsen, S., and Pedersen, E.B. (2010). Increased renal sodium absorption by inhibition of prostaglandin synthesis during fasting in healthy man. A possible role of the epithelial sodium channels. BMC nephrology *11*, 28.
Lee, E.H., Heo, J.S., Lee, H.K., Han, K.H., Kang, H.G., Ha, I.S., Choi, Y., and Cheong, H.I. (2010). A case of Bartter syndrome type I with atypical presentations. Korean journal of pediatrics *53*, 809-813.
Lepak, A., Nett, J., Lincoln, L., Marchillo, K., and Andes, D. (2006). Time course of microbiologic outcome and gene expression in Candida albicans during and following in vitro and in vivo exposure to fluconazole. Antimicrob Agents Chemother *50*, 1311-1319.
Li, J.H., Chou, C.L., Li, B., Gavrilova, O., Eisner, C., Schnermann, J., Anderson, S.A., Deng, C.X., Knepper, M.A., and Wess, J. (2009). A selective EP4 PGE2 receptor agonist alleviates disease in a new mouse model of X-linked nephrogenic diabetes insipidus. J Clin Invest *119*, 3115-3126.
Li, W., Zhang, Y., Bouley, R., Chen, Y., Matsuzaki, T., Nunes, P., Hasler, U., Brown, D., and Lu, H.A. (2011). Simvastatin enhances aquaporin-2 surface expression and urinary concentration in vasopressin-deficient Brattleboro rats through modulation of Rho GTPase. American journal of physiology. Renal physiology *301*, F309-318.
Liao, J.K., and Laufs, U. (2005). Pleiotropic effects of statins. Annual review of pharmacology and toxicology *45*, 89-118.
Liebenhoff, U., and Rosenthal, W. (1995). Identification of Rab3-, Rab5a- and synaptobrevin II-like proteins in a preparation of rat kidney vesicles containing the vasopressin-regulated water channel. FEBS Lett *365*, 209-213.
Lin, T.E., Adams, K.F., Jr., and Patterson, J.H. (2014). Potential roles of vaptans in heart failure: experience from clinical trials and considerations for optimizing therapy in target patients. Heart failure clinics *10*, 607-620.

Loonen, A.J., Knoers, N.V., van Os, C.H., and Deen, P.M. (2008). Aquaporin 2 mutations in nephrogenic diabetes insipidus. Seminars in nephrology *28*, 252-265.

Lu, H.J., Matsuzaki, T., Bouley, R., Hasler, U., Qin, Q.H., and Brown, D. (2008). The phosphorylation state of serine 256 is dominant over that of serine 261 in the regulation of AQP2 trafficking in renal epithelial cells. American journal of physiology. Renal physiology *295*, F290-294.

Maekawa, M., Ishizaki, T., Boku, S., Watanabe, N., Fujita, A., Iwamatsu, A., Obinata, T., Ohashi, K., Mizuno, K., and Narumiya, S. (1999). Signaling from Rho to the actin cytoskeleton through protein kinases ROCK and LIM-kinase. Science *285*, 895-898.

Manetti, F. (2012). LIM kinases are attractive targets with many macromolecular partners and only a few small molecule regulators. Med Res Rev *32*, 968-998.

McAvoy, T., and Nairn, A.C. (2010). Serine/threonine protein phosphatase assays. Curr Protoc Mol Biol *Chapter 18*, Unit18 18.

Miranda, C.A., Lee, J.W., Chou, C.L., and Knepper, M.A. (2014). Tolvaptan as a tool in renal physiology. American journal of physiology. Renal physiology *306*, F359-366.

Moeller, H.B., Knepper, M.A., and Fenton, R.A. (2009a). Serine 269 phosphorylated aquaporin-2 is targeted to the apical membrane of collecting duct principal cells. Kidney Int *75*, 295-303.

Moeller, H.B., MacAulay, N., Knepper, M.A., and Fenton, R.A. (2009b). Role of multiple phosphorylation sites in the COOH-terminal tail of aquaporin-2 for water transport: evidence against channel gating. American journal of physiology. Renal physiology *296*, F649-657.

Moeller, H.B., Praetorius, J., Rutzler, M.R., and Fenton, R.A. (2010). Phosphorylation of aquaporin-2 regulates its endocytosis and protein-protein interactions. Proceedings of the National Academy of Sciences of the United States of America *107*, 424-429.

Moeller, H.B., Rittig, S., and Fenton, R.A. (2013). Nephrogenic diabetes insipidus: essential insights into the molecular background and potential therapies for treatment. Endocrine reviews *34*, 278-301.

Morath, R., Klein, T., Seyberth, H.W., and Nusing, R.M. (1999). Immunolocalization of the four prostaglandin E2 receptor proteins EP1, EP2, EP3, and EP4 in human kidney. J. Am. Soc. Nephrol. *10*, 1851-1860.

Morishita, T., Tsutsui, M., Shimokawa, H., Sabanai, K., Tasaki, H., Suda, O., Nakata, S., Tanimoto, A., Wang, K.Y., Ueta, Y.*, et al.* (2005). Nephrogenic diabetes insipidus in mice lacking all nitric oxide synthase isoforms. Proceedings of the National Academy of Sciences of the United States of America *102*, 10616-10621.

Multari, G., Werner, B., Cervoni, M., Lubrano, R., Costantino, F., Demiraj, V., and Pozzilli, P. (2001). Peritoneal dialysis in an infant with type 1 diabetes and hyperosmolar coma. Journal of endocrinological investigation *24*, 104-106.

Murata, K., Mitsuoka, K., Hirai, T., Walz, T., Agre, P., Heymann, J.B., Engel, A., and Fujiyoshi, Y. (2000). Structural determinants of water permeation through aquaporin-1. Nature *407*, 599-605.

Nadella, K.S., Saji, M., Jacob, N.K., Pavel, E., Ringel, M.D., and Kirschner, L.S. (2009). Regulation of actin function by protein kinase A-mediated phosphorylation of Limk1. EMBO Rep *10*, 599-605.

Narayen, G., and Mandal, S.N. (2012). Vasopressin receptor antagonists and their role in clinical medicine. Indian journal of endocrinology and metabolism *16*, 183-191.

Nedvetsky, P.I., Tabor, V., Tamma, G., Beulshausen, S., Skroblin, P., Kirschner, A., Mutig, K., Boltzen, M., Petrucci, O., Vossenkamper, A.*, et al.* (2010). Reciprocal regulation of aquaporin-2 abundance and degradation by protein kinase A and p38-MAP kinase. Journal of the American Society of Nephrology : JASN *21*, 1645-1656.

Nedvetsky, P.I., Tamma, G., Beulshausen, S., Valenti, G., Rosenthal, W., and Klussmann, E. (2009). Regulation of aquaporin-2 trafficking. Handbook of experimental pharmacology, 133-157.

Nielsen, J., Hoffert, J.D., Knepper, M.A., Agre, P., Nielsen, S., and Fenton, R.A. (2008). Proteomic analysis of lithium-induced nephrogenic diabetes insipidus: mechanisms for aquaporin 2 down-regulation and cellular proliferation. Proceedings of the National Academy of Sciences of the United States of America *105*, 3634-3639.

Nielsen, S., DiGiovanni, S.R., Christensen, E.I., Knepper, M.A., and Harris, H.W. (1993). Cellular and subcellular immunolocalization of vasopressin-regulated water channel in rat kidney. Proceedings of the National Academy of Sciences of the United States of America *90*, 11663-11667.

Nishimoto, G., Zelenina, M., Li, D., Yasui, M., Aperia, A., Nielsen, S., and Nairn, A.C. (1999). Arginine vasopressin stimulates phosphorylation of aquaporin-2 in rat renal tissue. The American journal of physiology *276*, F254-259.

Niwa, R., Nagata-Ohashi, K., Takeichi, M., Mizuno, K., and Uemura, T. (2002). Control of actin reorganization by Slingshot, a family of phosphatases that dephosphorylate ADF/cofilin. Cell *108*, 233-246.

Niwa, T., Shiraga, T., and Takagi, A. (2005). Effect of antifungal drugs on cytochrome P450 (CYP) 2C9, CYP2C19, and CYP3A4 activities in human liver microsomes. Biological & pharmaceutical bulletin *28*, 1805-1808.

Noda, Y., Horikawa, S., Katayama, Y., and Sasaki, S. (2004). Water channel aquaporin-2 directly binds to actin. Biochem Biophys Res Commun *322*, 740-745.

Noda, Y., Sohara, E., Ohta, E., and Sasaki, S. (2010). Aquaporins in kidney pathophysiology. Nature reviews. Nephrology *6*, 168-178.

Ohashi, K. (2015). Roles of cofilin in development and its mechanisms of regulation. Dev Growth Differ *57*, 275-290.

Olesen, E.T., Rutzler, M.R., Moeller, H.B., Praetorius, H.A., and Fenton, R.A. (2011a). Vasopressin-independent targeting of aquaporin-2 by selective E-prostanoid receptor agonists alleviates nephrogenic diabetes insipidus. Proceedings of the National Academy of Sciences of the United States of America *108*, 12949-12954.

Olesen, E.T., Rutzler, M.R., Moeller, H.B., Praetorius, H.A., and Fenton, R.A. (2011b). Vasopressin-independent targeting of aquaporin-2 by selective E-prostanoid receptor agonists alleviates nephrogenic diabetes insipidus. Proc. Natl. Acad. Sci. U. S. A.

Oliverio, M.I., Delnomdedieu, M., Best, C.F., Li, P., Morris, M., Callahan, M.F., Johnson, G.A., Smithies, O., and Coffman, T.M. (2000). Abnormal water metabolism in mice lacking the type 1A receptor for ANG II. American journal of physiology. Renal physiology *278*, F75-82.

Pearce, D., Soundararajan, R., Trimpert, C., Kashlan, O.B., Deen, P.M., and Kohan, D.E. (2015). Collecting duct principal cell transport processes and their regulation. Clinical journal of the American Society of Nephrology : CJASN *10*, 135-146.

Peters, H.P., Robben, J.H., Deen, P.M., and Wetzels, J.F. (2007). Water in health and disease: new aspects of disturbances in water metabolism. The Netherlands journal of medicine *65*, 325-332.

Preston, G.M., and Agre, P. (1991). Isolation of the cDNA for erythrocyte integral membrane protein of 28 kilodaltons: member of an ancient channel family. Proceedings of the National Academy of Sciences of the United States of America *88*, 11110-11114.

Procino, G., Barbieri, C., Carmosino, M., Rizzo, F., Valenti, G., and Svelto, M. (2010). Lovastatin-induced cholesterol depletion affects both apical sorting and endocytosis of aquaporin-2 in renal cells. American journal of physiology. Renal physiology *298*, F266-278.

Procino, G., Barbieri, C., Carmosino, M., Tamma, G., Milano, S., De Benedictis, L., Mola, M.G., Lazo-Fernandez, Y., Valenti, G., and Svelto, M. (2011). Fluvastatin modulates renal water reabsorption in vivo through increased AQP2 availability at the apical plasma membrane of collecting duct cells. Pflugers Archiv : European journal of physiology *462*, 753-766.

Procino, G., Barbieri, C., Tamma, G., De Benedictis, L., Pessin, J.E., Svelto, M., and Valenti, G. (2008). AQP2 exocytosis in the renal collecting duct - involvement of SNARE isoforms and the regulatory role of Munc18b. J. Cell. Sci. *121*, 2097-2106.

Procino, G., Mastrofrancesco, L., Tamma, G., Lasorsa, D.R., Ranieri, M., Stringini, G., Emma, F., Svelto, M., and Valenti, G. (2012). Calcium-sensing receptor and aquaporin 2 interplay in hypercalciuria-associated renal concentrating defect in humans. An in vivo and in vitro study. PloS one *7*, e33145.

Procino, G., Milano, S., Carmosino, M., Barbieri, C., Nicoletti, M.C., Li, J.H., Wess, J., and Svelto, M. (2014). Combination of secretin and fluvastatin ameliorates the polyuria associated with X-linked nephrogenic diabetes insipidus in mice. Kidney Int *86*, 127-138.

Procino, G., Portincasa, P., Mastrofrancesco, L., Castorani, L., Bonfrate, L., Addabbo, F., Carmosino, M., Di Ciaula, A., and Svelto, M. (2016). Simvastatin increases AQP2 urinary excretion in hypercholesterolemic patients: A pleiotropic effect of interest for patients with impaired AQP2 trafficking. Clin Pharmacol Ther *99*, 528-537.

Qureshi, S., Galiveeti, S., Bichet, D.G., and Roth, J. (2014). Diabetes insipidus: celebrating a century of vasopressin therapy. Endocrinology *155*, 4605-4621.

Radin, M.J., Yu, M.J., Stoedkilde, L., Miller, R.L., Hoffert, J.D., Frokiaer, J., Pisitkun, T., and Knepper, M.A. (2012). Aquaporin-2 regulation in health and disease. Veterinary clinical pathology / American Society for Veterinary Clinical Pathology *41*, 455-470.

Randall, V.A., MacLennan, S.J., Martin, G.R., and Wilson, V.G. (1996). The effect of forskolin on 5-HT1-like and angiotensin II-induced vasoconstriction and cyclic AMP content of the rabbit isolated femoral artery. British journal of pharmacology *118*, 627-634.

Regan, J.W. (2003). EP2 and EP4 prostanoid receptor signaling. Life Sci. *74*, 143-153.

Ren, H., Yang, B., Ruiz, J.A., Efe, O., Ilori, T.O., Sands, J.M., and Klein, J.D. (2016). Phosphatase inhibition increases AQP2 accumulation in the rat IMCD apical plasma membrane. American journal of physiology. Renal physiology *311*, F1189-F1197.

Riento, K., and Ridley, A.J. (2003). Rocks: multifunctional kinases in cell behaviour. Nat Rev Mol Cell Biol *4*, 446-456.

Rinschen, M.M., Yu, M.J., Wang, G., Boja, E.S., Hoffert, J.D., Pisitkun, T., and Knepper, M.A. (2010). Quantitative phosphoproteomic analysis reveals vasopressin V2-receptor-dependent signaling pathways in renal collecting duct cells. Proceedings of the National Academy of Sciences of the United States of America *107*, 3882-3887.

Rogers, S.L., and Gelfand, V.I. (2000). Membrane trafficking, organelle transport, and the cytoskeleton. Curr Opin Cell Biol *12*, 57-62.

Roman, R.J. (2002). P-450 metabolites of arachidonic acid in the control of cardiovascular function. Physiological reviews *82*, 131-185.

Sakairi, Y., Jacobson, H.R., Noland, T.D., Capdevila, J.H., Falck, J.R., and Breyer, M.D. (1995). 5,6-EET inhibits ion transport in collecting duct by stimulating endogenous prostaglandin synthesis. The American journal of physiology *268*, F931-939.

Sanches, T.R., Volpini, R.A., Massola Shimizu, M.H., Braganca, A.C., Oshiro-Monreal, F., Seguro, A.C., and Andrade, L. (2012). Sildenafil reduces polyuria in rats with lithium-induced NDI. American journal of physiology. Renal physiology *302*, F216-225.

Sander, E.E., ten Klooster, J.P., van Delft, S., van der Kammen, R.A., and Collard, J.G. (1999). Rac downregulates Rho activity: reciprocal balance between both GTPases determines cellular morphology and migratory behavior. The Journal of cell biology *147*, 1009-1022.

Santos, S.R., Campos, E.V., Sanches, C., Gomez, D.S., and Ferreira, M.C. (2010). Fluconazole plasma concentration measurement by liquid chromatography for drug monitoring of burn patients. Clinics (Sao Paulo) *65*, 237-243.

Sato, E., Nakamura, T., Amaha, M., Nomura, M., Matsumura, D., Yamagishi, H., Ono, Y., and Ueda, Y. (2014). Effect of tolvaptan in patients with chronic kidney disease due to diabetic nephropathy with heart failure. International heart journal *55*, 533-538.

Savelkoul, P.J., De Mattia, F., Li, Y., Kamsteeg, E.J., Konings, I.B., van der Sluijs, P., and Deen, P.M. (2009). p.R254Q mutation in the aquaporin-2 water channel causing dominant nephrogenic diabetes insipidus is due to a lack of arginine vasopressin-induced phosphorylation. Hum Mutat *30*, E891-903.

Seibold, A., Brabet, P., Rosenthal, W., and Birnbaumer, M. (1992). Structure and chromosomal localization of the human antidiuretic hormone receptor gene. Am J Hum Genet *51*, 1078-1083.

Sellers, J.R. (2000). Myosins: a diverse superfamily. Biochimica et biophysica acta *1496*, 3-22.

Sinke, A.P., Kortenoeven, M.L., de Groot, T., Baumgarten, R., Devuyst, O., Wetzels, J.F., Loffing, J., and Deen, P.M. (2014). Hydrochlorothiazide attenuates lithium-induced nephrogenic diabetes insipidus independently of the sodium-chloride cotransporter. American journal of physiology. Renal physiology *306*, F525-533.

Sohara, E., Rai, T., Yang, S.S., Uchida, K., Nitta, K., Horita, S., Ohno, M., Harada, A., Sasaki, S., and Uchida, S. (2006). Pathogenesis and treatment of autosomal-

dominant nephrogenic diabetes insipidus caused by an aquaporin 2 mutation. Proceedings of the National Academy of Sciences of the United States of America *103*, 14217-14222.
Srichatrapimuk, S., and Sungkanuparph, S. (2016). Integrated therapy for HIV and cryptococcosis. AIDS Res Ther *13*, 42.
Stefan, E., Wiesner, B., Baillie, G.S., Mollajew, R., Henn, V., Lorenz, D., Furkert, J., Santamaria, K., Nedvetsky, P., Hundsrucker, C.*, et al.* (2007). Compartmentalization of cAMP-dependent signaling by phosphodiesterase-4D is involved in the regulation of vasopressin-mediated water reabsorption in renal principal cells. J Am Soc Nephrol *18*, 199-212.
Strushkevich, N., Usanov, S.A., and Park, H.W. (2010). Structural basis of human CYP51 inhibition by antifungal azoles. J Mol Biol *397*, 1067-1078.
Su, W., Huang, S.Z., Gao, M., Kong, X.M., Gustafsson, J.A., Xu, S.J., Wang, B., Zheng, F., Chen, L.H., Wang, N.P.*, et al.* (2017). Liver X Receptor beta (LXRbeta) Increases AQP2 Protein Level via a Post-transcriptional Mechanism in Renal Collecting Ducts. American journal of physiology. Renal physiology, ajprenal 00564 02016.
Sugimoto, Y., Namba, T., Shigemoto, R., Negishi, M., Ichikawa, A., and Narumiya, S. (1994). Distinct cellular localization of mRNAs for three subtypes of prostaglandin E receptor in kidney. Am. J. Physiol. Renal Physiol. *266*, F823-828.
Sugimoto, Y., and Narumiya, S. (2007). Prostaglandin E receptors. J Biol Chem *282*, 11613-11617.
Sun, T.X., Van Hoek, A., Huang, Y., Bouley, R., McLaughlin, M., and Brown, D. (2002). Aquaporin-2 localization in clathrin-coated pits: inhibition of endocytosis by dominant-negative dynamin. American journal of physiology. Renal physiology *282*, F998-1011.
Tamma, G., Klussmann, E., Maric, K., Aktories, K., Svelto, M., Rosenthal, W., and Valenti, G. (2001). Rho inhibits cAMP-induced translocation of aquaporin-2 into the apical membrane of renal cells. American journal of physiology. Renal physiology *281*, F1092-1101.
Tamma, G., Klussmann, E., Procino, G., Svelto, M., Rosenthal, W., and Valenti, G. (2003a). cAMP-induced AQP2 translocation is associated with RhoA inhibition through RhoA phosphorylation and interaction with RhoGDI. J Cell Sci *116*, 1519-1525.
Tamma, G., Lasorsa, D., Trimpert, C., Ranieri, M., Di Mise, A., Mola, M.G., Mastrofrancesco, L., Devuyst, O., Svelto, M., Deen, P.M.*, et al.* (2014). A protein kinase A-independent pathway controlling aquaporin 2 trafficking as a possible cause for the syndrome of inappropriate antidiuresis associated with polycystic kidney disease 1 haploinsufficiency. Journal of the American Society of Nephrology : JASN *25*, 2241-2253.
Tamma, G., Robben, J.H., Trimpert, C., Boone, M., and Deen, P.M.T. (2010). Regulation of AQP2 localization by Ser256 and S261 phosphorylation and ubiquitination. AJP: Cell Physiology.
Tamma, G., Wiesner, B., Furkert, J., Hahm, D., Oksche, A., Schaefer, M., Valenti, G., Rosenthal, W., and Klussmann, E. (2003b). The prostaglandin E2 analogue sulprostone antagonizes vasopressin-induced antidiuresis through activation of Rho. J. Cell. Sci. *116*, 3285-3294.
Tamma, G., Wiesner, B., Furkert, J., Hahm, D., Oksche, A., Schaefer, M., Valenti, G., Rosenthal, W., and Klussmann, E. (2003c). The prostaglandin E2 analogue

sulprostone antagonizes vasopressin-induced antidiuresis through activation of Rho. J Cell Sci *116*, 3285-3294.
Tong, J., Li, L., Ballermann, B., and Wang, Z. (2016). Phosphorylation and Activation of RhoA by ERK in Response to Epidermal Growth Factor Stimulation. PloS one *11*, e0147103.
Torres, A.C., Wickham, E.P., and Biskobing, D.M. (2011). Tolvaptan for the management of syndrome of inappropriate antidiuretic hormone secretion: lessons learned in titration of dose. Endocrine practice : official journal of the American College of Endocrinology and the American Association of Clinical Endocrinologists *17*, e97-100.
Troger, J., Moutty, M.C., Skroblin, P., and Klussmann, E. (2012). A-kinase anchoring proteins as potential drug targets. British journal of pharmacology *166*, 420-433.
Valenti, G., Procino, G., Carmosino, M., Frigeri, A., Mannucci, R., Nicoletti, I., and Svelto, M. (2000). The phosphatase inhibitor okadaic acid induces AQP2 translocation independently from AQP2 phosphorylation in renal collecting duct cells. J Cell Sci *113 (Pt 11)*, 1985-1992.
Verbalis, J.G. (2006). Whole-body volume regulation and escape from antidiuresis. The American journal of medicine *119*, S21-29.
Verhulst, A., D'Haese, P.C., and De Broe, M.E. (2004). Inhibitors of HMG-CoA reductase reduce receptor-mediated endocytosis in human kidney proximal tubular cells. Journal of the American Society of Nephrology : JASN *15*, 2249-2257.
Vossenkamper, A., Nedvetsky, P.I., Wiesner, B., Furkert, J., Rosenthal, W., and Klussmann, E. (2007). Microtubules are needed for the perinuclear positioning of aquaporin-2 after its endocytic retrieval in renal principal cells. American journal of physiology. Cell physiology *293*, C1129-1138.
Vukicevic, T., Schulz, M., Faust, D., and Klussmann, E. (2016). The Trafficking of the Water Channel Aquaporin-2 in Renal Principal Cells-a Potential Target for Pharmacological Intervention in Cardiovascular Diseases. Front Pharmacol *7*, 23.
Wade, J.B. (2011). Statins affect AQP2 traffic. American journal of physiology. Renal physiology *301*, F308.
Wang, P.J., Lin, S.T., Liu, S.H., Kuo, K.T., Hsu, C.H., Knepper, M.A., and Yu, M.J. (2017). Vasopressin-induced serine 269 phosphorylation reduces Sipa111 (signal-induced proliferation-associated 1 like 1)-mediated aquaporin-2 endocytosis. The Journal of biological chemistry.
Wells, C.D., Liu, M.Y., Jackson, M., Gutowski, S., Sternweis, P.M., Rothstein, J.D., Kozasa, T., and Sternweis, P.C. (2002). Mechanisms for reversible regulation between G13 and Rho exchange factors. J. Biol. Chem. *277*, 1174-1181.
Wennerberg, K., and Der, C.J. (2004). Rho-family GTPases: it's not only Rac and Rho (and I like it). J Cell Sci *117*, 1301-1312.
Yamaguchi, Y., Katoh, H., Yasui, H., Aoki, J., Nakamura, K., and Negishi, M. (2000). Galpha(12) and galpha(13) inhibit Ca(2+)-dependent exocytosis through Rho/Rho-associated kinase-dependent pathway. J. Neurochem. *75*, 708-717.
Yasui, M., Zelenin, S.M., Celsi, G., and Aperia, A. (1997). Adenylate cyclase-coupled vasopressin receptor activates AQP2 promoter via a dual effect on CRE and AP1 elements. The American journal of physiology *272*, F443-450.

Yui, N., Lu, H.A., Chen, Y., Nomura, N., Bouley, R., and Brown, D. (2013). Basolateral targeting and microtubule-dependent transcytosis of the aquaporin-2 water channel. American journal of physiology. Cell physiology *304*, C38-48.
Yui, N., Sasaki, S., and Uchida, S. (2016). Aquaporin-2 Ser-261 phosphorylation is regulated in combination with Ser-256 and Ser-269 phosphorylation. Biochem Biophys Res Commun.

7 PUBLICATION LIST

7.1 Articles

- Vukićević T, Schulz M, Faust D, Klussmann E. The Trafficking of the Water Channel Aquaporin-2 in Renal Principal Cells-a Potential Target forPharmacological Intervention in Cardiovascular Diseases. Front Pharmacol. 2016 Feb 11;7:23. doi: 10.3389/fphar.2016.00023. eCollection 2016.

7.2 Poster presentations

- Vukicevic T, Klussmann E. Small molecule triazolpropenon inhibits the cAMP-induced redistribution of the water channel aquaporin-2. *2nd German Pharm-Tox Summit.* Heidelberg, Germany, March 6-9, 2017.
- Vukicevic T, Hinze C, Dema A, Schrade K, Schmidt-Ott. MK, Klussmann E. The antimycotic drug fluconazole affects water homeostasis in the kidney by modulating the localization of aquaporin-2. *CMD Transcard Retreat 2016*, Bad Saarow, Germany, September 18-21, 2016.
- Vukicevic T, Schulz M, Dema A, Schächterle C, Klussmann E. Identification of novel proteins and their interacting partners controlling the localization of the water channel aquaporin-2. *FMP/MDC PhD Retreat 2015*, Bad Saarow, Germany, October 15-17, 2015.
- Vukicevic T, Klussmann E. Identification of novel proteins and their interacting partners controlling the localization of the water channel aquaporin-2. *Transcard Joint CMD PhD Retreat 2014*, Neuruppin, Germany, November 26-28, 2014.